

Core-collapse supernovae

Anders Jerkstrand^a, Dan Milisavljevic^b and Bernhard Müller (alphabetical)^c

^aStockholm University, Department of Astronomy, Roslagstullsbacken 21, 11421 Stockholm, Sweden.

^bPurdue University, Department of Physics and Astronomy, 525 Northwestern Ave., West Lafayette, IN 47907, USA.

^cMonash University, School of Physics and Astronomy, 10 College Walk, Clayton, VIC 3800, Australia.

© 2024 Elsevier Ltd. All rights reserved.

Chapter Article tagline: update of previous edition., reprint..

Nomenclature

SN	Supernova
CCSN	Core-collapse supernova
SNR	Supernova remnant
ZAMS	Zero-Age Main Sequence
RSG	Red Supergiant
BSG	Blue Supergiant
WR	Wolf-Rayet star
NS	Neutron star
BH	Black hole
GRB	Gamma-Ray Burst
PWN	Pulsar Wind Nebula
CSM	Circumstellar Medium
CSI	Circumstellar interaction
SESN	Stripped-envelope supernova
LTE	Local Thermodynamic Equilibrium
NLTE	Non-Local Thermodynamic Equilibrium

Abstract

Core-collapse supernovae (CCSNe) are the explosive end-points of stellar evolution for $M_{ZAMS} \gtrsim 8 M_{\odot}$ stars. The cores of these stars collapse to neutron stars, a process in which high neutrino luminosity drives off the overlying stellar layers, which get ejected with thousands of kilometers per second. These supernovae enrich their host galaxies with elements made both during the star's life and in the explosion, providing the main cosmic source of elements such as oxygen, neon and silicon. Their high luminosities ($\sim 10^{42}$ erg s⁻¹ at peak) make SNe beacons to large distances, and their light curves and spectra provide rich information on single and binary stellar evolution, nucleosynthesis, and a diverse set of high-energy physical processes. As the SN ejecta sweep up circumstellar and interstellar matter, it eventually enters a supernova remnant phase, exemplified by nearby, spatially resolved remnants such as Cas A and the Crab Nebula. In this phase, shocks and pulsar winds continue to light up the interior of the exploded stars, giving detailed information about their 3D structure. We review the central concepts of CCSNe, from the late stages of evolution of massive stars, through collapse, explosion, and electromagnetic display, to the final remnant phase. We briefly discuss still open questions, and current and future research avenues.

Key points

- **Core-collapse supernovae** occur when the cores of massive stars collapse to neutron stars, blowing off the outer layers.
- **Neutrinos** play a key role in transferring the gravitationally released energy of the core to kinetic energy of the mantle.
- **Supernova light curves and spectra** inform us about the mass and composition of the exploded star. CCSNe are the main cosmic source of most of the elements in the atomic number range $Z = 8 - 37$.
- **Supernova remnants** allow spatially resolved views of the debris and the central compact objects (typically pulsars) left behind.

1 Introduction

Core-collapse supernovae (CCSNe) are the explosions of massive stars, $M_{ZAMS} \gtrsim 8 M_{\odot}$, as they reach the end of their evolution. Such stars form iron cores at the end of their lives (apart from a small range of stars, $M_{ZAMS} \sim 8 - 9 M_{\odot}$, that may explode already at the ONeMg core stage), which eventually become unstable and collapse to neutron stars (NSs) or black holes (BHs), a process in which the overlying stellar layers get violently expelled. In this way, the cosmos is enriched in elements, with galactic chemical evolution models predicting CCSNe to dominate production of elements with atomic numbers $Z = 8 - 23, 29 - 37$, and possibly several of the yet heavier elements (Timmes et al., 1995; Kobayashi et al., 2020). In addition, compact objects (NSs and BHs) are formed, some of which lead to gamma-ray bursts (Woosley and Bloom, 2006) and NS mergers (Abbott et al., 2017), and energy and momentum are injected into the surroundings triggering

2 Core-collapse supernovae

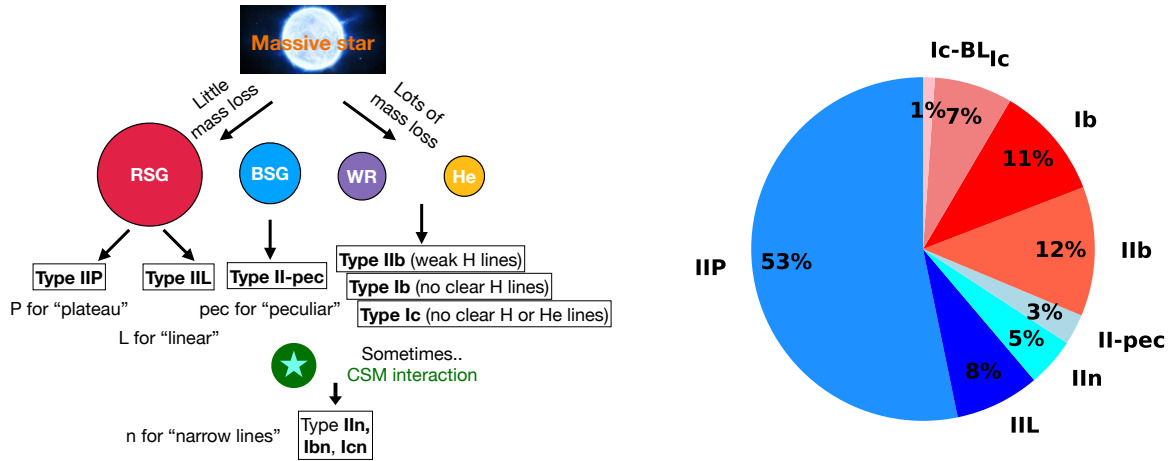


Fig. 1: *Left*: Progenitors and classification scheme of CCSNe. *Right*: Observed fractions of CCSN types in a volume-limited sample. Data from Li et al. (2011) and rates from Shivvers et al. (2017). Stars in the blue-tinted classes (about 2/3 of the total) have lost relatively little material over their lives, by winds and binary mass transfer, whereas those in the the red-tinted (about 1/3 of the total) have lost significant.

large-scale mass motions and regulating star formation (Colling et al., 2018).

One can estimate that about one CCSN occurs per second somewhere in the Universe, with a relatively good match between star formation rates for massive stars and CCSN rates (Botticella et al., 2012). CCSN progenitors live short lives and these SNe therefore occur in star-forming galaxies (Schulze et al., 2021). We currently (2025) discover about about one in every thousand CCSN, or 10,000 per year. The discovery rate has dramatically increased over the past two decades thanks to automated wide-field transient surveys such as Pan-STARRS, The Lick Observatory Supernova Survey, The Supernova SkyMapper, and the Zwicky Transient Facility (ZTF), and will soon take another major leap with the development of the Vera C. Rubin Observatory. Thanks to their immense brightness ($\sim 10^9 L_{\odot}$ at peak) we can observe SNe to large distances (hundreds of Mpc), but they are also common enough (about 2 per century in a Milky Way-like galaxy) that we can regularly study them in nearby galaxies (to several tens of Mpc, and sometimes yet further), and up-close in spatially resolved remnants in the Milky Way (typical distance a few kpc).

Classification system. The empirical classification of CCSNe (see Filippenko, 1997; Gal-Yam, 2017; Modjaz et al., 2019, for overviews) initially divides into the branches of Type I (hydrogen lines absent) and Type II (hydrogen lines present) - with Minkowski (1941) generally being credited with taking this first step for the taxonomy. The Type I class subdivides into Type Ib (helium lines present), and Type Ic (helium lines absent). Some Type Ic SNe have very broad lines, defining a specific Type Ic-BL class. There is also a Type Ia class, which are not CCSNe but thermonuclear explosions of white dwarfs. The distinction between the different Type I SN classes emerged in the mid 1980s (e.g. Wheeler and Levreault, 1985). The Type II branch subdivides into Type IIP (the light curve shows a plateau), Type IIL (the light curve shows a linear decline), Type II-pec (the light curve has a long initial rise) and Type IIb (spectra show weak H lines only, that later disappear). If narrow lines are seen, produced by the surrounding, slow circumstellar gas rather than the SN ejecta (which emit broad lines due to the high expansion velocity), the classification becomes Type IIn (Schlegel, 1990), Ibn (Pastorello et al., 2008), and Icn (Gal-Yam et al., 2021; Perley et al., 2022) respectively, depending on the composition of the circumstellar material (CSM). Figure 1 summarizes the classification system (left), and shows observationally inferred rates of the different classes (right). The most common type of supernova can be seen to be Type IIP, which make up just over half of all CCSNe by unit volume. An example of the light curves and spectra of a typical Type IIP SN (SN 2004et) is shown in Figure 2. Note the pronounced plateaus on the optical (V, R, I) bands, whereas UV/blue bands (U, B) decline and the infrared bands (J, H, K) increase over the diffusion phase ($\sim 0 - 100$ d).

It is today understood that the Type IIP/L-IIb-Ib-Ic differentiation arises due to different degrees of *mass loss* experienced by the star over its life up to explosion. Type IIb/Ib/Ic SNe are collectively called stripped-envelope supernovae (SESNe). This mass loss may occur both by stellar winds and by gravitational mass transfer to a companion star. Both these processes are mainly important in the post-main sequence phase when massive stars expand significantly, boosting their wind mass loss rates due to reduced surface gravity, as well as the chances of making Roche lobe contact with a binary companion. For a long time were Wolf-Rayet stars seen as the plausible progenitors of Type Ib/c SNe - however evidence has accumulated that most of these SNe instead appear to arise from lower-mass binary-stripped stars. There has historically been few known observational counterparts of these progenitors stars, as their bright companion stars tend to mask their light, but recently new discoveries have been reported (Drouot et al., 2023). One should also note that many Type II SN progenitors may have gained mass from a companion (Zapartas et al., 2019). Mass loss again manifests itself for the Type IIn, Ibn and Icn classes, believed to arise when the SN ejecta collide with (unusually) dense circumstellar material.

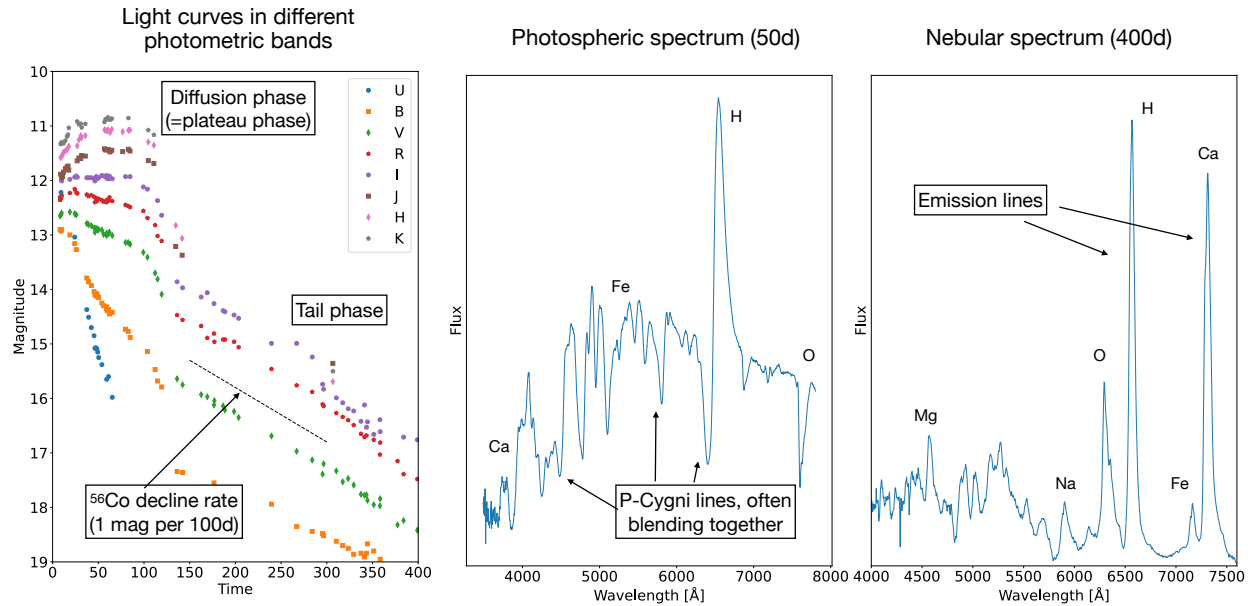


Fig. 2: Light curves in different photometric bands (left), photospheric spectrum (middle), and nebular spectrum (right) of a typical Type IIP SN. Data from Maguire et al. (2010).

2 Progenitors and explosion

2.1 Progenitor evolution up to collapse

The progenitors of core-collapse supernovae are *massive stars* with main sequence masses between about $8 M_{\odot}$ and $140 M_{\odot}$ if these evolved as single stars. For stars in binary systems the initial masses may be different due to mass exchange with their companions, and the lower and upper boundary for single stars or stars that have undergone mass transfer are subject to uncertainties in stellar physics. Such massive stars go through a sequence of six distinct burning stages (H, He, C, Ne, O, and Si burning) in the core and eventually develop an iron core after Si burning (Woosley et al., 2002; Woosley and Janka, 2005). Burning of lighter elements proceeds in shells outside the core and leaves the star with an “onion-shell” structure (Figure 3). The iron core has low entropy and is therefore mostly supported against gravity by (relativistic) electron degeneracy pressure, i.e., the pressure exerted by electrons as they occupy states of non-zero momentum and kinetic energy (up to about the *Fermi energy*) due to the Pauli exclusion principle. In addition to the electron degeneracy pressure, thermal radiation pressure also contributes, especially in more massive core-collapse supernova progenitors. As Si shell burning adds more mass to the iron core, it contracts and eventually reaches densities $\rho \gtrsim 10^9 \text{ g cm}^{-3}$.

At such high densities, the high Fermi energy of electrons allows electron captures on heavy nuclei, which drains the degeneracy pressure and therefore accelerates contraction. In addition, temperatures in the core become high enough for some measure of photodisintegration of heavy nuclei, which reduces radiation pressure support. Contraction thus becomes a runaway process and accelerates to a collapse on a dynamical time scale $\tau_{\text{dyn}} \sim (G\rho)^{-1/2}$, or a few hundred ms. The onset of collapse occurs when the iron core has grown to about $1.4 M_{\odot}$, corresponding roughly to the limiting Chandrasekhar mass of slightly neutron-rich matter. At this point, the core has reached central densities of a few 10^9 g cm^{-3} , central temperatures slightly below 10^{10} K , and has a radius of $\gtrsim 1000 \text{ km}$ (Woosley et al., 2002). In a narrow regime between low-mass and high-mass stars, where degenerate conditions in the core are encountered already after C burning, collapse may be initiated earlier by electron captures on Ne and Mg, giving rise to *electron-capture supernovae* (Nomoto, 1987; Leung and Nomoto, 2019). Such electron-capture supernovae may explain some observed low-energy explosions, but details of this evolutionary channel are still debated.

2.2 Collapse and bounce

Electron captures proceed at an accelerating pace until the the core reaches densities of $\sim 10^{12} \text{ g cm}^{-3}$. At this point, neutrinos from electron capture reactions become trapped and hence further loss of leptons from the core stops, but this is not sufficient to halt the collapse. The collapse eventually stops when the core exceeds nuclear saturation density ($\sim 2.7 \times 10^{14} \text{ g cm}^{-3}$). At this point, matter becomes significantly more incompressible due to repulsive nuclear interactions, and the inner core rebounds elastically (“bounce”). This results in the launching of a shock wave into the outer part of the core that is still collapsing supersonically. As the shock dissociates the infalling iron-group

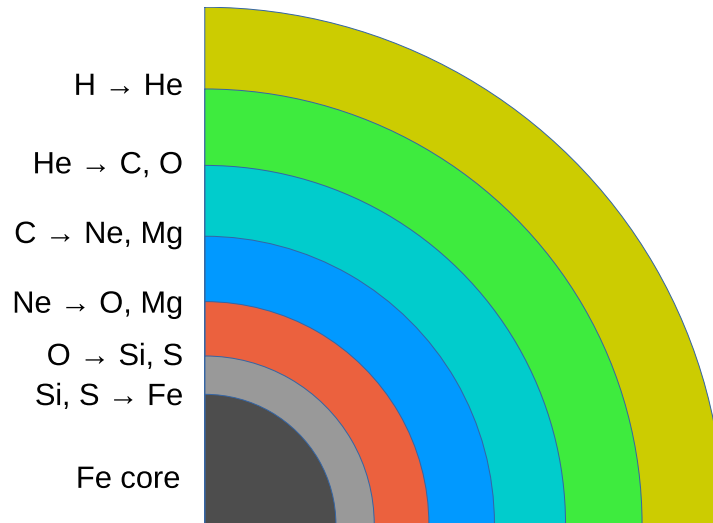


Fig. 3: Sketch (not to scale) of the onion shell structure of a massive star prior to the collapse of the iron core, in this case a red supergiant (RSG) progenitor with a hydrogen envelope. Inside the hydrogen envelope, there are shells of the ashes of hydrogen, helium, carbon, neon, and oxygen burning, and finally the iron core built by silicon burning. The respective burning processes are taking place at the bottom of the shells, but note that some burning shells may not be active at the time of collapse. The major fuels and ashes for each burning stage are indicated on the left.

material into free protons and neutrons and rapid neutrino losses occur once the post-shock densities drop below $\sim 10^{12} \text{ g cm}^{-3}$, the shock “stalls” and turns into an accretion shock within milliseconds (Bethe, 1990; Janka et al., 2007).

2.3 Structure of the Supernova Core

In the subsequent post-bounce phase, the stellar core consists of several distinct regions (Figure 4). At the centre, there is a proto-neutron star, which is still warm and relatively rich in protons with a neutron-to-proton ratio of about 3 : 1. The proto-neutron star can be divided into a core ($\sim 0.5 M_{\odot}$, region D in Figure 4) of low entropy and a continuously growing mantle (initially $\sim 0.9 M_{\odot}$, region C) of shock-heated material with higher-entropy. Below densities of a few $10^{13} \text{ g cm}^{-3}$, neutrino cooling of accreted matter becomes very efficient, and the mantle transitions into a roughly isothermal atmosphere with a steep density gradient (region B). Outside this cooling region, a heating region (also called “gain region”) develops between the proto-neutron star and the shock a few tens of milliseconds after bounce (region A in Figure 4). In this region, absorption of neutrinos from deeper layers outweighs neutrino emission, so that accreted material experiences net heating as it settles from the shock onto the proto-neutron star surface. The shock initially moves out only to a radius 100–200 km, where it remains as a standing accretion shock.

For the dynamics of supernova explosions, multi-dimensional fluid flow in the supernova core plays a crucial role (Herant et al., 1994; Burrows et al., 1995; Janka and Müller, 1996; for a review see Müller 2020). In the gain region, convection can occur because heating by neutrinos results in an unstable entropy gradient. Similarly, neutrino cooling at the proto-neutron star surface drives convection in the mantle region. Under certain conditions, the gain region may also be subject to the standing accretion shock instability (SASI, Blondin et al., 2003; Foglizzo et al., 2007; O’Connor and Couch, 2018) due to a feedback cycle of acoustic and vorticity waves. Pre-collapse asymmetries in the progenitor star due to the presence of convection shells driven by nuclear burning will often jump-start the development of violent multi-dimensional flow behind the shock (Couch et al., 2015; Müller et al., 2017a). Furthermore, turbulent fluid flow or differential rotation can drive various dynamo amplification mechanisms that generate strong magnetic fields (Akiyama et al., 2003; Raynaud et al., 2020; Matsumoto et al., 2022; Müller, 2024).

2.4 Explosion Mechanisms

Observations of supernovae and their progenitors indicate that massive stars with zero-age main sequence masses of probably up to 15–18 M_{\odot} (for single stars) explode (Smartt, 2015). This implies that some mechanism eventually “revives” the stalled accretion shock and pumps enough energy into the post-shock matter to eject the outer shells and explain the kinetic energies of observed explosions, which range from $\sim 10^{50} \text{ erg}$ to $\sim 2 \times 10^{51} \text{ erg}$ for Type IIP supernovae (e.g., Pejcha and Prieto, 2015) and may reach up to $\sim 10^{52} \text{ erg}$ for the rare class of broad-lined Ic supernovae, also known as *hypernovae*, with very high ejecta velocities. Several different explosion mechanisms have been proposed and studied extensively with numerical simulations.

In the *neutrino-driven mechanism*, the explosion is provided by the energy deposition of neutrinos in the gain region (Mezzacappa et al., 2020). Over the first seconds of its existence, the proto-neutron star radiates away several 10^{53} erg in neutrinos. The neutrino emission feeds on the internal energy of the proto-neutron star gained during the gravitational collapse. Even though only a small fraction of neutrinos are reabsorbed in the gain region, neutrino heating can provide an energy input of about 10^{52} erg over time scales of hundreds

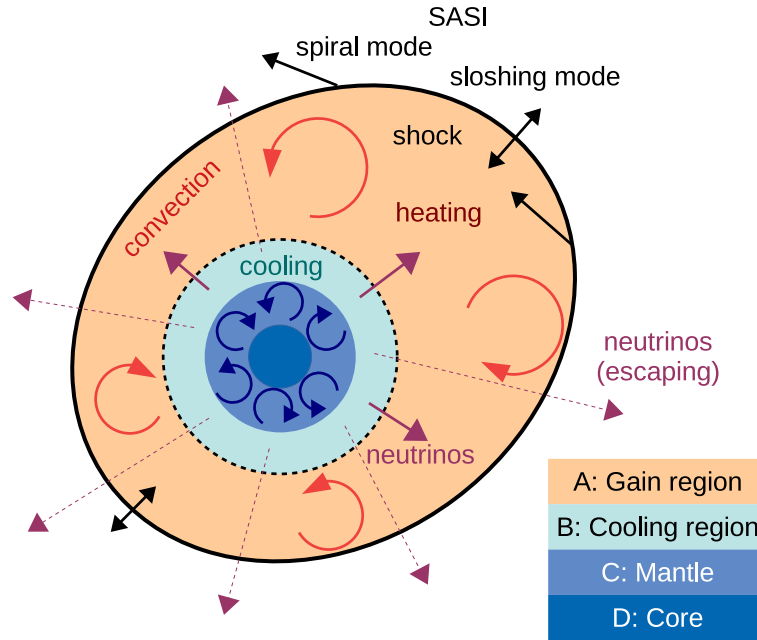


Fig. 4: Structure of the inner region of a core-collapse supernova inside the shock (thick outer curve) during the post-bounce phase before shock revival. At the centre, there is a proto-neutron star consisting of the core and mantle. Neutrinos (bordeaux arrows) are emitted from the cooling region at the proto-neutron star surface. Most of the neutrinos escape, but some are reabsorbed in the heating region (orange) behind the shock. Heating in the gain region drives convective turnover motions. These support the development of explosions, e.g., by providing effective “turbulent” pressure to support shock expansion. Another hydrodynamic instability, the standing accretion shock instability (SASI), which leads to sloshing or spiral (rotational) motions of the shock, can play a similar supportive role. Cooling at the proto-neutron star surface also drives convection in its mantle.

of milliseconds to a few seconds according to detailed neutrino transport simulations. Much of this energy needs to be used up to unbind the heated material from the vicinity of the neutron star, however, leaving a residual energy in the range of $\sim 10^{50} - 2 \times 10^{51}$ erg (Müller et al., 2017b; Bollig et al., 2021; Burrows et al., 2024), which is sufficient to explain the bulk of core-collapse supernova explosions. The detailed operation of the neutrino-driven mechanism is more complex than these simple order-of-magnitude considerations might insinuate, however. With the exception of the least massive core-collapse supernova progenitors, multi-dimensional effects in the supernova core are crucial for successful neutrino-driven explosions according to modern simulations. Multi-dimensional fluid flow supports the development of neutrino-driven explosions by providing additional “turbulent” pressure and mixing of hot, neutrino-heated material in the gain region, which increase the radius of the accretion shock (e.g., Müller, 2020). A sufficiently large shock radius is important for neutrino-driven shock revival, as this can help to increase the exposure time of accreted material to neutrino heating to the point where matter becomes unbound before settling on the proto-neutron star. Once the heating becomes sufficiently strong to exceed this threshold, it will trigger further shock expansion and a self-sustaining runaway process will set in (Janka, 2001). Numerical simulations suggest that shock revival often occurs when the interface between the silicon and oxygen shell falls into the shock. Due to a density jump at this shell interface, its infall is associated with a drop in pre-shock ram pressure that is often sufficient to trigger such a runaway.

Importantly, the onset of the explosion will not stop further accretion onto the proto-neutron star immediately. Instead, matter will continue to be channeled from the shock to the proto-neutron stars in accretion downflows, while neutrino-heating drives away hot matter in other directions (Figure 5). This cycle of simultaneous accretion and mass ejections may last for several seconds and channel up to $\sim 0.1 M_{\odot}$ into neutrino-driven outflows.

Rare explosions with kinetic energies of more than $\sim 2 \times 10^{51}$ erg cannot be readily explained by the neutrino-driven mechanism. The favoured explanation for such events is some form of *magnetorotational mechanism* (Akiyama et al., 2003; Burrows et al., 2007; Winteler et al., 2012; Obergaulinger and Reichert, 2020; Aloy and Obergaulinger, 2021; Müller, 2024). In the classic form of the magnetorotational mechanism, magnetic fields extract the rotational energy E_{rot} of a rapidly spinning proto-neutron star (ultimately coming from gravitational energy), which is roughly given in terms of its gravitational mass M , radius R , and spin period P by

$$E_{\text{rot}} = 2 \times 10^{52} \text{ erg} \left(\frac{M}{1.4 M_{\odot}} \right) \left(\frac{R}{12 \text{ km}} \right)^2 \left(\frac{P}{1 \text{ ms}} \right)^{-2}, \quad (1)$$

and hence provides a sufficient reservoir to account for hypernova energies if extraction is efficient. Strong proto-neutron star surface fields of order 10^{15} G are required to extract the rotational energy on a short enough time scale to achieve shock revival. For the shortest possible neutron star spin periods of ~ 1 ms (to avoid centrifugal breakup), the maximum rotational energy roughly corresponds to the

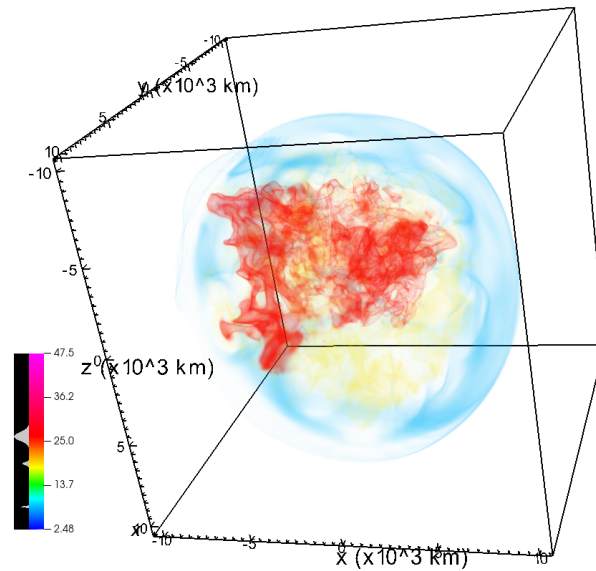


Fig. 5: Three-dimensional simulation of the supernova explosion of a $3.5M_{\odot}$ stripped-envelope progenitor from Müller et al. (2019), one second after the formation of a proto-neutron star and several hundred milliseconds after the onset of the explosion. The volume rendering shows the entropy in the flow. The shock is visible as a blue translucent surface. It is pushed outward by expanding neutrino-heated bubbles (yellow, red). The neutrino-driven outflows are strongly asymmetric, with considerably more neutrino-heated matter in one hemisphere. Much of the shocked matter is still channelled down to the proto-neutron star around the neutrino-heated bubbles. The continuing accretion of material allows the proto-neutron star to maintain strong neutrino emission, which pumps more energy into the expanding bubbles.

maximum kinetic energies inferred for hypernovae (Mazzali et al., 2014a). As an alternative to such (hypothetical) millisecond magnetars, the *collapsar mechanism* relies on the rotational energy of a black hole accretion disk as a power source. The magnetohydrodynamically powered outflows can take the form of bipolar jets, but there may be a more isotropic, wind-like outflow component from the proto-neutron star or the disk as well. The polar regions around the compact object will eventually become strongly evacuated, and both the millisecond magnetar scenario and the collapsar scenario can accommodate the launching of relativistic jets as seen in the gamma-ray bursts associated with many hypernovae (Woosley and Bloom, 2006). There are two principal uncertainties about explosion scenarios involving rotation and magnetic fields. First, the problem of angular momentum transport in stellar interiors and hence the pre-collapse rotation as well as the magnetic field strengths and configurations in massive stars before core collapse are not yet fully understood (see Chapters “Evolution and final fates of massive stars”). Second, the amplification of pre-collapse magnetic fields by compression during collapse is likely not sufficient to reach the field strengths required for magnetorotational explosion. Field amplification by magnetohydrodynamic instabilities after collapse must play a major role, but is challenging to study in simulations because of extreme requirements on spatial resolution (Mösta et al., 2015).

As an alternative to these two traditional scenarios, *phase-transition driven explosions* have been proposed to occur in some massive stars. In this scenario, the proto-neutron star becomes unstable when its core becomes dense enough to reach a putative first-order hadron-quark phase transition, collapses to a more compact state, rebounds, and thus launches a second shock wave that explodes the star (Fischer et al., 2018). Whether that phase transition is of first-order as required, and whether it could trigger explosions in a certain mass range are debated (Zha et al., 2021; Jakobus et al., 2022).

2.5 Explosion Dynamics and Nucleosynthesis

Both in the neutrino-driven scenario and in the magnetorotational scenario, the “engine” continues to operate for significant time after shock revival, as we already alluded to in the previous section. The dynamics during this phase largely determines the properties of the explosion and the compact remnant. It also shapes the production of heavy elements (nucleosynthesis) during the explosion, which will influence the electromagnetic display of the supernova (Section 3), the composition and structure of supernova remnants (Section 4), and contributes to the chemical evolution of the host galaxy.

The dynamics of this early explosion phase, which lasts hundreds of milliseconds to seconds, has been explored most thoroughly in simulations of neutrino-driven explosions. The energy of such explosions is set by the amount of neutrino-heated matter that is marginally unbound from the vicinity of the proto-neutron star and then delivers an additional energy of ~ 5 – 6 MeV per nucleon due to the recombination of nucleons into α -particles and then partially into heavy nuclei. The amount of ejected neutrino-heated material depends on how long

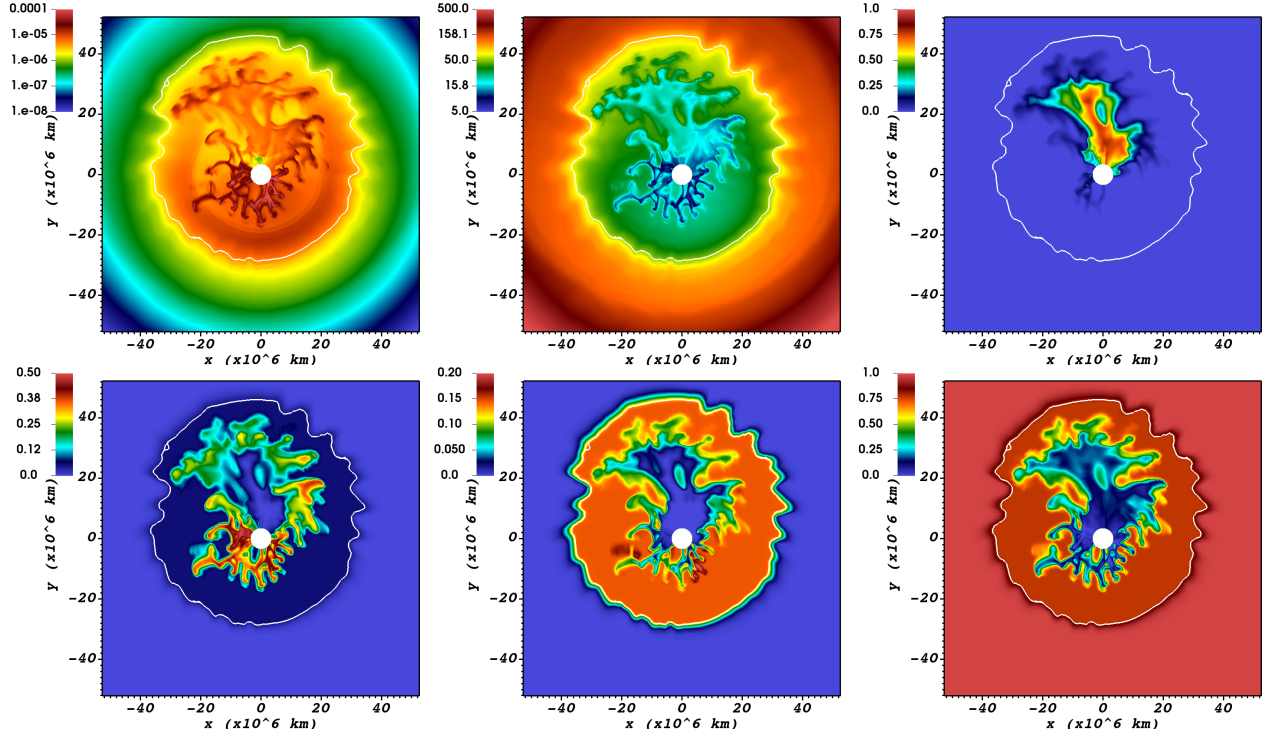


Fig. 6: Rayleigh-Taylor instability in the simulation (Mauder et al., 2024) of a Type Ib/c supernova of a $3.5 M_{\odot}$ stripped-envelope progenitor (same as in Figure 5). The figures show slices through the three-dimensional model about one hour after the onset of the explosion. The top row shows density (left, units of g cm^{-3}), entropy (middle, units of k_{B} per nucleon), and the mass fraction of iron-group elements (right). The bottom row shows the mass fractions of oxygen (left), carbon (middle) and helium (right). The white line indicates a helium mass fraction of 0.8, and demarcates the composition interface between the core and the unburned helium envelope, which has already been hit by the shock and expanded from its initial radius. Distinctive Rayleigh-Taylor plumes have formed and mix material from deep inside the star outward. Note that the large-scale asymmetry in the iron-group ejecta corresponds to the unipolar asymmetry of the early explosion in Figure 5.

the cycle of mass accretion and ejection is sustained, i.e., it is tightly coupled to the amount of matter accreted onto the proto-neutron star. Accretion eventually terminates when the explosion is strong enough for shocked matter to be accelerated roughly to the escape velocity to avoid being accreted (Marek and Janka, 2009; Müller et al., 2016a). Accretion will generally last longer in progenitors with massive and dense O shells around the Si-Fe core. After accretion has stopped, a neutrino-driven wind outflow from the neutron star will develop (Duncan et al., 1986).

Since there are also outflows of neutrino-heated matter, *net* accretion onto the proto-neutron star is expected to terminate well before the explosion engine shuts off, often already a few hundred milliseconds after the shock is revived (Müller et al., 2019). The dynamics of accretion is not only important for the final neutron star mass, however. Due to the asymmetries in the explosion, the neutron star can receive a substantial *kick* to oppose the net momentum of the ejecta. The acceleration of the neutron star occurs primarily by its gravitational attraction to the ejecta into the direction where the explosion is weaker (gravitational tug-bot mechanism, Scheck et al. 2006; Wongwathanarat et al. 2013). Since the accretion downflows hit the neutron star with a finite impact parameter, they will deposit angular momentum and can spin up the neutron star even when the progenitor core had no rotation or slow rotation (Wongwathanarat et al., 2013).

The explosion dynamics also affects the composition of the inner ejecta. As the shock moves through the star and heats the shells around the core, it will trigger *explosive burning* as long as the post-shock temperatures are high enough. Since the post-shock matter can be treated as a radiation-dominated gas, the post-shock temperature T_{sh} is about

$$T_{\text{sh}} \approx \sqrt{\frac{3(\beta - 1)}{a\beta}} \rho v_{\text{sh}}^2, \quad (2)$$

in terms of the pre-shock density ρ , the shock velocity v_{sh} and the compression ratio $\beta \approx 3-7$ in the shock; here a is the radiation constant. About 3.5×10^9 K is required for explosive O burning into (mostly) Si and S, and about 5×10^9 K is needed to further burn Si and other intermediate-mass elements into iron-group elements (Iliadis, 2007). Explosive burning to the iron-group will mostly produce ^{56}Ni in shells that have no or at most very little neutron excess. ^{56}Ni is also made by recombination of nucleons and α -particles in the neutrino-heated matter that is ejected from the vicinity of the proto-neutron star; it will later play a crucial role for the CCSN light curve. However, the nucleosynthesis becomes more complicated if the shock-heated matter expands rapidly. Under these conditions, freeze-out of hot ejecta in

8 Core-collapse supernovae

nuclear statistical equilibrium will leave an excess abundance of α -particles whose reactions on heavier nuclei modify the abundances seen in “normal” freeze-out. This α -rich freeze-out is the main source for ^{44}Ti , whose decay is an important power source for the later phase of the light curve (Section 3) and the emission from supernova remnant (Section 4). For significant neutron- or proton-excess, more complex nucleosynthesis processes can occur (see, e.g., Woosley et al., 2002; Wanajo, 2023) and produce, e.g., elements beyond the iron-group (Wanajo et al., 2011).

2.6 Evolution to Shock Breakout

After one of the aforementioned mechanisms has powered up the explosion, the shock wave still needs to propagate to the stellar surface until the explosion becomes visible by electromagnetic radiation. This can take hours to days in red supergiant stars with extended envelopes, and as a little as several minutes in very compact stripped-envelope progenitors.

As the shock propagates to the surface, the shock velocity v_{sh} changes as the kinetic energy of the explosion is distributed over a large amount of material, and as the pre-shock density declines. A rough approximation for v_{sh} in terms of the explosion energy E_{exp} , ejecta mass M_{ej} , pre-shock density ρ and shock radius is given by (Matzner and McKee, 1999)

$$v_{\text{sh}}(r) \approx 0.794 \left(\frac{E_{\text{exp}}}{M_{\text{ej}}} \right)^{1/2} \left(\frac{M_{\text{ej}}}{\rho(r)r^3} \right)^{0.19}. \quad (3)$$

Although the shock may transiently accelerate at shell interfaces in the star where the density drops strongly, the ejecta *behind* the shock generally experience deceleration by a positive pressure gradient (bigger pressure outside) behind the shock. Such a decelerated flow is subject to the *Rayleigh-Taylor instability* (Chevalier, 1976; Müller et al., 1991; Zhou, 2017) if denser, low-entropy material comes to lie below lighter, high-entropy material; in some sense the flow behaves as under an outward-directed “effective gravity”. The Rayleigh-Taylor instability can drive significant outward mixing of heavy elements from the inner shells of the explosion, and drag light elements downwards (Figure 6). Other fluid instabilities such as the Richtmyer-Meshkov instability (Zhou, 2017) may also occur.

These mixing instabilities are seeded by the initial asymmetries that inherently develop during the first few second of the explosion in the neutrino-driven and magnetorotational scenario. How much mixing occurs as the shock propagates through the envelope depends both on the initial seed asymmetries as well as the progenitor structure (Müller, 2020). Red supergiant stars tend to experience significant mixing by the Rayleigh-Taylor instability with significant development of small-scale plumes. Explosions of compact stripped-envelope progenitors tend to experience less mixing so that the ejecta geometry more strongly reflects the initial explosion asymmetries.

Generally, the dynamics of the ejecta behind the shock can be rather complex. In addition to mixing instabilities, episodes of acceleration and deceleration of the shock can lead to the formation of *reverse shocks*, which can both trigger and inhibit mixing, and decelerate material to a degree that it will fall back onto the compact remnant.

Such *fallback* is thought to play a most prominent role in massive progenitors with big helium and carbon-oxygen cores. In such progenitors, accretion may continue for a long time after the shock is revived, and eventually push the neutron star over its maximum mass towards black hole collapse. Furthermore, because of a large binding energy of the envelope, the explosion energy may be insufficient to eject all the matter outside the proto-neutron star. The dynamics of fallback may be of significant importance for shaping the mass distribution of black holes. For compact objects, a quantitative comparison with the observed populations of neutron stars and black holes is intertwined with the problem of single and binary stellar evolution. One important insight from recent years is that neutrino-driven explosions produce a wide range of gravitational neutron star masses, reaching to $1.7 M_{\odot}$ and beyond (Müller et al., 2017c; Burrows et al., 2024). This is in line with observations (Özel and Freire, 2016) that have overturned the long-held assumption that neutron stars are generically born with masses around $1.35 M_{\odot}$.

Due to adiabatic cooling of the ejecta, the dynamics of the expanding blast waves become less affected by pressure effects as the shock moves closer to and eventually breaks out of the stellar surface. Beyond shock breakout, large parts of the ejecta therefore approach homologous expansion, i.e., the radial velocity becomes proportional to radius. Homologous expansion only holds approximately, however. Complex dynamics involving reverse shocks and fallback can continue after shock breakout, and the interaction with the circumstellar environment is a major factor during the supernova remnant phase (Section 4) and in some instances for the dynamics of the observable transient (Section 3). Radioactive decay and strong outflows from the compact remnant will affect both the thermal evolution and hence the electromagnetic emission from the ejecta, as well as their kinematic and spatial structure. For example, heating by the decay of radioactive ^{56}Ni can further accelerate and inflate Ni-rich bubbles (Blondin et al., 2001; Gabler et al., 2021). Repercussions of this “Ni bubble effect” and outflows such as pulsar winds can be studied directly both from nebular spectra (Section 3) and in the remnant phase (Section 4).

3 Light curves and spectra

As the shock breaks out of the star, the electromagnetic display begins. Figure 7 shows a compilation of light curves for the different SN types discussed in section 1. We see that SNe reach peak brightness sometime between 10-100d, with a characteristic luminosity value of $\sim 10^{42}$ erg s^{-1} . Variations around that luminosity is about a factor 10 up and down ($10^{41} - 10^{43}$ erg s^{-1}). After a relatively steep decline from peak (end of “diffusion phase”), the light curves show a kink as the SN goes into the “tail” phase. The brightness declines over time to a characteristic value $\sim 10^{40}$ erg s^{-1} by 1 year. The different phases, and the driving mechanisms and key parameters for each, will be described below.

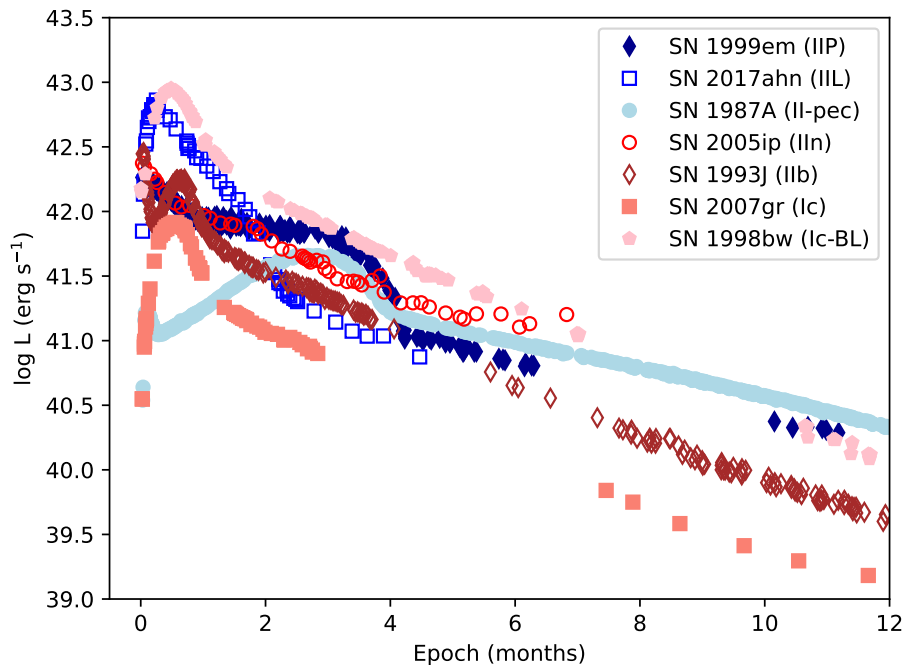


Fig. 7: Pseudo-bolometric ($UBVRI$, no correction for light outside these bands) light curves of characteristic SNe from each of the main classes (no Type Ib SN is plotted but these are similar to Type IIb and Ic SNe). Data from [Menzies et al. \(1987\)](#); [Catchpole et al. \(1987\)](#); [Barbon et al. \(1995\)](#); [Richmond et al. \(1996\)](#); [Patat et al. \(2001\)](#); [Sollerman et al. \(2002\)](#); [Elmhamdi et al. \(2003\)](#); [Galama et al. \(1998\)](#); [Valenti et al. \(2008\)](#); [Hunter et al. \(2009\)](#); [Stritzinger et al. \(2012\)](#); [Tartaglia et al. \(2021\)](#).

3.1 Shock breakout phase

The electromagnetic display begins when the shock wave reaches the stellar surface, or, if the star has a dense wind, as the shock approaches the optically thin point in the wind. The actual shock breakout gives a very brief transient (minutes/hours), with most radiation in X-rays and UV. Some of this hard radiation will photoionize the CSM which then emits recombination lines over a few hours or days ([Quimby et al., 2007](#)). As the star gives no sign of its impending collapse, observation of the shock breakout phase can occur only serendipitously, which has happened only a few times, e.g. for SN 2008D ([Soderberg et al., 2008](#); [Modjaz et al., 2009](#)) and SN 2016gkg ([Bersten et al., 2018](#)). Shock breakout observations hold promise to diagnose in particular progenitor radius (larger radii give more energetic bursts), shock velocity (higher velocity gives higher-frequency spectral energy distribution), and very late mass loss (impacts the time evolution); see [Waxman and Katz \(2017\)](#) for a theory review. One of the topics on the current research fore-front of shock breakout is to understand how the intrinsic 3D structure of the stellar envelope affects the shock break-out signal (e.g. [Goldberg et al., 2022](#), Fig. 8).

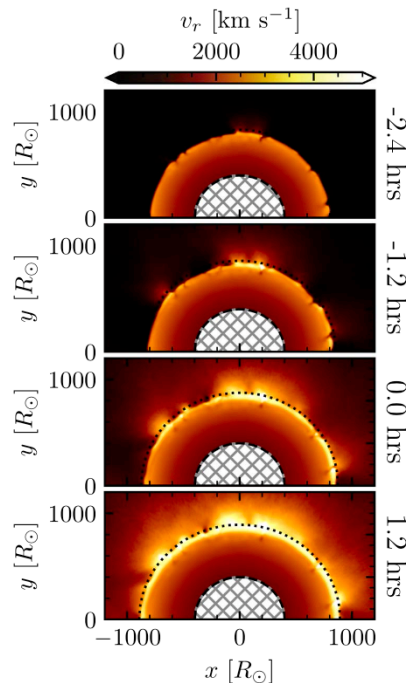


Fig. 8: Shock breakout simulated in 3D for a RSG. From [Goldberg et al. \(2022\)](#).

3.2 Diffusion phase

Following shock breakout, the light curve enters the *diffusion phase*, governed by the diffusive release of internal energy on a time-scale of weeks to months. The early light curve evolves in a way that depends on how much internal energy has been deposited by the shock passage, what fraction of this energy will be radiated rather than adiabatically converted to bulk kinetic expansion energy, and on the time scale of the diffusion process. By equipartition, the initial internal energy is close to half of the total shock-deposited energy, the value of which is given by the outcome of the competing inward ram pressure and outward thermal pressure described in Section 2. The radiation efficiency depends mainly on the progenitor radius R_0 (scaling approximately with $\sim R_0^{0.8}$; luminosity $L \propto E^{5/6} M_{ej}^{-1/2} R_0^{2/3} \kappa^{-1/3}$, diffusion time $\Delta t \propto E^{-1/6} M_{ej}^{1/2} R_0^{1/6} \kappa^{1/6} \rightarrow E_{rad}/E = L \times \Delta t/E \propto E^{-1/3} R_0^{5/6}$, Popov, 1993; Kasen and Woosley, 2009, where κ is a space and time averaged opacity), and is for all progenitors $\ll 1$; i.e. almost all energy deposited by the shock will be converted to kinetic bulk expansion energy of the stellar debris rather than being radiated away. For a Red Supergiant ($R_0 \approx 500 R_\odot$), its value is around 1%, giving $\sim 10^{51} \times 0.01 = 10^{49}$ erg of emitted radiation. The time scale of diffusive energy release Δt depends most sensitively on the ejecta mass, scaling with $M_{ej}^{1/2}$, (or $M_{ej}^{3/4}$, depending on the role of recombination). For RSGs $M_{ej} \approx 10 M_\odot$ which gives a time-scale of a few months. In these Type IIP SNe the bolometric light curve is initially declining (although the optical light curves rise as cooling brings an increasing fraction of the spectral energy distribution from X-ray/UV into the optical), then a recombination wave sets in after about three weeks, as the ejecta temperature reaches the H recombination temperature of ~ 6000 K, which flattens the light curve to a plateau. The brightness on this plateau depends most sensitively on the explosion energy ($L \sim E^{5/6}$) and observations give values of 0.1 – 1 B (1 B = 10^{51} erg) (e.g. Martinez et al., 2022).

Radioactive elements produced in the explosion also influence the diffusion phase light-curve. In Type IIP SNe the radioactivity extends the plateau by about 20% by sustaining and boosting the opacity (e.g. Kasen and Woosley, 2009), while in compact star ($\lesssim 50 R_\odot$) explosions, where the explosion-deposited internal energy becomes strongly degraded by adiabatic expansion, it plays a yet larger role. For explosions of Blue Supergiants (BSG) and He cores, the internal energy provided by the radioactive decay chain $^{56}\text{Ni} \rightarrow ^{56}\text{Co} \rightarrow ^{56}\text{Fe}$ governs the light curve from a few days already. The powering mechanism is mainly that gamma-rays emitted in the radioactive decay Compton scatter in the ejecta, a process in which high-energy electrons are created which subsequently heat, ionize and excite the gas. The total energy provided by radioactivity is not overly large; $E_{decay} = 2 \times 10^{49} \times (M(^{56}\text{Ni})/0.1 M_\odot)$ erg, but the delayed injection (decay time scales 8.8d and 111d for the two steps) avoids the strong adiabatic degradation that the shock-deposited energy suffers from. For radioactivity-powered light curves (Type Ib, Ic, IIb), the diffusion phase brightness and duration give information about the mass of ^{56}Ni (approximately proportional to the peak luminosity) and the quantity $\kappa^{1/2} M_{ej}^{3/4} E^{-1/4}$ (approximately proportional to the diffusion phase duration for SESNe, note difference to expression for Type IIP SNe above). Ejecta mass is more robustly inferred than explosion energy due to the stronger scaling ($M_{ej}^{3/4}$ vs $E^{-1/4}$). Typical inferred values are $M(^{56}\text{Ni}) \sim 0.1 M_\odot$ and $M_{ej} = (1 - 5) M_\odot \times E_{51}^{1/3} \kappa_{0.1}^{-2/3}$, with the energy in units of 10^{51} erg and opacity in units of $0.1 \text{ cm}^2 \text{ g}^{-1}$ (e.g. Drout et al., 2011; Bersten et al., 2012; Prentice et al., 2016). With detailed modelling (e.g. Blinnikov et al., 1998) and combining with spectral information, degeneracies with E and κ can be mitigated - for example is the photospheric velocity around peak light, inferable e.g. from the O I 7774 absorption line, a good indicator of the quantity $\sqrt{2E}/M_{ej}$ (Dessart et al., 2015). Detailed light curve modelling has also shown that symmetry breaking is strong in the explosion, with good fits requiring the initially innermost layers (rich in ^{56}Ni) to be strongly mixed outwards over the minutes and hours after explosion (e.g. Shigeyama et al., 1990); this provides important constraints on the explosion hydrodynamics and the various scenarios and mechanisms discussed in Section 2.

In addition to explosion-deposited energy and radioactivity, another power source of potential importance is circumstellar interaction (CSI). A steady wind from the progenitor star sets up a $\rho(r) \propto r^{-2}$ circumstellar medium (CSM), containing a mass of

$$M_{\text{CSM}}(r) = 3 \times 10^{-3} M_\odot \left(\dot{M}/10^{-5} M_\odot \text{ yr}^{-1} \right) \left(v_w/10 \text{ km s}^{-1} \right)^{-1} \left(r/10^{16} \text{ cm} \right), \quad (4)$$

where \dot{M} is the mass-loss rate and v_w is the wind velocity. While this may seem small, if only a percent or so of the SN kinetic energy ($\sim 10^{51}$ erg) is converted to radiation by collision with this CSM, this could overtake the radiated energy budget. Should \dot{M}/v_w be much larger than the canonical RSG wind value ($\sim 6 \times 10^{14} \text{ g cm}^{-1}$), this will be the case as the swept-up CSM mass within the diffusion time then becomes $\geq 1\%$ of the SN ejecta mass. Observations of very early light curves and spectra have indicated that some massive stars also appear to eject large amounts of mass in eruptive episodes prior to explosion (Ofek et al., 2013), which is not yet well theoretically understood. Such late mass loss will further increase the role of CSI (Margutti et al., 2017).

A final power source that may come into play is the compact remnant; if a fast-rotating, highly magnetized neutron star is formed, but spin-down occurs over weeks or months rather than seconds as needed in the magnetorotational explosion scenario (Section 2), a pulsar wind is formed that may provide most of the energy input to the nebula. We see such a situation today in the Crab nebula (Section 4), and it is also a contender to explain the light curves of some unusually bright SNe over weeks and months (Maeda et al., 2007b; Woosley, 2010; Inserra et al., 2013; Nicholl et al., 2013; Lunnan et al., 2018; Moriya et al., 2018).

Spectra. In the diffusion phase the expanding nebula is optically thick, and spectral formation can be reasonably well described as blackbody radiation emitted from a photosphere experiencing scattering in the outermost layers. The density profile in the outer line-forming region is quite steep, a v^{-7} power law or yet steeper (Matzner and McKee, 1999). The rapid, differential expansion leads to a characteristic line profile called a *P-Cygni* line, where absorption is seen on the blue side of the rest wavelength and emission on the red side - the peak is at the rest wavelength which facilitates line identifications. In Type II SNe the photospheric spectra probe largely unprocessed, H-rich gas (although dredge-up of CNO-burning products can occur in some progenitors, Fransson et al., 1989) and is therefore a good metallicity probe (Dessart et al., 2013; Anderson et al., 2018), whereas in SESNe also the outermost layers contain nuclear processed

material, from H and/or He burning. For this latter class, signatures of He, O, Na, Ca, Si and Fe are typically seen in photospheric spectra (e.g. Liu et al., 2016; Shahbandeh et al., 2022). The time evolution of photospheric and line scattering velocities, inferred from the P-Cygni profiles, give important information on the SN envelope structure. The line transfer in supernovae (or in any other nebulae with rapid differential expansion) behave in a particular way; photons scatter in the resonance layer in the same way for any $\tau_S \gtrsim 1$, where τ_S is the so-called Sobolev optical depth, a local quantity. P-Cygni lines therefore give upper (no absorption) or lower (absorption) limits to ion densities rather than absolute values, which makes abundance determinations more challenging than in static nebulae. Because the photosphere recedes towards lower velocities with time, more structure in the spectrum emerges continuously, which reduces line blending and facilitates the composition analysis.

Polarimetry. Information about the geometry of the SN may be obtained by photometric polarimetry, or, for bright enough sources, spectroscopic polarimetry (see Wang and Wheeler, 2008, for a review). Asymmetry in the free electron morphology induces polarization in Thomson-scattered light, and asymmetry in element distributions induces asymmetry in the P-Cygni lines. Observations give typical polarization levels varying between $\sim 0.1\%$ up to a few percent. Close-to axisymmetric morphologies (e.g. from some magneto-rotational explosion scenarios) would give a straight line in the so-called Q/U plane, whereas 3D morphologies with small clumps would give broad, scattered distributions. The most commonly observed pattern - a loop - instead indicates 3D morphologies with quite large structures (plume sizes $R_{cl} \gtrsim 1/4R_{phot}$, Tanaka et al., 2017). Such a morphology for the outer SN material is broadly consistent with what is seen in the spatially resolved Cas A remnant (see section 4.2). For the deeper lying regions, a good moment for spectropolarimetry is when the SN is transitioning from the photospheric to the nebular phase - the large asymmetries of the core then combine with still lingering opacity to give a maximum in the polarization signal (Leonard et al., 2006). While the data clearly show significant asymmetries, there is also much diversity (Nagao et al., 2024). While some constraints have been derived based on crafted multi-D ejecta (Dessart et al., 2024), more detailed conclusions await the computation of polarization signals from 3D explosion simulations and comparison with data.

3.3 Tail phase

The expanding nebula eventually (after 1-4 months, depending on the ejecta mass, explosion energy and powering mechanism) reaches an extended and dilute enough state that generated radiation can escape on short time-scale with little or no interaction. The SN is then said to have entered the *tail phase* or the *nebular phase* (see Jerkstrand, 2017, for a review).

Light curves. The bolometric light curve in this phase follows the instantaneous radioactive energy deposition, which equals the radioactive decay rate times a trapping factor, which is unity for full trapping but can be below unity if decay particles like gamma rays partially escape. The effective opacity for gamma rays is about $0.03 \text{ cm}^2 \text{ g}^{-1}$, and the trapping time is of order (expression derived from setting the radial gamma-ray optical depth to unity for a uniform sphere):

$$t_{\gamma\text{-trap}} = 100\text{d} \left(\frac{M_{ej}}{3 M_{\odot}} \right) \left(\frac{E}{10^{51} \text{ erg}} \right)^{-1/2}. \quad (5)$$

The early tail phase in Type IIP SNe ($t \sim 120 - 200\text{d}$, $M_{ej} \sim 10 M_{\odot}$) has close to full trapping and therefore offers a good opportunity to determine the amount of ^{56}Ni synthesised - values $0.01 - 0.1 M_{\odot}$ are typically found (Rodríguez et al., 2021). Mapping out how the ^{56}Ni yield depends on the M_{ej} and E parameters, inferrable from the diffusion phase (e.g. Müller et al., 2017c), puts important constraints on the SN explosion mechanism. If the bolometric luminosity can be determined for epochs later than 2-3 yr, the masses of other radioisotopes such as ^{57}Ni and ^{44}Ti can also be estimated, as these take over the powering at late epochs. In particular, ^{44}Ti is a sensitive probe of the innermost, high-entropy regions originating from just outside the proto-NS (Wongwathanarat et al., 2017). Direct detection of the gamma-ray/X-ray lines emitted in the ^{44}Ti decay both for SN 1987A (Boggs et al., 2015) and Cas A (Renaud et al., 2006) have here been of value.

In SESNe the $M_{ej}E^{-1/2}$ quantity is typically a factor 2-10 lower than in Type IIP SNe (Sec. 3.2), and Eq. 5 shows that gamma-ray trapping is typically incomplete already in the early tail phase ($\sim 50\text{-}100\text{d}$ for these SNe), so ^{56}Ni mass estimates from the tail are for these SNe model-dependent. One can fit $M(^{56}\text{Ni})$ and $t_{\gamma\text{-trap}}$ simultaneously, the results give a median ^{56}Ni mass of $0.08 M_{\odot}$ and a median trapping time of 117d (Afsariardchi et al., 2021). The ^{56}Ni mass values inferred from the tail are in good agreement with those inferred from the diffusion phase brightness, and the mean value is a factor 2-3 higher than in Type IIP SNe, a difference driven by an apparent dearth of SESNe with ^{56}Ni masses below $\sim 0.03 M_{\odot}$. Population synthesis studies considering binary mass loss for SESN progenitors have provided explanations for this difference in ^{56}Ni masses between the SN classes (Schneider et al., 2021).

Spectra. The spectrum in the tail phase changes character to an emission-line spectrum (Fig. 9, right panel). The widths of the emission lines reflect the kinematics, with expansion velocities (thousands of km/s) being much larger than the thermal velocities (few km/s). The dominant emission lines come from low-lying metastable states in neutral and singly ionized atoms of abundant elements. These can be populated by thermal collisional excitations at the characteristic nebula temperature (a few thousand degrees); examples are [O I] 6300, 6364, [Fe II] 7155, and [Ca II] 7291, 7323¹, which provide much of the cooling (Kozma and Fransson, 1998). For some lines, for example $H\alpha$, Mg I] 4571 and O I 9263, population of the parent state by recombination can also be important. By combining information from several lines one may attempt deduction of physical parameters and composition for the inner, metal-rich core of the SN, which is only visible in this phase. This allows the direct testing of modern theories for massive star and SN nucleosynthesis (e.g. Heger et al., 2003; Chieffi and Limongi, 2013). The densities are in the nebular phase too low for a Local Thermodynamic Equilibrium (LTE) assumption

¹[] means a forbidden transition (occurs via magnetic dipole (M1) or electric quadrupole (E2) transition), while] means semi-forbidden (occurs via electric dipole (E1) transition with spin change).

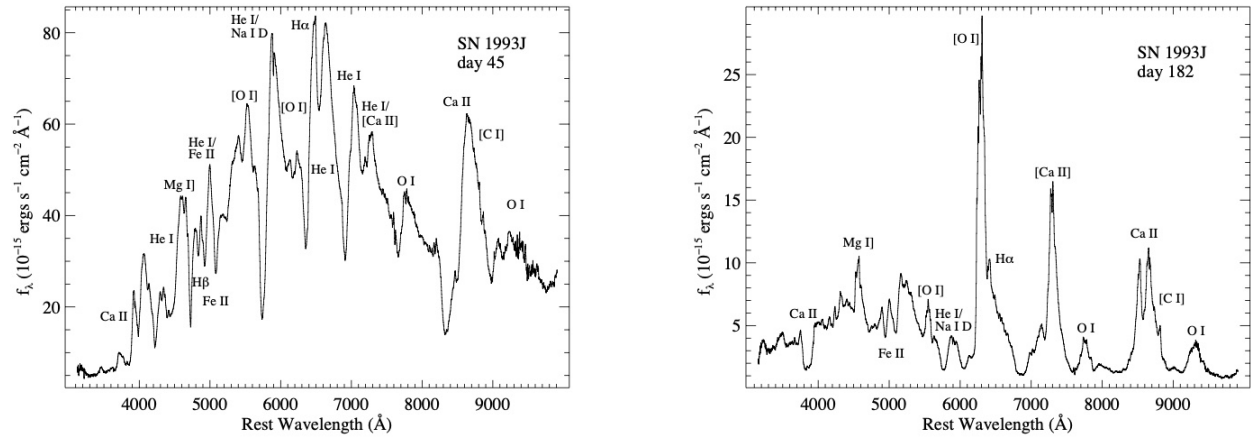


Fig. 9: Spectral evolution as the SN transitions from the photospheric phase (left) to the nebular phase (right), here for the Type IIb SN 1993J. In the photospheric phase the spectrum shows P-Cygni profiles with blueshifted absorption and redshifted emission (but with peak at the rest wavelength). In the nebular phase the spectrum takes on an emission-line character. From [Matheson et al. \(2000a\)](#).

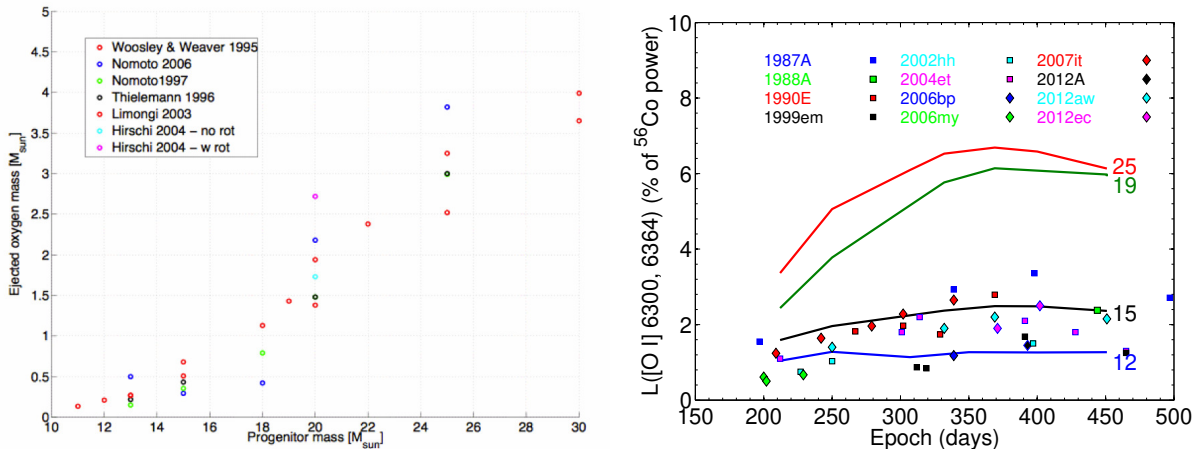


Fig. 10: *Left*: Theoretical SN yields of oxygen as function of progenitor mass (M_{ZAMS}). Data from [Woosley and Weaver \(1995\)](#); [Thielemann et al. \(1996\)](#); [Nomoto et al. \(1997, 2006\)](#); [Limongi and Chieffi \(2003\)](#); [Hirschi et al. \(2004\)](#). *Right*: Luminosities in [O I] 6300, 6364 for twelve Type IIP SNe compared to models for different M_{ZAMS} (12, 15, 19, 25 M_{\odot}). From [Jerkstrand et al. \(2015b\)](#).

in general, and modelling requires solving non-LTE (NLTE) rate equations. Because the stellar nucleosynthesis production of oxygen is a monotonic and strongly increasing function of stellar mass (Fig. 10), inference of the oxygen mass from nebular lines may be used to constrain the progenitor star mass. The fact that oxygen has several strong and relatively unblended lines in the optical from its dominant neutral ionization stage, enables this to be done in a relatively robust way. Oxygen masses in the range 0.1-1 M_{\odot} are inferred for the vast majority of CCSNe, in line with expected production in $M_{ZAMS} \lesssim 18 - 20 M_{\odot}$ stars ([Jerkstrand et al., 2014, 2015a, 2018](#); [Silverman et al., 2017](#); [Dessart et al., 2021](#)). Higher yields, implicating more massive stars, appear mostly associated with Ic-BL SNe ([Sollerman et al., 2000](#); [Mazzali et al., 2001](#); [Jerkstrand et al., 2017](#)), a subclass of the Type Ic category with unusually high velocities, often associated with GRBs. However, a few cases of massive progenitors giving regular Type Ibc SNe also exist (e.g. [Valenti et al., 2012](#); [Karamahmetoglu et al., 2023](#)). These events are too rare to account for all or most stars over $M_{ZAMS} \approx 20 M_{\odot}$, which seems to suggest that most massive progenitors fail to explode, but some succeed by, presumably, the operation by the magneto-rotational or collapsar mechanisms discussed in Section 2. Signatures of other hydrostatically made elements include He ([Li and McCray, 1995](#)), N ([Barentloo et al., 2024](#)) and Mg ([Jerkstrand et al., 2015a](#)). Information on explosive nucleosynthesis can be obtained from lines such as [Fe II] 7155 and [Ni II] 7378, the latter which probes changes in the neutron-to-proton ratio in stellar evolution and/or explosion ([Fröhlich et al., 2006](#); [Maeda et al., 2007a](#); [Jerkstrand et al., 2015b,c](#)). The mid-infrared iron-group lines are in turn good diagnostics of the ^{56}Ni -bubble expansion discussed in Section 1, having shown that the relatively small mass of radioactive material expands to fill $\gtrsim 20\%$ of the SN core volume ([Li et al., 1993](#); [Jerkstrand et al., 2012](#)).

It has long been known that nebular lines profiles provide a rich source of information on the multi-dimensional structure of the nebula ([Filippenko and Sargent, 1989](#); [Spyromilio et al., 1993](#)). In homology, ejecta material in sheets perpendicular to the line-of-sight (LOS) has the same LOS velocity, and for a given spectral line, each wavelength shift $\Delta\lambda$ relative to line center therefore probes emissivity by

the sheet moving with corresponding line-of-sight velocity $v_{LOS} = \Delta\lambda/\lambda_0 c$. By this tomography effect, bulk line properties (width, shift, skewness) probe the large-scale morphology, whereas fine-structure (wiggles, spikes) probes clumping and fragmentation. Observed line profiles indicate emissivity over a broad range of velocities for most elements, indicating strong hydrodynamic mixing, in line with results from light curve modelling. The mixing has been inferred to occur on macroscopic but not microscopic scales, so different elements still probe different, compositionally distinct, nuclear burning layers in the star. Fine-structure in line profiles is observed to be quite constant over time, and similar between different lines of the same ion (Matheson et al., 2000b), which indicates that variations in physical conditions over time and space do not swamp out the underlying morphology of an element distribution. The complex debris field obtained in modern neutrino-driven explosion simulations give a wide diversity of line profiles (van Baal et al., 2023), including the often observed double-peaked ones (Mazzali et al., 2005; Modjaz et al., 2008; Maeda et al., 2008; Taubenberger et al., 2009; Milisavljevic et al., 2010; Fang et al., 2022). By comparing the domain spanned by all viewing angles to observations, specific explosion models can be tested (van Baal et al., 2024).

The tail phase also sees the activation of a rich chemistry in CCSNe, with initially ($t \gtrsim$ few months) molecules such as CO and SiO forming in the inner, metal-rich regions, and later ($t \gtrsim$ years) dust (see Sarangi et al., 2018, for a review). Dust forms in the cooling expanding gas of SNe just as it does around cool stars, in planetary nebulae and novae. These processes can alter the physical conditions in the nebula, allow new probes through IR and radio emission by molecules and dust, and make SNe important cosmic dust factories. The significance of the cosmic dust contribution depends on how efficiently the formed dust is destroyed again when strong shock waves are later formed as the SN enters the supernova remnant phase. The composition of SN dust is an active area of research, with possibilities including silicates (Rho et al., 2008a), amorphous carbon (Matsuura et al., 2015), and metal needles (Dwek, 2004).

4 Supernova remnant phase

As the SN continues to homologously expand in its nebular phase, it continuously sweeps up more and more of the CSM and eventually reaches the interstellar medium (ISM). The timescales for when the CSM and ISM are encountered by the blast wave depend on the forward shock velocity, as well as properties of the mass loss. The characteristic velocity of the supernova ejecta v_{ej} having a typical kinetic energy $E_{SN} \sim 10^{51}$ erg $\sim (1/2)M_{ej}v_{ej}^2$ can be expressed as

$$v_{ej} \sim 10^4 \text{ km s}^{-1} \left(\frac{E_{SN}}{10^{51} \text{ erg}} \right)^{1/2} \left(\frac{M_{ej}}{M_{\odot}} \right)^{-1/2}, \quad (6)$$

where M_{ej} is the mass of the SN ejecta. The forward shock will decelerate as it sweeps up material, while a reverse shock develops that moves opposite in direction of the forward shock (in the Lagrangian frame) and excites the slower moving ejecta (Raymond, 2018). Between the shocked supernova ejecta and shocked CSM/ISM, which each have different composition and entropy, is an area of pressure equilibrium called the contact discontinuity. The shock waves of SNRs can also accelerate particles to relativistic energies and are a source of cosmic rays (Blasi, 2013).

The lifespan of an SNR is approximately 10^{5-6} yr, and its evolution is often grouped into four stages (see, e.g., Bamba and Williams 2022). In the first stage of *free expansion*, the stellar ejecta retain their initial velocity without significant deceleration and expand homologously such that the radius of the blast wave is $r(t) = v_{ej}t$, where t is time since explosion. The blast wave gains mass as it sweeps up surrounding material of density $\rho(r)$, where $\rho(r)_{CSM} \propto r^{-2}$ for wind-like mass loss and $\rho(r)_{ISM} \propto \rho_0$ for constant density ISM. The free expansion stage ends when the mass swept up $M_{swept} \sim M_{ej}$. If expansion is primarily in an ISM-like environment, this transition occurs at a radius of

$$r_{\text{free expansion}} \sim 2 \text{ pc} \left(\frac{M_{ej}}{M_{\odot}} \right)^{1/3} \left(\frac{\rho_0}{10^{-24} \text{ g cm}^{-3}} \right)^{-1/3}, \quad (7)$$

and time

$$t_{\text{free expansion}} \sim \frac{r}{v_{ej}} \sim 200 \text{ yr} \left(\frac{E_{SN}}{10^{51} \text{ erg}} \right)^{-1/2} \left(\frac{M_{ej}}{M_{\odot}} \right)^{5/6} \left(\frac{\rho_0}{10^{-24} \text{ g cm}^{-3}} \right)^{-1/3}. \quad (8)$$

Subsequent remnant phases include the adiabatic *Sedov* phase ($t \sim 10^{2-4}$ yr; $r \sim t^{2/5}$; $M_{ej} < M_{swept}$) and the pressure-driven *snowplow* phase ($t \sim 10^{4-5}$ yr; $r \sim t^{1/4}$; $M_{ej} \ll M_{swept}$) that develops as the SN interacts with more and more of the surrounding material, the gas cools radiatively at constant momentum, and the SN retains only vestiges of the initial ejecta mass and its distribution. In the final *dissipation* phase, the shock slows down to a velocity comparable to the sound velocity, and the SNR merges with the ISM.

Throughout its evolution, the SNR will sweep up a substantial amount of ISM ($\sim 10^4 M_{\odot}$), and the interaction results in multi-wavelength emission. Radio emission is largely from synchrotron radiation associated with electrons accelerated in regions run over by the forward shock, whereas the ionized broad inner ejecta region that has been reverse-shocked emits across infrared-through-X-ray wavelengths as a result of various thermal and non-thermal processes. The forward-shocked CSM/ISM can also emit at these wavelengths. After timescales of 10^{5-6} yr, the ejecta expand into the dilute plasma of the ISM, filling the space between stars, and create cavities that can reach up to several hundred parsecs in diameter. Molecules and dust in the ejecta feed into molecular clouds, which in turn become the building blocks

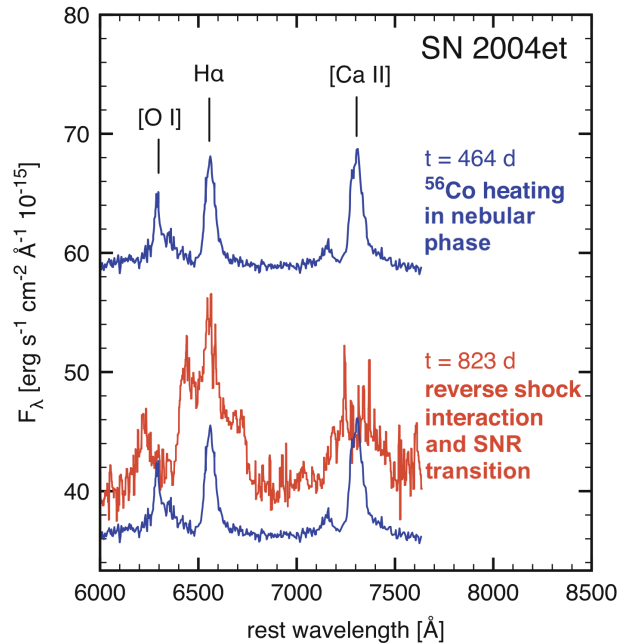


Fig. 11: Optical spectra of SN 2004et showing its transition from the nebular to supernova remnant phase. At $t=464$ d, the emission from the [O I], $H\alpha$, and [Ca II] lines is powered by radioactive ^{56}Co . At $t=823$ d, the kinematic distribution of these ions undergo a dramatic broadening, consistent with emission now being dominated by the reverse shock exciting outer, higher velocity ejecta. Asymmetry in the profile is due to internal extinction of optically-emitting material from the far side of the supernova by dust. Note that the $t=823$ d spectrum will likely also have new contributions from [N II] 6548, 6583 and [O II] 7319, 7330. Adapted from Milisavljevic and Fesen (2017) using data from Kotak et al. (2009).

for new stars and planetary systems. Overall SNRs are vital contributors to the heating and chemical evolution of galaxies.

There is no generally accepted definition for the point when a SN is said to have become a SNR. Historically, the SNR phase has been attributed to the time when a SN departs from free expansion and begins to strongly interact with its surrounding environment, or when both UV/optical line and continuum emission from a SN’s ejecta fall below that generated by interaction with either surrounding CSM/ISM or via emission from a central compact stellar remnant (Fesen, 2001b). However, such generalizations fail to incorporate scenarios when SN-CSM interaction is strong immediately after explosion, as in the case of SNe IIn. Sometimes the transition from supernova to supernova remnant is defined simply when it reaches an age of ≥ 100 years (Branch and Wheeler, 2017).

A convenient definition, applicable for most cases when there is no strong SN-CSM interaction immediately after the SN, is the time at which SN–CSM interaction leading to reverse shock heating of inner ejecta dominates observed emission (Milisavljevic and Fesen, 2017). At these epochs, which follows from the late tail phase, broad, boxy lines of $H\alpha$ and/or metal lines such as He I 5876 and [O III] 4959, 5007 (e.g. Matheson et al., 2000a) are observed in optical spectra. These broad lines ($v \gtrsim 4000$ km s^{-1}), which can often be observed simultaneously with narrower lines associated with forward shocked CSM ($v \lesssim 2000$ km s^{-1}), arise from the fast, outermost layers of the SN, absorbing X-rays from the reverse shock created by the CSM collision (Chevalier and Fransson, 1994). Often asymmetry is observed in profiles of these line emissions, giving a false sense of preferential blueshifted ejecta velocity, that is in fact attributable to dust within the ejecta. Conspicuous line substructure is a common and long-lasting phenomenon in the late-time spectra, and is linked to large scale coherent structure in the ejecta (Milisavljevic et al., 2010). For some core-collapse H-rich SNe, the timescale to transition to the SNR stage as defined this way can be as short 1–2 years (see, e.g., Black et al. 2017; Dessart et al. 2023; Figure 11).

Whereas most supernova remnants in the Milky Way were initially identified as extended radio sources with nonthermal radio spectra, the majority of extragalactic supernova remnants have been found via optical narrow-band imaging surveys that utilize the line strength diagnostic ratio $[\text{S II}]/H\alpha > 0.4$ (Long, 2017). Most extragalactic SNRs are unresolved or barely resolved ($r_{\text{SNR}} \lesssim 1''$), and lack an associated classification because they are evolved (> 1000 yr) and the original supernova was not observed. The possibility to monitor extragalactic supernovae many years after discovery was first recognized in the late 1980s with the optical re-detections of SN 1980K (Fesen and Becker, 1988) and SN 1957D (Long et al., 1989). Since then, there have been several examples of continued monitoring of SNe as they transition between supernova phases (diffusion and tail) to the supernova remnant phase (Milisavljevic et al., 2012). In the majority of cases when late-time monitoring is possible, some long-lived energy source related to interaction between the SN and ISM/CSM, or contributions from a pulsar/magnetar star, is present. In the case of SN 1987A in the LMC, a fortuitous nearby distance has made it possible to monitor the supernova continuously from detection of neutrinos to transition to the supernova remnant phase (McCray, 2017).

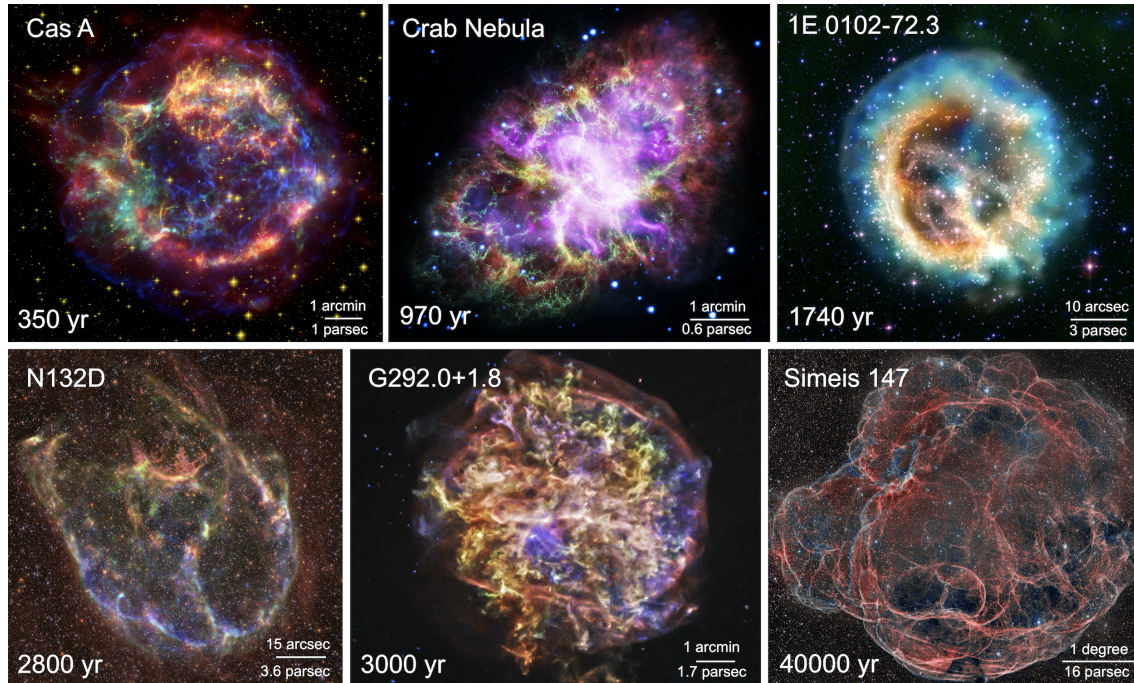


Fig. 12: Supernova remnants of core collapse supernovae. Approximate ages and physical scales adopted from Reed et al. (1995), Hester (2008), Banovetz et al. (2023), Temim et al. (2022), and Ng et al. (2007). Image credits: Cas A (NASA/CXC/SAO/STScI/JPL-Caltech/Steward/O. Krause et al.), Crab Nebula (NASA, ESA, and J. DePasquale, STScI), E0102 (NASA/SAO/CXC/STScI/MIT/D. Dewey et al./J. DePasquale), N132D (NASA/CXC/CXO/HST/STScI/J. Schmidt), G292 (NASA/CXC/SAO), and Simeis 147 (Georges Attard).

4.1 Galactic Supernova Remnants

Currently, there are approximately 300 SNRs catalogued in the Milky Way (Green, 2019).² Multiple diagnostics exist to distinguish whether remnants are associated with core-collapse versus Type Ia supernovae. A fundamental means is to look for the presence of a compact object (neutron star or black hole) or to perform spectroscopy of a light echo of the original supernova (if present). Various methods at X-ray wavelengths exist, including estimates of iron abundance (Reynolds et al., 2007), X-ray line morphologies (Lopez et al., 2009), and Fe–K line energy centroids (Patnaude et al., 2015). Attempts at relating specific SN types with SNRs can also involve connecting SNRs with historical records of “guest stars” as has been possible with the Crab Nebula (Clark and Stephenson, 1977).³ However, since these ancient sightings lack spectroscopic information, and are often incomplete in terms of the precise location of the SN and the evolution of the light curve, they can lead to uncertain conclusions. The Crab is the only Milky Way SNR that has a firm historical account of the parent supernova associated with a core collapse explosion.

The morphology of a supernova remnant is dependent on both the explosion dynamics and the environment into which the supernova expands into. Figure 12 shows core collapse supernova remnants with a variety of morphologies reflecting diverse progenitor systems, environments, and ages. Most young ($\lesssim 1000$ yr) galactic SNRs have strong individual characteristics that are not always shared by other young SNRs or easily connected to SN subclasses. Differences largely arise from the role CSM/ISM can play in affecting remnant’s properties and evolution. The surrounding environment will have been sculpted by prior mass loss of the progenitor system; the mass loss may be a smooth wind or clumpy or eruptive; and the gas may deviate from a homogeneous distribution due to effects of rotation or the influence of a binary companion. Asymmetries intrinsic to the SN explosion can also contribute to the morphology, especially for SNRs still in free expansion. The evolution of massive stars toward the ends of their life cycles is likely to be nonspherical and may have extensive inter-shell mixing (Arnett and Meakin, 2011), and hence asymmetries introduced by a turbulent progenitor star interior can seed explosion asymmetries that persist until the SNR phase. Large-scale magnetic fields can also contribute to SNR morphology at advanced ages (West et al., 2016).

SNRs are typically divided into (i) shell-like remnants, in which emission comes almost entirely from a distinct shell, (ii) filled-center or Crab-like remnants, which have a central pulsar wind nebula (PWN) and whose brightness decreases radially outward, and (iii) composite remnants that blend shell and Crab-like properties. Shell-like remnants pass through the typical four stages of supernova remnant evolution, whereas the dynamics of Crab-like remnants are more complex because the central source provides electromagnetic radiation and high-

²An up-to-date listing can be found at <https://www.mrao.cam.ac.uk/surveys/snrs/>. See also <http://snrcat.physics.umanitoba.ca/>.

³The term “guest star” is a literal translation from ancient Chinese astronomical records and refers to a star that suddenly appears in the sky where no star had been observed before, and then fades away after some time. Modern astronomy recognizes that these “guest stars” were actually manifestations of cataclysmic events such as novae and supernovae.

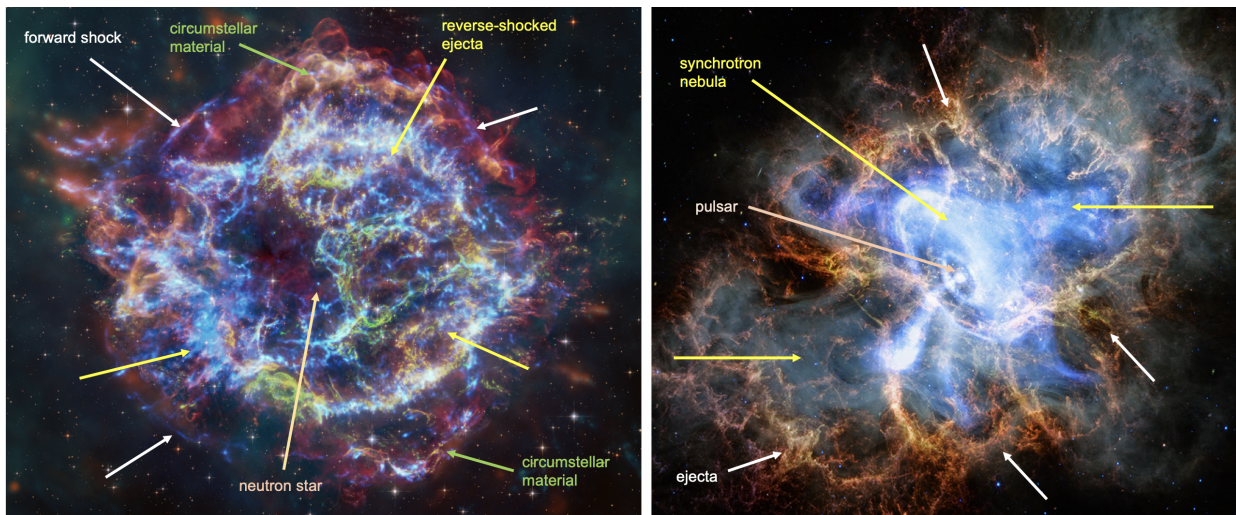


Fig. 13: Multiwavelength images of Cassiopeia A [X-ray: NASA/CXC/SAO; Optical: NASA/ESA/STScI; IR: NASA/ESA/CSA/STScI/Milisavljevic et al., NASA/JPL/CalTech; Image Processing: NASA/CXC/SAO/J. Schmidt and K. Arcand] and the Crab Nebula [X-ray, Chandra: NASA/CXC/SAO; Infrared, Webb: NASA/STScI/T. Temim et al.; Image Processing: NASA/CXC/SAO/J. Major].

energy particles that influence surrounding gas and the SNR evolution. Approximately 80% of SNRs are shell-like, 10% are composite, and a few percent are Crab-like. In addition to these classifications is a relatively rare number of *mixed morphology* remnants that exhibit a shell-like morphology in the radio band and centrally peaked thermal emission in the X-ray band (Rho and Petre, 1998). Unlike composite remnants, mixed morphology remnants lack a PWN.

SNRs where hydrogen emission is weak or non-existent in the ejecta and is instead dominated by heavy metals including oxygen, neon, sulfur, argon, and calcium, are known as oxygen-rich SNRs. O-rich SNRs likely originate from massive stars that were largely stripped of their hydrogen envelopes. Only a handful of O-rich remnants have so far been identified in our Galaxy and in nearby galaxies. Cassiopeia A (Cas A), which is regarded as the prototypical O-rich SNR (Fesen, 2001a), Puppis A (Winkler and Kirshner, 1985), and G292+1.8 (Goss et al., 1979) are among the Galactic members. N132D (Danziger and Dennefeld, 1976) and 0540-69.3 (Mathewson et al., 1980) are in the Large Magellanic Cloud. 1E 0102.2-7219 (Dopita et al., 1981), 0103-72.6 (Park et al., 2003), and B0049-73.6 (Hendrick et al., 2005) are in the Small Magellanic Cloud. Several mixed-morphology SNRs, including CTB 1, HB 3, and W28, have also shown evidence of O-rich ejecta (Lazendic and Slane, 2006; Pannuti et al., 2010, 2017). An ultraluminous O-rich SNR has been found in NGC 4449 (Balick and Heckman, 1978; Milisavljevic and Fesen, 2008).

4.2 Cassiopeia A - The prototypical core-collapse SNR

Cas A (Figure 13) is the youngest Galactic core-collapse SNR known (≈ 350 yr; Fesen et al. 2006). This youth and a relatively nearby distance ($3.4_{-0.1}^{+0.3}$ kpc; Reed et al. 1995; Alarie et al. 2014) have made Cas A extremely important to investigate the physics of core collapse through resolved, multiwavelength observations. Although there is no credible historical record of the original supernova (Koo and Park, 2017), Cas A is the only core-collapse remnant with a secure SN classification. Spectroscopy performed on light echoes associated with the original supernova, from multiple lines of sight, found that the supernova was most similar to SNe I Ib events SN 1993J and 2003bg near maximum light (Krause et al., 2008; Rest et al., 2008, 2011). This makes the remnant very helpful in attempts to connect unresolved SNe with nearby, resolved SNRs (Milisavljevic and Fesen, 2017).

The bulk of the ejecta of Cas A are distributed in a ring called the “main shell” that emits strongly at X-ray, optical, and infrared wavelengths (Figure 13). These ejecta, having a total mass of $\approx 3 M_{\odot}$, are composed primarily of oxygen, sulfur, argon, neon, and iron (Ennis et al., 2006; DeLaney et al., 2010; Hwang and Laming, 2012) that has encountered the reverse shock. The ejecta contain considerable amounts of dust ($\approx 0.5 M_{\odot}$; De Looze et al. 2017) with varying compositions and sizes (Rho et al., 2008b). Dust emission is also present throughout the surrounding CSM seen along the periphery of the remnant that has been heated by the forward shock. Approximately $0.5 M_{\odot}$ of ejecta have not yet encountered the reverse shock and emit in the infrared (DeLaney et al., 2014; Laming and Temim, 2020).

Models for Cas A suggest that the $15\text{--}25 M_{\odot}$ zero-age-main-sequence progenitor star lost the majority of its mass prior to explosion as a $\approx 4\text{--}6 M_{\odot}$ star (Chevalier and Oishi, 2003; Hwang and Laming, 2012; Lee et al., 2014). The mass loss was likely encouraged through interaction with a binary companion (Young et al., 2006; Sato et al., 2020). Deep observations targeting the center of expansion have ruled out the possibility of a surviving companion star for the putative binary progenitor system (Kochanek, 2018; Kerzendorf et al., 2019), which is in tension with claims of OB companions detected at the locations of extragalactic stripped-envelope explosions (Maud et al., 2004; Ryder et al., 2018; Fox et al., 2022). If the progenitor system was indeed a binary, the two stars may have merged or were disrupted prior to collapse. More exotic scenarios such as a surviving white dwarf, neutron star, or black hole are unlikely but cannot be ruled out.

Cas A exhibits exceptionally high velocity Si- and S-rich material in a jet/counter-jet arrangement in the NE and SW directions (Fesen,

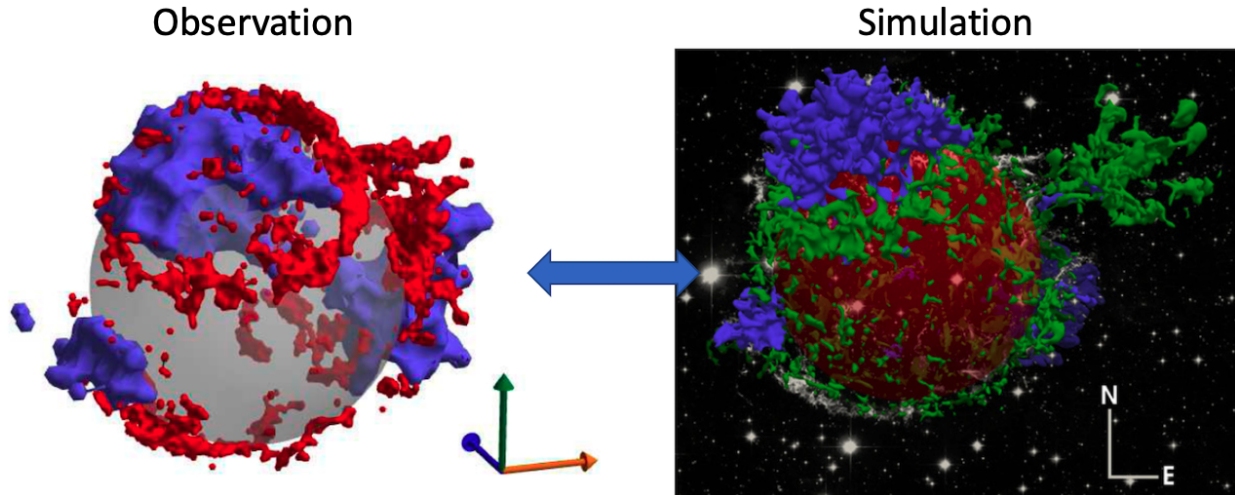


Fig. 14: Comparison of 3D kinematic reconstruction of Cas A showing optical (red) data tracing S- and O-rich ejecta (Milisavljevic et al., 2013) and X-ray (blue) data tracing Fe-rich ejecta (DeLaney et al., 2010) to a simulation that evolved a Cas A-like core-collapse explosion to the remnant phase where green traces shocked S- and Si-rich ejecta, and blue again traces shocked Fe-rich ejecta (Orlando et al., 2016). The two viewing perspectives are approximately the same. An interactive web app of observational data is available [here](#), and the simulation data can be explored [here](#).

2001a; Hwang et al., 2004). The known extent of this jet region contains fragmented knots of debris traveling up to 15000 km/s, which is three times the velocity of the bulk of the O- and S-rich main shell. The large opening half-angle $\approx 40^\circ$ is inconsistent with a highly collimated flow (Milisavljevic and Fesen, 2013), and the energy in this region ($\sim 10^{50}$ erg) is a fraction of the total energy of the original supernova ($\sim 10^{51}$ erg) that is best understood as being driven by low-mode convective instabilities encouraged by uneven neutrino heating during core collapse (Vink, 2004; Grefenstette et al., 2014). Nonetheless, some jet-like mechanism carved a path allowing interior material from the Si- S-Ar-Ca region near the core out past the mantle and H- and He-rich photosphere (Laming et al., 2006; Fesen and Milisavljevic, 2016). The NE-SW outflows of Cas A may be a common feature of core-collapse supernovae, and supports the view that varying levels of participation from a rapidly rotating neutron star may exist in SNe (Mazzali et al., 2008; Soderberg et al., 2010; Mazzali et al., 2014b; Metzger et al., 2015; Milisavljevic et al., 2018).

“First-light” images of Cas A taken by *Chandra* revealed a central X-ray point source (Tananbaum, 1999; Pavlov et al., 2000), that is presumably its remnant neutron star. This neutron star is part of the family of *central compact objects* (CCOs), which are young, exhibit X-ray emission that is steady and predominantly thermal, have magnetic fields that are two orders of magnitude lower than those of typical young NS, and lack surrounding pulsar wind nebulae (Pavlov et al., 2004). Deep imaging with the James Webb Space Telescope did not detect the CCO and place strong constraints on scenarios involving a possible fallback disk (Milisavljevic et al., 2024).

4.3 Crab Nebula - The prototypical SNR with a pulsar wind nebula

The Crab Nebula was the first example of a Galactic supernova remnant that was connected with the historical record of a “guest star” in 1054 CE (Lundmark, 1921; Mayall, 1939). The event reached an apparent magnitude brighter than -5 (associated with absolute magnitude approaching -18 mag), was visible during daylight hours for 23 days, and remained visible for approximately two years (Duyvendak, 1942).

Moving from the inside out, the Crab Nebula consists of the Crab pulsar, the synchrotron nebula, and a bright expanding shell of thermal gas in a network of filaments (Figure 13). The Crab pulsar has a period $P = 33$ ms, a period derivative of $\dot{P} = 4.21 \times 10^{-13}$, and spin-down luminosity of $L_{spin} = 4\pi^2 I \frac{\dot{P}}{P^3} \sim 5 \times 10^{38} \text{ erg s}^{-1}$, where I is the moment of inertia of the pulsar ($\approx 1.1 \times 10^{45} \text{ g cm}^2$). The majority of the pulsar’s spin-down luminosity is carried away by some combination of magnetic dipole radiation and an ultrarelativistic wind that powers the nebula and is confined by the thermal ejecta into which it expands (Hester, 2008). Much of the filamentary ejecta, which are possibly mixed with some material from the pre-supernova wind (Fesen et al., 1992), breaks up into inward pointing fingers of emission due to Rayleigh-Taylor instabilities introduced by PWN pressure.

The Crab Nebula is an interesting contrast to Cas A. Although a historical record exists of its light curve, to date no light echoes have been detected and hence no confirmation of its specific core-collapse classification has been possible. It has expansion velocities (< 2000 km/s) far lower than commonly seen in SNe, an extremely luminous pulsar, and ejecta showing only helium enrichment. The total mass of its ejecta is $2-7 M_\odot$ (Fesen et al., 1997; Owen and Barlow, 2015), and, as estimated from the small carbon and oxygen abundances in the helium-rich nebula, the plausible mass of the progenitor is $8-13 M_\odot$ (Nomoto, 1987; Owen and Barlow, 2015).

Debate continues as to which SN subtype best matches its properties (Davidson and Fesen, 1985; Smith, 2013; Yang and Chevalier, 2015). SN 1054 was more luminous than a normal Type II SN (-18 mag vs. -15.6 mag), yet its kinetic energy ($\leq 10^{50}$ erg) is surprisingly low compared to the canonical $\sim 10^{51}$ erg. It was originally speculated that most of the mass and 90% of the kinetic energy of SN 1054 reside

in an invisible freely expanding envelope of cold and neutral ejecta far outside the Crab (Chevalier, 1977). However, this fast envelope has never been detected to remarkably low upper limits (Lundqvist and Tziamtzis 2012; but see also Hester 2008). Fesen et al. (1997) suggested that SN 1054 was a low energy SN with additional luminosity provided by circumstellar interaction. Smith (2013) supports this view and identified potential Crab-like analogs in many recent Type II events. Tominaga et al. (2013) found that the high peak luminosity could instead be related to the large extent of the progenitor star and not necessarily associated with strong circumstellar interaction.

Many models originally favored an electron capture SN origin (e.g., Nomoto et al. 1982 and Kitaura et al. 2006) in light of the Crab’s low energy explosion and unique chemical abundances that included a high Ni/Fe ratio. In this scenario, a massive star whose mass is slightly smaller than the mass required to form an Fe core can still make an electron degenerate O+Ne+Mg core, which can trigger core collapse through electron-capture reactions. However, this explanation comes with many discrepancies. Electron capture explosions are generally faint ($M_V > -15$ mag) and thus inconsistent with the relatively luminous SN unless SN-CSM interaction was involved, and the proper motion of the pulsar in the Crab Nebula has an associated velocity ($\approx 160 \text{ km s}^{-1}$; Kaplan et al. 2008) that is too high to originate from an electron capture explosion (Stockinger et al., 2020). Modern simulations can now produce core-collapse SN explosion of similar low energies, and the latest measurement of the Ni/Fe abundance ratios in the Crab are consistent with those expected from a low-mass Fe core-collapse SN (Temim et al., 2024).

4.4 3D morphology and modeling SN-SNR evolution

Nearby, young SNRs can be kinematically mapped via scanning of long slit spectroscopy, widefield integral field unit spectrographs (e.g., MUSE on the Very Large Telescope; SITELLE on Canada-France-Hawaii Telescope), or Fabry-Perot imaging spectroscopy. If the ejecta motion and center of expansion are known via 2D proper motion studies, and trajectories are assumed to be ballistic, a three dimensional reconstruction can be created by converting the radial velocities of the expanding gas to a z-space coordinate from the plane. To date, kinematic maps of SNRs have been made for Cas A (DeLaney et al., 2010; Milisavljevic and Fesen, 2015), the Crab Nebula (Martin et al., 2021), N132D (Law et al., 2020), 0540-69.3 (Larsson et al., 2021), 1E 0102.2-7219 (Vogt et al., 2018), and SN 1987A (Larsson et al., 2016).

Figure 14 shows a detailed 3D reconstruction of Cas A, and Figure 15 shows a comparison of the Mercator projections of Cas A (Milisavljevic and Fesen, 2013), the Crab (Martin et al., 2021), 3C58 (Lopez and Fesen, 2018). The 3D kinematic reconstruction of Cas A shows that its ejecta are arranged in several well-defined and nearly circular rings with diameters between approximately $30''$ (0.5 pc) and $2'$ (2 pc), demonstrating that the distribution of its metal-rich ejecta is not random. The sizes and arrangement of the large-scale rings reflect properties of the explosion dynamics and subsequent evolution of the expanding debris. Three large concentrations of Fe-rich ejecta, which are good tracers of the original explosion dynamics, lie within and bounded by ring structures. This complementary arrangement is consistent with the “Ni bubble effect” having influenced the remnant’s expansion dynamics shortly after the original explosion, wherein the observed ejecta rings represent cross-sections of large cavities in the expanding ejecta created by a post-explosion input of energy from plumes of radioactive Ni-rich ejecta. Nickel bubbles may be a common phenomenon of young, core-collapse SNRs (Li et al., 1993; Milisavljevic et al., 2012).

The Crab exhibits a much more complex structure compared to Cas A. The largest and deepest structures of the Crab are similar both in size and shape as those seen in 3C 58. In these cases, Rayleigh-Taylor instabilities encouraged by the PWN are likely dominating the morphology of the ejecta. The general boundaries of the 3D volume occupied by the Crab are not strictly ellipsoidal as commonly assumed, and instead appear to follow a “heart-shaped” distribution that is symmetrical about the plane of the pulsar wind torus. Conspicuous restrictions in the bulk distribution of gas consistent with constrained expansion coincide with positions of the dark bays and east–west band of He-rich filaments, which may be associated with interaction with a pre-existing circumstellar disc. The distribution of filaments follows an intricate honeycomb-like arrangement with straight and rounded boundaries at large and small scales that are anticorrelated with distance from the centre of expansion. Comparing the observed morphology to the recent simulations of Stockinger et al. (2020), Martin et al. (2021) disfavoured associating SN 1054 with an electron capture supernova and instead with an Fe-core progenitor with less second dredge-up.

Pristine structures and features recovered in resolved SNRs reflect fundamental properties of the explosion dynamics and the early interaction of the SN blast wave with the inhomogeneous CSM. Hence, these kinematic maps provide unique opportunities to test the origins of turbulent mixing and explosion asymmetry predicted in simulations. The ability to link the physical and chemical characteristics of core-collapse SNRs to the explosion processes associated with their parent SNe through hydrodynamic / magnetohydrodynamic (MHD) models has been improving over the last decade (Figure 14). Modeling the SN–SNR connection involves many factors, including: the structure and chemical stratification of the stellar progenitor at collapse, the explosive nucleosynthetic processes, the effects of post-explosion anisotropies, the dynamics and chemical evolution of ejecta since the SN, and the interaction of the SNR with the surrounding ambient medium (Orlando et al., 2020, 2021).

5 Summary and outlook

The theory of the supernova explosion mechanism (Sec. 2), the study of supernova light curves and spectra (Sec. 3), and the study of supernova remnants (Sec. 4) have always fertilised each other, and recent progress in these fields has further improved the prospects for this. As with any scientific field, progress arises over iterations in a loop between models and data, with both forward (processing hydrodynamic simulations with radiative transfer codes) and backward modelling (analysing data with analytic methods) playing important

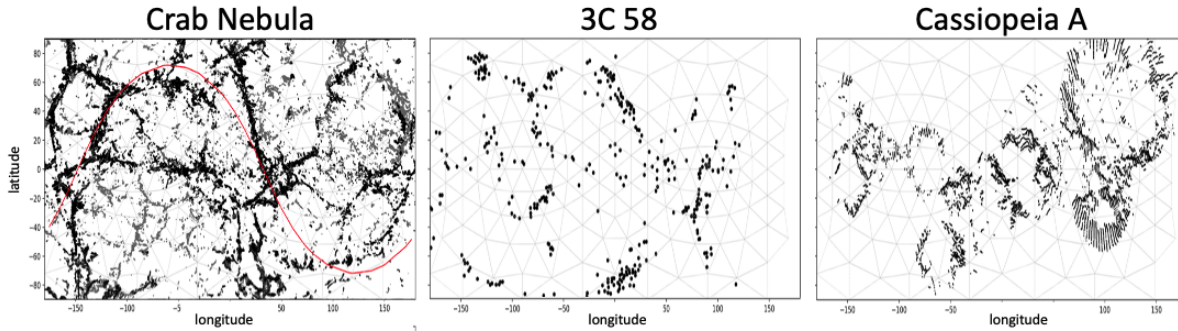


Fig. 15: Mercator projections of optically-emitting material represented in the 3D reconstructions of the Crab Nebula (Martin et al., 2021), 3C 58 (Lopez and Fesen, 2018) and Cas A (Milisavljevic and Fesen, 2013). For the Crab, the densest and deepest material is represented in black, while the faster expanding material is in grey. The red line shows the pulsar torus plane as fitted by Ng and Romani (2004). Adapted from Martin et al. (2021).

roles. The full ab-initio forward modelling is challenged by the enormous computing costs involved in simulating the explosion and evolution of supernovae - the ejecta needs to be evolved to times of weeks or months, but even the first second of core-collapse can take millions of CPU hours. There is therefore a vast range of methods in the range between “full ab-initio” and “toy models” - the challenge is to patch and sort the results from these into a coherent and consistent framework. As spatially resolved SN remnants clearly show us - SNe are extraordinarily complex objects, and this task is therefore a grand challenge.

We consider it fair to say that simulations are now in a position to inform us at quite some depth about the physical principles behind CCSN explosions, and also to allow for a quantitative understanding of some of the observed properties of SNe and their compact remnants. Admittedly, this relies to a large extent still on *phenomenological* models that require calibration, but the capabilities of fully self-consistent models are growing rapidly.

A key question that simulations have started to address is how the progenitor mass, metallicity, rotation, and possibly binarity, determine whether a massive star explodes as a CCSN or collapses into a BH. There is significant evidence from identified supernova progenitors in archival images that there is a dearth of explosions from red supergiants above progenitor masses of $M_{ZAMS} \sim 18 M_{\odot}$ (Smartt, 2015). Three-dimensional modelling of supernova explosions is not yet at the stage where the mass range of successful explosions can be confidently predicted. However, parameterised models of neutrino-driven explosions (Müller et al., 2016a; Sukhbold et al., 2016) can account for the absence of explosions at high masses and suggest that, despite model uncertainties, inherent characteristics of the progenitor star strongly influence explodability, such as mass size of the iron-silicon core, whose edge defines a natural point for the initiation of an explosion. An important research avenue for this question is also the ongoing monitoring of millions of red supergiants, waiting to see if some of them disappear without exploding as a SN (Kochanek et al., 2008).

Furthermore, the physics revealed by simulations of neutrino-driven explosions can explain some of the systematics of observed explosion and remnant properties (e.g. Fryer et al., 2012). Since longer accretion onto the proto-neutron star implies more energetic explosions, one naturally expects a correlation between the progenitor structure and the explosion energy in the neutrino-driven paradigm. Progenitors with more massive C/O cores tend to accrete for longer and hence reach higher explosion energies. Population studies using calibrated phenomenological explosion models suggest that neutrino-driven explosions can thus produce a range of explosion energies from $\sim 10^{50}$ erg to $\sim 2 \times 10^{51}$ erg, which are loosely correlated with progenitor mass (Müller et al., 2016b). A correlation between the ^{56}Ni mass and the ejecta mass is also theoretically expected, quite regardless of the explosion mechanism, because higher explosion energies permit substantially more explosive burning to the iron-group in the innermost shells of the ejecta due to the shock managing to heat a larger region over the Si-burn limit (5×10^9 K). In the neutrino-driven mechanism, the neutrino-heated ejecta may also produce substantial ^{56}Ni by nucleon recombination. Models of neutrino-driven explosions are in general good agreement with the observed range of nickel masses of up to $\sim 0.15 M_{\odot}$ - the ^{56}Ni mass is arguably the most robustly inferred quantity from observations.

In contrast to this, it has turned out quite difficult to determine unique values for E and M_{ej} ; for Type IIP SNe there are several parameter degeneracies at play, e.g., velocity information not breaking degeneracy with R_0 (Goldberg et al., 2019), and the plateau light curve not being sensitive to the total mass but just the envelope mass (Dessart and Hillier, 2019). Parameter degeneracies may be mitigated by including the early shock cooling phase, but this in turn has turned out to be sensitive to yet further parameters related to the CSM (Morozova et al., 2018), as well as to the detailed 3D structure of the outermost material. For SESNe it is challenging to accurately infer E because the diffusion time has only a weak dependency on it ($\propto E^{-1/4}$) and the peak luminosity none (depending rather on the ^{56}Ni mass). The timing of gamma-ray escape in the tail phase, having a stronger E dependency than the diffusion time ($t_{trap} \propto E^{-1/2}$), can be of use to break the degeneracy. A completely different way to estimate E can be done the cases when the SN runs into a massive CSM (luminous Type IIn SNe), turning $\geq 50\%$ of the kinetic energy into radiation - a handful of cases here have given $E \gtrsim 0.5$ B (e.g. Fransson et al., 2014). Even here there can be caveats, as it is sometimes difficult to distinguish a CCSN and thermonuclear SN origin for Type IIn SNe (Jerkstrand et al., 2020).

5.1 Outlook

As we look to the future, there is reason for optimism for exciting progress in the years ahead. Automated transient surveys have revolutionized the field of supernovae over the past 20 years, and with the Legacy Survey of Space and Time soon starting up at the Vera C. Rubin Observatory there will be yet another leap forward in the number of detected transients. While in the past there were so few SNe detected that one followed them all, we now have to be very selective. This means an early entry of theory and simulations into the process, for providing inputs into what is of most relevance to follow up on, and with which instrumentation. The improvements in detection efficiencies will also, with the upcoming generation of Extremely Large Telescopes (ELTs), be matched with improvements in the long-term monitoring data we can obtain. The emphasis both with the ELTs and the James Webb Space Telescope is on the infrared - and indeed this defines much of the vista to be explored in the coming years, with rich expected signatures of nucleosynthesis, molecules, and dust.

It is our view that future progress in SN research lies in combining models and data covering multiple phases and multiple wavelength windows. In this new multi-messenger era, observations of neutrinos (Müller, 2019) and gravitational waves (Abdikamalov et al., 2022; Vartanyan et al., 2023) are also anticipated to contribute tremendously to a better understanding of CCSNe in the event of an explosion in the Milky Way or its close neighborhood. As many sections in this review has emphasized, any limited patch of data and models typically does not give unique solutions and answers - the grand challenge lies with combining the patches and doing a holistic analysis. In that sense, SN research by necessity will continue to transition from individual or small-group efforts into larger, global collaborative ones - and this is all and well, in the true spirit of science.

Acknowledgments

The authors thank S. Valenti for support in sourcing the data and putting together Figure 7, and K. Maguire for sourcing the data for Figure 2. We thank M. Modjaz, K. Maeda, S. Valenti, T. Foglizzo, J. Goldberg, and T. Temim for discussion and comments on the manuscript. A.J. acknowledges support by the European Research Council, the Swedish National Research Council, and the Knut and Alice Wallenberg foundation. D.M. acknowledges NSF support from grants PHY-2209451 and AST-2206532. B.M. acknowledge support by the Australian Research Council (ARC) through grants FT160100035 and DP240101786 (BM, AH), by Australia Limited’s ASTAC scheme, the National Computational Merit Allocation Scheme (NCMAS), and by an Australasian Leadership Computing Grant (ALCG).

See Also: Nebular spectra; Jerkstrand (2017). Classification; Gal-Yam (2017). SN neutrino emission; Janka (2017). Dust formation in SNe; Sarangi et al. (2018). Supernova remnants; Vink (2020). Supernova-to-supernova remnant transition; Milisavljevic and Fesen (2017).

References

- Abbott BP, Abbott R, Abbott TD, Acernese F, Ackley K, Adams C, Adams T, Addesso P, Adhikari RX, Adya VB, Affeldt C, Afrough M, Agarwal B, Agathos M, Agatsuma K, Aggarwal N, Aguiar OD, Aiello L, Ain A, Ajith P, Allen B, Allen G, Allocca A, Altin PA, Amato A, Ananyeva A, Anderson SB, Anderson WG, Angelova SV, Antier S, Appert S, Arai K, Araya MC, Areeda JS, Arnaud N, Arun KG, Ascenzi S, Ashton G, Ast M, Aston SM, Astone P, Atallah DV, Aufmuth P, Aulbert C, AultONEal K, Austin C, Avila-Alvarez A, Babak S, Bacon P, Bader MKM, Bae S, Baker PT, Baldaccini F, Ballardini G, Ballmer SW, Banagiri S, Barayoga JC, Barclay SE, Barish BC, Barker D, Barkett K, Barone F, Barr B, Barsotti L, Barsuglia M, Barta D, Barthelmy SD, Bartlett J, Bartos I, Bassiri R, Basti A, Batch JC, Bawaj M, Bayley JC, Bazzan M, Bécsy B, Beer C, Bejger M, Belahcene I, Bell AS, Berger BK, Bergmann G, Bero JJ, Berry CPL, Bersanetti D, Bertolini A, Betzwieser J, Bhagwat S, Bhandare R, Bilenko IA, Billingsley G, Billman CR, Birch J, Birney R, Birnholtz O, Biscans S, Biscoveanu S, Bisht A, Bitossi M, Biwer C, Bizouard MA, Blackburn JK, Blackman J, Blair CD, Blair DG, Blair RM, Bloemen S, Bock O, Bode N, Boer M, Bogaert G, Bohe A, Bondu F, Bonilla E, Bonnand R, Boom BA, Bork R, Boschi V, Bose S, Bossie K, Bouffanais Y, Bozzi A, Bradaschia C, Brady PR, Branchesi M, Brau JE, Briant T, Brillat A, Brinkmann M, Brisson V, Brockill P, Broida JE, Brooks AF, Brown DA, Brown DD, Brunett S, Buchanan CC, Buikema A, Bulik T, Bulten HJ, Buonanno A, Buskulic D, Buy C, Byer RL, Cabero M, Cadonati L, Cagnoli G, Cahillane C, Calderón Bustillo J, Callister TA, Calloni E, Camp JB, Canepa M, Canizares P, Cannon KC, Cao H, Cao J, Capano CD, Capocasa E, Carbognani F, Caride S, Carney MF, Casanueva Diaz J, Casentini C, Caudill S, Cavaglia M, Cavalier F, Cavalieri R, Cella G, Cepeda CB, Cerdá-Durán P, Cerretani G, Cesarini E, Chamberlin SJ, Chan M, Chao S, Charlton P, Chase E, Chassande-Mottin E, Chatterjee D, Chatziioannou K, Cheeseboro BD, Chen HY, Chen X, Chen Y, Cheng HP, Chia H, Chincarini A, Chiummo A, Chmiel T, Cho HS, Cho M, Chow JH, Christensen N, Chu Q, Chua AJK, Chua S, Chung AKW, Chung S and Ciani G (2017), Oct. Multi-messenger Observations of a Binary Neutron Star Merger. *ApJ* 848 (2), L12. doi:10.3847/2041-8213/aa91c9. 1710.05833.
- Abdikamalov E, Pagliaroli G and Radice D (2022), Gravitational Waves from Core-Collapse Supernovae, Bambi C, Katsanevas S and Kokkotas KD, (Eds.), *Handbook of Gravitational Wave Astronomy*, pp. 21.
- Afsariardchi N, Drout MR, Khatami DK, Matzner CD, Moon DS and Ni YQ (2021), Sep. The Nickel Mass Distribution of Stripped-envelope Supernovae: Implications for Additional Power Sources. *ApJ* 918 (2), 89. doi:10.3847/1538-4357/ac0aeb. 2009.06683.
- Akiyama S, Wheeler JC, Meier DL and Lichtenstadt I (2003), Feb. The Magnetorotational Instability in Core-Collapse Supernova Explosions. *ApJ* 584 (2): 954–970. doi:10.1086/344135. astro-ph/0208128.
- Alarie A, Bilodeau A and Drissen L (2014), Jul. A hyperspectral view of Cassiopeia A. *MNRAS* 441 (4): 2996–3008. doi:10.1093/mnras/stu774.
- Aloy MÁ and Obergaulinger M (2021), Jan. Magnetorotational core collapse of possible GRB progenitors - II. Formation of protomagnetars and collapsars. *MNRAS* 500 (4): 4365–4397. doi:10.1093/mnras/staa3273. 2008.03779.
- Anderson JP, Dessart L, Gutiérrez CP, Krühler T, Galbany L, Jerkstrand A, Smartt SJ, Contreras C, Morrell N, Phillips MM, Stritzinger MD, Hsiao EY, González-Gaitán S, Agliozzo C, Castellón S, Chambers KC, Chen TW, Flewelling H, Gonzalez C, Hosseinzadeh G, Huber M, Fraser M, Inserra C, Kankare E, Mattila S, Magnier E, Maguire K, Lowe TB, Sollerman J, Sullivan M, Young DR and Valenti S (2018), May. The lowest-

- metallicity type II supernova from the highest-mass red supergiant progenitor. *Nature Astronomy* 2: 574–579. doi:10.1038/s41550-018-0458-4. 1805.04434.
- Arnett WD and Meakin C (2011), Jun. Toward Realistic Progenitors of Core-collapse Supernovae. *ApJ* 733, 78. doi:10.1088/0004-637X/733/2/78. 1101.5646.
- Balick B and Heckman T (1978), Nov. An unusual supernova remnant with broad emission lines near NGC 4449. *ApJ* 226: L7–L10. doi:10.1086/182819.
- Bamba A and Williams BJ (2022), Supernova Remnants: Types and Evolution, Bambi C and Sanganello A, (Eds.), Handbook of X-ray and Gamma-ray Astrophysics, pp. 77.
- Banovetz J, Milisavljevic D, Sravan N, Weil KE, Subrayan B, Fesen RA, Patnaude DJ, Plucinsky PP, Law CJ, Blair WP and Morse JA (2023), May. Hubble Space Telescope Proper Motion Measurements of Supernova Remnant N132D: Center of Expansion and Age. *ApJ* 948 (1), 33. doi:10.3847/1538-4357/acb8b6. 2301.02128.
- Barbon R, Benetti S, Cappellaro E, Patat F, Turatto M and Iijima T (1995), May. SN 1993J in M 81: One year of observations at Asiago. *A&AS* 110: 513.
- Barmantloo S, Jerkstrand A, Iwamoto K, Hachisu I, Nomoto K, Sollerman J and Woosley S (2024), Sep. Nebular nitrogen line emission in stripped-envelope supernovae - a new progenitor mass diagnostic. *MNRAS* 533 (2): 1251–1280. doi:10.1093/mnras/stae1811. 2403.08911.
- Bersten MC, Benvenuto OG, Nomoto K, Ergon M, Folatelli G, Sollerman J, Benetti S, Botticella MT, Fraser M, Kotak R, Maeda K, Ochner P and Tomasella L (2012), Sep. The Type IIb Supernova 2011dh from a Supergiant Progenitor. *ApJ* 757 (1), 31. doi:10.1088/0004-637X/757/1/31. 1207.5975.
- Bersten MC, Folatelli G, García F, van Dyk SD, Benvenuto OG, Orellana M, Buso V, Sánchez JL, Tanaka M, Maeda K, Filippenko AV, Zheng W, Brink TG, Cenko SB, de Jaeger T, Kumar S, Moriya TJ, Nomoto K, Perley DA, Shivvers I and Smith N (2018), Feb. A surge of light at the birth of a supernova. *Nature* 554 (7693): 497–499. doi:10.1038/nature25151. 1802.09360.
- Bethe HA (1990), Oct. Supernova mechanisms. *Reviews of Modern Physics* 62 (4): 801–866. doi:10.1103/RevModPhys.62.801.
- Black CS, Milisavljevic D, Margutti R, Fesen RA, Patnaude D and Parker S (2017), Oct. The Transition of a Type IIIc Supernova into a Supernova Remnant: Late-time Observations of SN 2013by. *ApJ* 848 (1), 5. doi:10.3847/1538-4357/aa8999. 1709.02257.
- Blasi P (2013), Nov. The origin of galactic cosmic rays. *A&A Rev* 21, 70. doi:10.1007/s00159-013-0070-7. 1311.7346.
- Blinnikov SI, Eastman R, Bartunov OS, Popolitov VA and Woosley SE (1998), Mar. A Comparative Modeling of Supernova 1993J. *ApJ* 496 (1): 454–472. doi:10.1086/305375. astro-ph/9711055.
- Blondin JM, Borkowski KJ and Reynolds SP (2001), Aug. Dynamics of Fe Bubbles in Young Supernova Remnants. *ApJ* 557 (2): 782–791. doi:10.1086/321674. astro-ph/0010285.
- Blondin JM, Mezzacappa A and DeMarino C (2003), Feb. Stability of Standing Accretion Shocks, with an Eye toward Core-Collapse Supernovae. *ApJ* 584: 971–980. doi:10.1086/345812.
- Boggs SE, Harrison FA, Miyasaka H, Grefenstette BW, Zoglauer A, Fryer CL, Reynolds SP, Alexander DM, An H, Barret D, Christensen FE, Craig WW, Forster K, Giommi P, Hailey CJ, Hornstrup A, Kitaguchi T, Koglin JE, Madsen KK, Mao PH, Mori K, Perri M, Pivovarov MJ, Puccetti S, Rana V, Stern D, Westergaard NJ and Zhang WW (2015), May. ⁴⁴Ti gamma-ray emission lines from SN1987A reveal an asymmetric explosion. *Science* 348 (6235): 670–671. doi:10.1126/science.aaa2259.
- Bollig R, Yadav N, Kresse D, Janka HT, Müller B and Heger A (2021), Jul. Self-consistent 3D Supernova Models From -7 Minutes to +7 s: A 1-bethe Explosion of a 19 M_⊙ Progenitor. *ApJ* 915 (1), 28. doi:10.3847/1538-4357/abf82e. 2010.10506.
- Botticella MT, Smartt SJ, Kennicutt RC, Cappellaro E, Sereno M and Lee JC (2012), Jan. A comparison between star formation rate diagnostics and rate of core collapse supernovae within 11 Mpc. *A&A* 537, A132. doi:10.1051/0004-6361/201117343. 1111.1692.
- Branch D and Wheeler JC (2017). Supernova Explosions. doi:10.1007/978-3-662-55054-0.
- Burrows A, Hayes J and Fryxell BA (1995), Sep. On the Nature of Core-Collapse Supernova Explosions. *ApJ* 450: 830–850. doi:10.1086/176188.
- Burrows A, Dessart L, Livne E, Ott CD and Murphy J (2007), Jul. Simulations of Magnetically Driven Supernova and Hypernova Explosions in the Context of Rapid Rotation. *ApJ* 664 (1): 416–434. doi:10.1086/519161. astro-ph/0702539.
- Burrows A, Wang T and Vartanyan D (2024), Mar. Physical Correlations and Predictions Emerging from Modern Core-collapse Supernova Theory. *ApJ* 964 (1), L16. doi:10.3847/2041-8213/ad319e. 2401.06840.
- Catchpole RM, Menzies JW, Monk AS, Wargau WF, Pollaco D, Carter BS, Whitelock PA, Marang F, Laney CD, Balona LA, Feast MW, Lloyd Evans THH, Sekiguchi K, Laing JD, Kilkenny DM, Spencer Jones J, Roberts G, Cousins AWJ, van Vuuren G and Winkler H (1987), Nov. Spectroscopic and photometric observations of SN 1987A - II. Days 51 to 134. *MNRAS* 229: 15P–25. doi:10.1093/mnras/229.1.15P.
- Chevalier RA (1976), Aug. The hydrodynamics of Type II supernovae. *ApJ* 207: 872–887. doi:10.1086/154557.
- Chevalier RA (1977), Jan., Was SN 1054 A Type II Supernova?, Schramm DN, (Ed.), Supernovae, Astrophysics and Space Science Library, 66, pp. 53.
- Chevalier RA and Fransson C (1994), Jan. Emission from Circumstellar Interaction in Normal Type II Supernovae. *ApJ* 420: 268. doi:10.1086/173557.
- Chevalier RA and Oishi J (2003), Aug. Cassiopeia A and Its Clumpy Presupernova Wind. *ApJ* 593 (1): L23–L26. doi:10.1086/377572. astro-ph/0306376.
- Chieffi A and Limongi M (2013), Feb. Pre-supernova Evolution of Rotating Solar Metallicity Stars in the Mass Range 13-120 M_⊙ and their Explosive Yields. *ApJ* 764 (1), 21. doi:10.1088/0004-637X/764/1/21.
- Clark DH and Stephenson FR (1977). The historical supernovae.
- Colling C, Hennebelle P, Geen S, Iffrig O and Bournaud F (2018), Dec. Impact of galactic shear and stellar feedback on star formation. *A&A* 620, A21. doi:10.1051/0004-6361/201833161. 1809.01037.
- Couch SM, Chatzopoulos E, Arnett WD and Timmes FX (2015), Jul. The Three-dimensional Evolution to Core Collapse of a Massive Star. *ApJ* 808: L21. doi:10.1088/2041-8205/808/1/L21.
- Danziger IJ and Dennefeld M (1976), Jul. Supernova ejecta in the Large Magellanic Cloud. *ApJ* 207: 394–407. doi:10.1086/154507.
- Davidson K and Fesen RA (1985), Jan. Recent developments concerning the Crab Nebula. *ARA&A* 23: 119–146. doi:10.1146/annurev.aa.23.090185.001003.
- De Looze I, Barlow MJ, Swinyard BM, Rho J, Gomez HL, Matsuura M and Wesson R (2017), Mar. The dust mass in Cassiopeia A from a spatially resolved Herschel analysis. *MNRAS* 465 (3): 3309–3342. doi:10.1093/mnras/stw2837. 1611.00774.
- DeLaney T, Rudnick L, Stage MD, Smith JD, Isensee K, Rho J, Allen GE, Gomez H, Kozasa T, Reach WT, Davis JE and Houck JC (2010), Dec. The Three-dimensional Structure of Cassiopeia A. *ApJ* 725 (2): 2038–2058. doi:10.1088/0004-637X/725/2/2038. 1011.3858.
- DeLaney T, Kassim NE, Rudnick L and Perley RA (2014), Apr. The Density and Mass of Unshocked Ejecta in Cassiopeia A through Low Frequency Radio Absorption. *ApJ* 785 (1), 7. doi:10.1088/0004-637X/785/1/7. 1403.0032.
- Dessart L and Hillier DJ (2019), May. The difficulty of inferring progenitor masses from type-II-Plateau supernova light curves. *A&A* 625, A9. doi:10.1051/0004-6361/201834732. 1903.04840.

- Dessart L, Hillier DJ, Waldman R and Livne E (2013), Aug. Type II-Plateau supernova radiation: dependences on progenitor and explosion properties. *MNRAS* 433 (2): 1745–1763. doi:10.1093/mnras/stt861. 1305. 3386.
- Dessart L, Hillier DJ, Woosley S, Livne E, Waldman R, Yoon SC and Langer N (2015), Oct. Radiative-transfer models for supernovae IIb/Ib/Ic from binary-star progenitors. *MNRAS* 453 (2): 2189–2213. doi:10.1093/mnras/stv1747. 1507. 07783.
- Dessart L, Hillier DJ, Sukhbold T, Woosley SE and Janka HT (2021), Aug. The explosion of 9–29 M_{\odot} stars as Type II supernovae: Results from radiative-transfer modeling at one year after explosion. *A&A* 652, A64. doi:10.1051/0004-6361/202140839. 2105. 13029.
- Dessart L, Hillier DJ, Woosley SE and Kuncarayakti H (2023), Sep. Modeling of the nebular-phase spectral evolution of stripped-envelope supernovae. New grids from 100 to 450 days. *A&A* 677, A7. doi:10.1051/0004-6361/202346626. 2306. 12092.
- Dessart L, Hillier DJ and Leonard DC (2024), Apr. The evolution of continuum polarization in type II supernovae as a diagnostic of ejecta morphology. *A&A* 684, A16. doi:10.1051/0004-6361/202347808. 2401. 07330.
- Dopita MA, Tuohy IR and Mathewson DS (1981), Sep. An oxygen-rich young supernova remnant in the Small Magellanic Cloud. *ApJ* 248: L105–L108. doi:10.1086/183635.
- Drout MR, Soderberg AM, Gal-Yam A, Cenko SB, Fox DB, Leonard DC, Sand DJ, Moon DS, Arcavi I and Green Y (2011), Nov. The First Systematic Study of Type Ibc Supernova Multi-band Light Curves. *ApJ* 741 (2), 97. doi:10.1088/0004-637X/741/2/97. 1011. 4959.
- Drout MR, Götzberg Y, Ludwig BA, Groh JH, de Mink SE, O’Grady AJG and Smith N (2023), Dec. An observed population of intermediate-mass helium stars that have been stripped in binaries. *Science* 382 (6676): 1287–1291. doi:10.1126/science.ade4970. 2307. 00061.
- Duncan RC, Shapiro SL and Wasserman I (1986), Oct. Neutrino-driven Winds from Young, Hot Neutron Stars. *ApJ* 309: 141. doi:10.1086/164587.
- Duyvendak JJJ (1942), Apr. Further Data Bearing on the Identification of the Crab Nebula with the Supernova of 1054 A.D. Part I. The Ancient Oriental Chronicles. *PASP* 54 (318): 91–94. doi:10.1086/125409.
- Dwek E (2004), Jun. The Detection of Cold Dust in Cassiopeia A: Evidence for the Formation of Metallic Needles in the Ejecta. *ApJ* 607 (2): 848–854. doi:10.1086/382653. astro-ph/0401074.
- Elmhamdi A, Danziger IJ, Chugai N, Pastorello A, Turatto M, Cappellaro E, Altavilla G, Benetti S, Patat F and Salvo M (2003), Feb. Photometry and spectroscopy of the Type IIP SN 1999em from outburst to dust formation. *MNRAS* 338 (4): 939–956. doi:10.1046/j.1365-8711.2003.06150.x. astro-ph/0209623.
- Ennis JA, Rudnick L, Reach WT, Smith JD, Rho J, DeLaney T, Gomez H and Kozasa T (2006), Nov. Spitzer IRAC Images and Sample Spectra of Cassiopeia A’s Explosion. *ApJ* 652 (1): 376–386. doi:10.1086/508142. astro-ph/0610838.
- Fang Q, Maeda K, Kuncarayakti H, Tanaka M, Kawabata KS, Hattori T, Aoki K, Moriya TJ and Yamanaka M (2022), Apr. Statistical Properties of the Nebular Spectra of 103 Stripped-envelope Core-collapse Supernovae. *ApJ* 928 (2), 151. doi:10.3847/1538-4357/ac4f60. 2201. 11467.
- Fesen RA (2001a), Mar. An Optical Survey of Outlying Ejecta in Cassiopeia A: Evidence for a Turbulent, Asymmetric Explosion. *ApJS* 133: 161–186. doi:10.1086/319181.
- Fesen RA (2001b), May, The SN-SNR connection, Holt SS and Hwang U, (Eds.), Young Supernova Remnants, American Institute of Physics Conference Series, 565, AIP, 119–128.
- Fesen RA and Becker RH (1988), Sep., Optical Detection of the Remnant of SN 1980K in NGC 6946, Bulletin of the American Astronomical Society, 20, pp. 962.
- Fesen RA and Milisavljevic D (2016), Feb. An HST Survey of the Highest-velocity Ejecta in Cassiopeia A. *ApJ* 818 (1), 17. doi:10.3847/0004-637X/818/1/17. 1512. 05049.
- Fesen RA, Martin CL and Shull JM (1992), Nov. The Synchrotron Bays of the Crab Nebula: A Magnetic Structure Associated with a Presupernova Circumstellar Disk. *ApJ* 399: 599. doi:10.1086/171951.
- Fesen RA, Shull JM and Hurford AP (1997), Jan. An Optical Study of the Circumstellar Environment Around the Crab Nebula. *AJ* 113: 354–363. doi:10.1086/118258.
- Fesen RA, Hammell MC, Morse J, Chevalier RA, Borkowski KJ, Dopita MA, Gerardy CL, Lawrence SS, Raymond JC and van den Bergh S (2006), Jul. The Expansion Asymmetry and Age of the Cassiopeia A Supernova Remnant. *ApJ* 645: 283–292. doi:10.1086/504254. astro-ph/0603371.
- Filippenko AV (1997), Jan. Optical Spectra of Supernovae. *ARA&A* 35: 309–355. doi:10.1146/annurev.astro.35.1.309.
- Filippenko AV and Sargent WLW (1989), Oct. Spectroscopic Evidence for Inhomogeneities in the Ejecta of the Type Ib Supernova 1985F. *ApJ* 345: L43. doi:10.1086/185548.
- Fischer T, Bastian NUF, Wu MR, Baklanov P, Sorokina E, Blinnikov S, Typel S, Klähn T and Blaschke DB (2018), Oct. Quark deconfinement as a supernova explosion engine for massive blue supergiant stars. *Nature Astronomy* 2: 980–986. doi:10.1038/s41550-018-0583-0. 1712. 08788.
- Foglizzo T, Galletti P, Scheck L and Janka HT (2007), Jan. Instability of a Stalled Accretion Shock: Evidence for the Advective-Acoustic Cycle. *ApJ* 654 (2): 1006–1021. doi:10.1086/509612. astro-ph/0606640.
- Fox OD, Van Dyk SD, Williams BF, Drout M, Zapartas E, Smith N, Milisavljevic D, Andrews JE, Bostroem KA, Filippenko AV, Gomez S, Kelly PL, de Mink SE, Priel J, Rest A, Ryder S, Sravan N, Strolger L, Wang Q and Weil KE (2022), Apr. The Candidate Progenitor Companion Star of the Type Ib/c SN 2013ge. *ApJ* 929 (1), L15. doi:10.3847/2041-8213/ac5890. 2203. 01357.
- Fransson C, Cassatella A, Gilmozzi R, Kirshner RP, Panagia N, Sonneborn G and Wamsteker W (1989), Jan. Narrow Ultraviolet Emission Lines from SN 1987A: Evidence for CNO Processing in the Progenitor. *ApJ* 336: 429. doi:10.1086/167022.
- Fransson C, Ergon M, Challis PJ, Chevalier RA, France K, Kirshner RP, Marion GH, Milisavljevic D, Smith N, Bufano F, Friedman AS, Kangas T, Larsson J, Mattila S, Benetti S, Chornock R, Czekala I, Soderberg A and Sollerman J (2014), Dec. High-density Circumstellar Interaction in the Luminous Type IIin SN 2010jl: The First 1100 Days. *ApJ* 797 (2), 118. doi:10.1088/0004-637X/797/2/118. 1312. 6617.
- Fröhlich C, Hauser P, Liebendörfer M, Martínez-Pinedo G, Thielemann FK, Bravo E, Zinner NT, Hix WR, Langanke K, Mezzacappa A and Nomoto K (2006), Jan. Composition of the Innermost Core-Collapse Supernova Ejecta. *ApJ* 637 (1): 415–426. doi:10.1086/498224. astro-ph/0410208.
- Fryer CL, Belczynski K, Wiktorowicz G, Dominik M, Kalogera V and Holz DE (2012), Apr. Compact Remnant Mass Function: Dependence on the Explosion Mechanism and Metallicity. *ApJ* 749 (1), 91. doi:10.1088/0004-637X/749/1/91. 1110. 1726.
- Gabler M, Wongwathanarat A and Janka HT (2021), Apr. The infancy of core-collapse supernova remnants. *MNRAS* 502 (3): 3264–3293. doi:10.1093/mnras/stab116. 2008. 01763.
- Gal-Yam A (2017), Observational and Physical Classification of Supernovae, Alsabti AW and Murdin P, (Eds.), Handbook of Supernovae, pp. 195.
- Gal-Yam A, Yaron O, Pastorello A, Taubenberger S, Fraser M and Perley D (2021), Feb. Introducing a new Supernova classification type: SN Icn. *Transient Name Server AstroNote* 76: 1–76.
- Galama TJ, Vreeswijk PM, van Paradijs J, Kouveliotou C, Augusteijn T, Bönnhardt H, Brewer JP, Doublier V, Gonzalez JF, Leibundgut B, Lidman C, Hainaut OR, Patat F, Heise J, in’t Zand J, Hurley K, Groot PJ, Strom RG, Mazzali PA, Iwamoto K, Nomoto K, Umeda H, Nakamura T, Young TR, Suzuki T, Shigeyama T, Koshut T, Kippen M, Robinson C, de Wildt P, Wijers RAMJ, Tanvir N, Greiner J, Pian E, Palazzi E, Frontera F, Masetti N, Nicastro L, Feroci M, Costa E, Piro L, Peterson BA, Tinney C, Boyle B, Cannon R, Stathakis R, Sadler E, Begam MC and Ianna P (1998), Oct. An unusual supernova in the error box of the γ -ray burst of 25 April 1998. *Nature* 395 (6703): 670–672. doi:10.1038/27150.

- astro-ph/9806175.
- Goldberg JA, Bildsten L and Paxton B (2019), Jul. Inferring Explosion Properties from Type II-Plateau Supernova Light Curves. *ApJ* 879 (1), 3. doi:10.3847/1538-4357/ab22b6. 1903.09114.
- Goldberg JA, Jiang YF and Bildsten L (2022), Jul. Shock Breakout in Three-dimensional Red Supergiant Envelopes. *ApJ* 933 (2), 164. doi:10.3847/1538-4357/ac75e3. 2206.04134.
- Goss WM, Shaver PA, Zealey WJ, Murdin P and Clark DH (1979), Aug. Optical identification and spectrum of the supernova remnant G292.0+1.8. *MNRAS* 188: 357–363. doi:10.1093/mnras/188.2.357.
- Green DA (2019), Aug. A revised catalogue of 294 Galactic supernova remnants. *Journal of Astrophysics and Astronomy* 40 (4), 36. doi:10.1007/s12036-019-9601-6. 1907.02638.
- Grefenstette BW, Harrison FA, Boggs SE, Reynolds SP, Fryer CL, Madsen KK, Wik DR, Zoglauer A, Ellinger CI, Alexander DM, An H, Barret D, Christensen FE, Craig WW, Forster K, Giommi P, Hailey CJ, Hornstrup A, Kaspi VM, Kitaguchi T, Koglin JE, Mao PH, Miyasaka H, Mori K, Perri M, Pivovarov MJ, Puccetti S, Rana V, Stern D, Westergaard NJ and Zhang WW (2014), Feb. Asymmetries in core-collapse supernovae from maps of radioactive ^{44}Ti in Cassiopeia A. *Nature* 506: 339–342. doi:10.1038/nature12997. 1403.4978.
- Heger A, Fryer CL, Woosley SE, Langer N and Hartmann DH (2003), Jul. How Massive Single Stars End Their Life. *ApJ* 591 (1): 288–300. doi:10.1086/375341. astro-ph/0212469.
- Hendrick SP, Reynolds SP and Borkowski KJ (2005), Apr. An Fe-Ni Bubble in the Small Magellanic Cloud Supernova Remnant B0049-73.6. *ApJ* 622 (2): L117–L120. doi:10.1086/429862.
- Herant M, Benz W, Hix WR, Fryer CL and Colgate SA (1994), Nov. Inside the supernova: A powerful convective engine. *ApJ* 435: 339–361. doi:10.1086/174817.
- Hester JJ (2008), Sep. The Crab Nebula : an astrophysical chimera. *ARA&A* 46: 127–155. doi:10.1146/annurev.astro.45.051806.110608.
- Hirschi R, Meynet G and Maeder A (2004), Oct. Stellar evolution with rotation. XII. Pre-supernova models. *A&A* 425: 649–670. doi:10.1051/0004-6361:20041095. astro-ph/0406552.
- Hunter DJ, Valenti S, Kotak R, Meikle WPS, Taubenberger S, Pastorello A, Benetti S, Stanishev V, Smartt SJ, Trundle C, Arkharov AA, Bufano F, Cappellaro E, Di Carlo E, Dolci M, Elias-Rosa N, Frandsen S, Fynbo JU, Hopp U, Larionov VM, Laursen P, Mazzali P, Navasardyan H, Ries C, Riffeser A, Rizzi L, Tsvetkov DY, Turatto M and Wilke S (2009), Dec. Extensive optical and near-infrared observations of the nearby, narrow-lined type Ic γ ASTROBJ ζ SN 2007gr γ /ASTROBJ ζ : days 5 to 415. *A&A* 508 (1): 371–389. doi:10.1051/0004-6361/200912896. 0909.3780.
- Hwang U and Laming JM (2012), Feb. A Chandra X-Ray Survey of Ejecta in the Cassiopeia A Supernova Remnant. *ApJ* 746, 130. doi:10.1088/0004-637X/746/2/130. 1111.7316.
- Hwang U, Laming JM, Badenes C, Berendse F, Blondin J, Cioffi D, DeLaney T, Dewey D, Fesen R, Flanagan KA, Fryer CL, Ghavamian P, Hughes JP, Morse JA, Plucinsky PP, Petre R, Pohl M, Rudnick L, Sankrit R, Slane PO, Smith RK, Vink J and Warren JS (2004), Nov. A Million Second Chandra View of Cassiopeia A. *ApJ* 615: L117–L120. doi:10.1086/426186. astro-ph/0409760.
- Iliadis C (2007). Nuclear Physics of Stars.
- Inserra C, Smartt SJ, Jerkstrand A, Valenti S, Fraser M, Wright D, Smith K, Chen TW, Kotak R, Pastorello A, Nicholl M, Bresolin F, Kudritzki RP, Benetti S, Botticella MT, Burgett WS, Chambers KC, Ergon M, Flewelling H, Fynbo JPU, Geier S, Hodapp KW, Howell DA, Huber M, Kaiser N, Leloudas G, Magill L, Magnier EA, McCrum MG, Metcalfe N, Price PA, Rest A, Sollerman J, Sweeney W, Taddia F, Taubenberger S, Tonry JL, Wainscoat RJ, Waters C and Young D (2013), Jun. Super-luminous Type Ic Supernovae: Catching a Magnetar by the Tail. *ApJ* 770 (2), 128. doi:10.1088/0004-637X/770/2/128. 1304.3320.
- Jakobus P, Müller B, Heger A, Motornenko A, Steinheimer J and Stoecker H (2022), Oct. The role of the hadron-quark phase transition in core-collapse supernovae. *MNRAS* 516 (2): 2554–2574. doi:10.1093/mnras/stac2352. 2204.10397.
- Janka HT (2001), Mar. Conditions for shock revival by neutrino heating in core-collapse supernovae. *A&A* 368: 527–560. doi:10.1051/0004-6361:20010012. astro-ph/0008432.
- Janka HT (2017), Neutrino Emission from Supernovae, Alsabti AW and Murdin P, (Eds.), Handbook of Supernovae, pp. 1575.
- Janka HT and Müller E (1996), Feb. Neutrino heating, convection, and the mechanism of Type-II supernova explosions. *A&A* 306: 167–198.
- Janka HT, Langanke K, Marek A, Martínez-Pinedo G and Müller B (2007), Apr. Theory of core-collapse supernovae. *Phys. Rep.* 442 (1–6): 38–74. doi:10.1016/j.physrep.2007.02.002. astro-ph/0612072.
- Jerkstrand A (2017), Spectra of Supernovae in the Nebular Phase, Alsabti AW and Murdin P, (Eds.), Handbook of Supernovae, pp. 795.
- Jerkstrand A, Fransson C, Maguire K, Smartt S, Ergon M and Spyromilio J (2012), Oct. The progenitor mass of the Type IIP supernova SN 2004et from late-time spectral modeling. *A&A* 546, A28. doi:10.1051/0004-6361/201219528. 1208.2183.
- Jerkstrand A, Smartt SJ, Fraser M, Fransson C, Sollerman J, Taddia F and Kotak R (2014), Apr. The nebular spectra of SN 2012aw and constraints on stellar nucleosynthesis from oxygen emission lines. *MNRAS* 439 (4): 3694–3703. doi:10.1093/mnras/stu221. 1311.2031.
- Jerkstrand A, Ergon M, Smartt SJ, Fransson C, Sollerman J, Taubenberger S, Bersten M and Spyromilio J (2015a), Jan. Late-time spectral line formation in Type IIb supernovae, with application to SN 1993J, SN 2008ax, and SN 2011dh. *A&A* 573, A12. doi:10.1051/0004-6361/201423983. 1408.0732.
- Jerkstrand A, Smartt SJ, Sollerman J, Inserra C, Fraser M, Spyromilio J, Fransson C, Chen TW, Barbarino C, Dall’Ora M, Botticella MT, Della Valle M, Gal-Yam A, Valenti S, Maguire K, Mazzali P and Tomasella L (2015b), Apr. Supersolar Ni/Fe production in the Type IIP SN 2012ec. *MNRAS* 448 (3): 2482–2494. doi:10.1093/mnras/stv087. 1410.8394.
- Jerkstrand A, Timmes FX, Magkotsios G, Sim SA, Fransson C, Spyromilio J, Müller B, Heger A, Sollerman J and Smartt SJ (2015c), Jul. Constraints on Explosive Silicon Burning in Core-collapse Supernovae from Measured Ni/Fe Ratios. *ApJ* 807 (1), 110. doi:10.1088/0004-637X/807/1/110. 1505.05323.
- Jerkstrand A, Smartt SJ, Inserra C, Nicholl M, Chen TW, Krühler T, Sollerman J, Taubenberger S, Gal-Yam A, Kankare E, Maguire K, Fraser M, Valenti S, Sullivan M, Cartier R and Young DR (2017), Jan. Long-duration Superluminous Supernovae at Late Times. *ApJ* 835 (1), 13. doi:10.3847/1538-4357/835/1/13. 1608.02994.
- Jerkstrand A, Ertl T, Janka HT, Müller E, Sukhbold T and Woosley SE (2018), Mar. Emission line models for the lowest mass core-collapse supernovae - I. Case study of a 9 M_{\odot} one-dimensional neutrino-driven explosion. *MNRAS* 475 (1): 277–305. doi:10.1093/mnras/stx2877. 1710.04508.
- Jerkstrand A, Maeda K and Kawabata KS (2020), Jan. A type Ia supernova at the heart of superluminous transient SN 2006gy. *Science* 367 (6476): 415–418. doi:10.1126/science.aaw1469. 2002.10768.
- Kaplan DL, Chatterjee S, Gaensler BM and Anderson J (2008), apr. A Precise Proper Motion for the Crab Pulsar, and the Difficulty of Testing Spin-Kick Alignment for Young Neutron Stars. *The Astrophysical Journal* 677 (2): 1201–1215. ISSN 0004-637X. doi:10.1086/529026.
- Karamahmetoglu E, Sollerman J, Taddia F, Barbarino C, Feindt U, Fremling C, Gal-Yam A, Kasliwal MM, Petrushevska T, Schulze S, Stritzinger MD and Zapartas E (2023), Oct. A population of Type Ibc supernovae with massive progenitors. Broad lightcurves not uncommon in (i)PTF. *A&A* 678, A87. doi:10.1051/0004-6361/202245231. 2210.09402.

- Kasen D and Woosley SE (2009), Oct. Type II Supernovae: Model Light Curves and Standard Candle Relationships. *ApJ* 703 (2): 2205–2216. doi:10.1088/0004-637X/703/2/2205. 0910.1590.
- Kerzendorf WE, Do T, de Mink SE, Götzberg Y, Milisavljevic D, Zapartas E, Renzo M, Justham S, Podsiadlowski P and Fesen RA (2019), Mar. No surviving non-compact stellar companion to Cassiopeia A. *A&A* 623, A34. doi:10.1051/0004-6361/201732206. 1711.00055.
- Kitaura FS, Janka HT and Hillebrandt W (2006), Apr. Explosions of O-Ne-Mg cores, the Crab supernova, and subluminal type II-P supernovae. *A&A* 450 (1): 345–350. doi:10.1051/0004-6361:20054703. astro-ph/0512065.
- Kobayashi C, Karakas AI and Lugaro M (2020), Sep. The Origin of Elements from Carbon to Uranium. *ApJ* 900 (2), 179. doi:10.3847/1538-4357/abae65. 2008.04660.
- Kochanek CS (2018), Jan. Cas A and the Crab were not stellar binaries at death. *MNRAS* 473 (2): 1633–1643. doi:10.1093/mnras/stx2423. 1701.03109.
- Kochanek CS, Beacom JF, Kistler MD, Prieto JL, Stanek KZ, Thompson TA and Yüksel H (2008), Sep. A Survey About Nothing: Monitoring a Million Supergiants for Failed Supernovae. *ApJ* 684 (2): 1336–1342. doi:10.1086/590053. 0802.0456.
- Koo BC and Park C (2017), Supernova Remnant Cassiopeia A, Alsabti AW and Murdin P, (Eds.), Handbook of Supernovae, pp. 161.
- Kotak R, Meikle WPS, Farrah D, Gerardy CL, Foley RJ, Van Dyk SD, Fransson C, Lundqvist P, Sollerman J, Fesen R, Filippenko AV, Mattila S, Silverman JM, Andersen AC, Höflich PA, Pozzo M and Wheeler JC (2009), Oct. Dust and The Type II-Plateau Supernova 2004et. *ApJ* 704 (1): 306–323. doi:10.1088/0004-637X/704/1/306. 0904.3737.
- Kozma C and Fransson C (1998), Mar. Late Spectral Evolution of SN 1987A. I. Temperature and Ionization. *ApJ* 496 (2): 946–966. doi:10.1086/305409. astro-ph/9712223.
- Krause O, Birkmann SM, Usuda T, Hattori T, Goto M, Rieke GH and Misselt KA (2008), May. The Cassiopeia A Supernova Was of Type IIb. *Science* 320: 1195–. doi:10.1126/science.1155788. 0805.4557.
- Laming JM and Temim T (2020), Dec. Element Abundances in the Unshocked Ejecta of Cassiopeia A. *ApJ* 904 (2), 115. doi:10.3847/1538-4357/abc1e5. 2010.07718.
- Laming JM, Hwang U, Radics B, Lekli G and Takács E (2006), Jun. The Polar Regions of Cassiopeia A: The Aftermath of a Gamma-Ray Burst? *ApJ* 644: 260–273. doi:10.1086/503553. astro-ph/0603434.
- Larsson J, Fransson C, Spyromilio J, Leibundgut B, Challis P, Chevalier RA, France K, Jerkstrand A, Kirshner RP, Lundqvist P, Matsuura M, McCray R, Smith N, Sollerman J, Garnavich P, Heng K, Lawrence S, Mattila S, Migotto K, Sonneborn G, Taddia F and Wheeler JC (2016), Dec. Three-dimensional Distribution of Ejecta in Supernova 1987A at 10,000 Days. *ApJ* 833 (2), 147. doi:10.3847/1538-4357/833/2/147. 1609.04413.
- Larsson J, Sollerman J, Lyman JD, Spyromilio J, Tenhu L, Fransson C and Lundqvist P (2021), Dec. Clumps and Rings of Ejecta in SNR 0540-69.3 as Seen in 3D. *ApJ* 922 (2), 265. doi:10.3847/1538-4357/ac2a41. 2109.03683.
- Law CJ, Milisavljevic D, Patnaude DJ, Plucinsky PP, Gladders MD, Schmidt J, Sravan N, Banovetz J, Sano H, McGraw JM, Takahashi G and Orlando S (2020), May. Three-dimensional Kinematic Reconstruction of the Optically Emitting, High-velocity, Oxygen-rich Ejecta of Supernova Remnant N132D. *ApJ* 894 (1), 73. doi:10.3847/1538-4357/ab873a. 2004.00016.
- Lazendic JS and Slane PO (2006), Aug. Enhanced Abundances in Three Large-Diameter Mixed-Morphology Supernova Remnants. *ApJ* 647 (1): 350–366. doi:10.1086/505380. astro-ph/0505498.
- Lee JJ, Park S, Hughes JP and Slane PO (2014), Jul. X-Ray Observation of the Shocked Red Supergiant Wind of Cassiopeia A. *ApJ* 789 (1), 7. doi:10.1088/0004-637X/789/1/7. 1304.3973.
- Leonard DC, Filippenko AV, Ganeshalingam M, Serduke FJD, Li W, Swift BJ, Gal-Yam A, Foley RJ, Fox DB, Park S, Hoffman JL and Wong DS (2006), Mar. A non-spherical core in the explosion of supernova SN 2004dj. *Nature* 440 (7083): 505–507. doi:10.1038/nature04558. astro-ph/0603297.
- Leung SC and Nomoto K (2019), Feb. Final evolution of super-AGB stars and supernovae triggered by electron capture. *Publ. Astron. Soc. Aust.* 36, e006. doi:10.1017/pasa.2018.49.
- Li H and McCray R (1995), Mar. The He I Emission Lines of SN 1987A. *ApJ* 441: 821. doi:10.1086/175405.
- Li H, McCray R and Sunyaev RA (1993), Dec. Iron, Cobalt, and Nickel in SN 1987A. *ApJ* 419: 824. doi:10.1086/173534.
- Li W, Leaman J, Chornock R, Filippenko AV, Poznanski D, Ganeshalingam M, Wang X, Modjaz M, Jha S, Foley RJ and Smith N (2011), Apr. Nearby supernova rates from the Lick Observatory Supernova Search - II. The observed luminosity functions and fractions of supernovae in a complete sample. *MNRAS* 412 (3): 1441–1472. doi:10.1111/j.1365-2966.2011.18160.x. 1006.4612.
- Limongi M and Chieffi A (2003), Jul. Evolution, Explosion, and Nucleosynthesis of Core-Collapse Supernovae. *ApJ* 592 (1): 404–433. doi:10.1086/375703. astro-ph/0304185.
- Liu YQ, Modjaz M, Bianco FB and Graur O (2016), Aug. Analyzing the Largest Spectroscopic Data Set of Stripped Supernovae to Improve Their Identifications and Constrain Their Progenitors. *ApJ* 827 (2), 90. doi:10.3847/0004-637X/827/2/90. 1510.08049.
- Long KS (2017), Galactic and Extragalactic Samples of Supernova Remnants: How They Are Identified and What They Tell Us, Alsabti AW and Murdin P, (Eds.), Handbook of Supernovae, pp. 2005.
- Long KS, Blair WP and Krzeminski W (1989), May. Discovery of Optical Emission from the Remnant of SN 1957D in M83. *ApJ* 340: L25. doi:10.1086/185430.
- Lopez LA and Fesen RA (2018), Feb. The Morphologies and Kinematics of Supernova Remnants. *Space Sci. Rev.* 214, 44. doi:10.1007/s11214-018-0481-x. 1804.00024.
- Lopez LA, Ramirez-Ruiz E, Badenes C, Huppenkothen D, Jeltama TE and Pooley DA (2009), Nov. Typing Supernova Remnants Using X-Ray Line Emission Morphologies. *ApJ* 706 (1): L106–L109. doi:10.1088/0004-637X/706/1/L106. 0910.3208.
- Lundmark K (1921), Oct. Suspected New Stars Recorded in Old Chronicles and Among Recent Meridian Observations. *PASP* 33 (195): 225. doi:10.1086/123101.
- Lundqvist P and Tziatzis A (2012), Jun. Constraints on fast ejecta in the Crab supernova remnant from optical spectral lines. *MNRAS* 423 (2): 1571–1582. doi:10.1111/j.1365-2966.2012.20979.x.
- Lunnan R, Chornock R, Berger E, Jones DO, Rest A, Czekala I, Dittmann J, Drout MR, Foley RJ, Fong W, Kirshner RP, Laskar T, Leibler CN, Margutti R, Milisavljevic D, Narayan G, Pan YC, Riess AG, Roth KC, Sanders NE, Scolnic D, Smartt SJ, Smith KW, Chambers KC, Draper PW, Flewelling H, Huber ME, Kaiser N, Kudritzki RP, Magnier EA, Metcalfe N, Wainscoat RJ, Waters C and Willman M (2018), Jan. Hydrogen-poor Superluminous Supernovae from the Pan-STARRS1 Medium Deep Survey. *ApJ* 852 (2), 81. doi:10.3847/1538-4357/aa9f1a. 1708.01619.
- Maeda K, Kawabata K, Tanaka M, Nomoto K, Tominaga N, Hattori T, Minezaki T, Kuroda T, Suzuki T, Deng J, Mazzali PA and Pian E (2007a), Mar. SN 2006aj Associated with XRF 060218 at Late Phases: Nucleosynthesis Signature of a Neutron Star-driven Explosion. *ApJ* 658 (1): L5–L8. doi:10.1086/513564. astro-ph/0703107.
- Maeda K, Tanaka M, Nomoto K, Tominaga N, Kawabata K, Mazzali PA, Umeda H, Suzuki T and Hattori T (2007b), Sep. The Unique Type Ib Supernova 2005bf at Nebular Phases: A Possible Birth Event of a Strongly Magnetized Neutron Star. *ApJ* 666 (2): 1069–1082. doi:10.1086/520054. 0705.2713.
- Maeda K, Kawabata K, Mazzali PA, Tanaka M, Valenti S, Nomoto K, Hattori T, Deng J, Pian E, Taubenberger S, Iye M, Matheson T, Filippenko

- AV, Aoki K, Kosugi G, Ohya Y, Sasaki T and Takata T (2008), Feb. Asphericity in Supernova Explosions from Late-Time Spectroscopy. *Science* 319 (5867): 1220. doi:10.1126/science.1149437. 0801.1100.
- Maguire K, Di Carlo E, Smartt SJ, Pastorello A, Tsvetkov DY, Benetti S, Spiro S, Arkharov AA, Beccari G, Botticella MT, Cappellaro E, Cristallo S, Dolci M, Elias-Rosa N, Fiaschi M, Gorshanov D, Harutyunyan A, Larionov VM, Navasardyan H, Pietrinferni A, Raimondo G, di Rico G, Valenti S, Valentini G and Zampieri L (2010), May. Optical and near-infrared coverage of SN 2004et: physical parameters and comparison with other Type IIP supernovae. *MNRAS* 404 (2): 981–1004. doi:10.1111/j.1365-2966.2010.16332.x. 0912.3111.
- Marek A and Janka H (2009), Mar. Delayed Neutrino-Driven Supernova Explosions Aided by the Standing Accretion-Shock Instability. *ApJ* 694: 664–696. doi:10.1088/0004-637X/694/1/664.
- Margutti R, Kamble A, Milisavljevic D, Zapartas E, de Mink SE, Drout M, Chornock R, Risaliti G, Zauderer BA, Bietenholz M, Cantiello M, Chakraborti S, Chomiuk L, Fong W, Grefenstette B, Guidorzi C, Kirshner R, Parrent JT, Patnaude D, Soderberg AM, Gehrels NC and Harrison F (2017), Feb. Ejection of the Massive Hydrogen-rich Envelope Timed with the Collapse of the Stripped SN 2014C. *ApJ* 835 (2), 140. doi:10.3847/1538-4357/835/2/140. 1601.06806.
- Martin T, Milisavljevic D and Drissen L (2021), Apr. 3D mapping of the Crab Nebula with SITELLE - I. Deconvolution and kinematic reconstruction. *MNRAS* 502 (2): 1864–1881. doi:10.1093/mnras/staa4046. 2101.02709.
- Martinez L, Bersten MC, Anderson JP, Hamuy M, González-Gaitán S, Förster F, Orellana M, Stritzinger M, Phillips MM, Gutiérrez CP, Burns C, Contreras C, de Jaeger T, Ertini K, Folatelli G, Galbany L, Hoeflich P, Hsiao EY, Morrell N, Pessi PJ and Suntzeff NB (2022), Apr. Type II supernovae from the Carnegie Supernova Project-I. II. Physical parameter distributions from hydrodynamical modelling. *A&A* 660, A41. doi:10.1051/0004-6361/202142076. 2111.06529.
- Matheson T, Filippenko AV, Barth AJ, Ho LC, Leonard DC, Bershady MA, Davis M, Finley DS, Fisher D, González RA, Hawley SL, Koo DC, Li W, Lonsdale CJ, Schlegel D, Smith HE, Spinrad H and Wirth GD (2000a), Sep. Optical Spectroscopy of Supernova 1993J During Its First 2500 Days. *AJ* 120 (3): 1487–1498. doi:10.1086/301518. astro-ph/0006263.
- Matheson T, Filippenko AV, Ho LC, Barth AJ and Leonard DC (2000b), Sep. Detailed Analysis of Early to Late-Time Spectra of Supernova 1993J. *AJ* 120 (3): 1499–1515. doi:10.1086/301519. astro-ph/0006264.
- Mathewson DS, Dopita MA, Tuohy IR and Ford VL (1980), Dec. A new oxygen-rich supernova remnant in the Large Magellanic Cloud. *ApJ* 242: L73–L76. doi:10.1086/183406.
- Matsumoto J, Asahina Y, Takiwaki T, Kotake K and Takahashi HR (2022), Oct. Magnetic support for neutrino-driven explosion of 3D non-rotating core-collapse supernova models. *MNRAS* 516 (2): 1752–1767. doi:10.1093/mnras/stac2335. 2202.07967.
- Matsuura M, Dwek E, Barlow MJ, Babler B, Baes M, Meixner M, Cernicharo J, Clayton GC, Dunne L, Fransson C, Fritz J, Gear W, Gomez HL, Groenewegen MAT, Indebetouw R, Ivison RJ, Jerkstrand A, Leboutailler V, Lim TL, Lundqvist P, Pearson CP, Roman-Duval J, Royer P, Staveley-Smith L, Swinyard BM, van Hoof PAM, van Loon JT, Verstappen J, Wesson R, Zanardo G, Blommaert JADL, Decin L, Reach WT, Sonneborn G, Van de Steene GC and Yates JA (2015), Feb. A Stubbornly Large Mass of Cold Dust in the Ejecta of Supernova 1987A. *ApJ* 800 (1), 50. doi:10.1088/0004-637X/800/1/50. 1411.7381.
- Matzner CD and McKee CF (1999), Jan. The Expulsion of Stellar Envelopes in Core-Collapse Supernovae. *ApJ* 510 (1): 379–403. doi:10.1086/306571. astro-ph/9807046.
- Maud JR, Smartt SJ, Kudritzki RP, Podsiadlowski P and Gilmore GF (2004), Jan. The massive binary companion star to the progenitor of supernova 1993J. *Nature* 427 (6970): 129–131. doi:10.1038/nature02161. astro-ph/0401090.
- Mauder T, Callan FP, Sim SA, Heger A and Müller B (2024), Oct. Synthetic Light Curves and Spectra for the Photospheric Phase of a 3D Stripped-Envelope Supernova Explosion Model. *arXiv e-prints*, arXiv:2410.20829doi:10.48550/arXiv.2410.20829. 2410.20829.
- Mayall NU (1939), Jan. The Crab Nebula, a Probable Supernova. *Leaflet of the Astronomical Society of the Pacific* 3 (119): 145.
- Mazzali PA, Nomoto K, Patat F and Maeda K (2001), Oct. The Nebular Spectra of the Hypernova SN 1998bw and Evidence for Asymmetry. *ApJ* 559 (2): 1047–1053. doi:10.1086/322420. astro-ph/0106095.
- Mazzali PA, Kawabata KS, Maeda K, Nomoto K, Filippenko AV, Ramirez-Ruiz E, Benetti S, Pian E, Deng J, Tominaga N, Ohya Y, Iye M, Foley RJ, Matheson T, Wang L and Gal-Yam A (2005), May. An Asymmetric Energetic Type Ic Supernova Viewed Off-Axis, and a Link to Gamma Ray Bursts. *Science* 308 (5726): 1284–1287. doi:10.1126/science.1111384. astro-ph/0505199.
- Mazzali PA, Valenti S, Della Valle M, Chincarini G, Sauer DN, Benetti S, Pian E, Piran T, D'Elia V, Elias-Rosa N, Margutti R, Pasotti F, Antonelli LA, Bufano F, Campana S, Cappellaro E, Covino S, D'Avanzo P, Fiore F, Fugazza D, Gilmozzi R, Hunter D, Maguire K, Maiorano E, Marziani P, Masetti N, Mirabel F, Navasardyan H, Nomoto K, Palazzi E, Pastorello A, Panagia N, Pellizza LJ, Sari R, Smartt S, Tagliaferri G, Tanaka M, Taubenberger S, Tominaga N, Trundle C and Turatto M (2008), Aug. The Metamorphosis of Supernova SN 2008D/XRF 080109: A Link Between Supernovae and GRBs/Hypernovae. *Science* 321 (5893): 1185. doi:10.1126/science.1158088. 0807.1695.
- Mazzali PA, McFadyen AI, Woosley SE, Pian E and Tanaka M (2014a), Sep. An upper limit to the energy of gamma-ray bursts indicates that GRBs/SNe are powered by magnetars. *MNRAS* 443 (1): 67–71. doi:10.1093/mnras/stu1124. 1406.1209.
- Mazzali PA, McFadyen AI, Woosley SE, Pian E and Tanaka M (2014b), Sep. An upper limit to the energy of gamma-ray bursts indicates that GRBs/SNe are powered by magnetars. *MNRAS* 443 (1): 67–71. doi:10.1093/mnras/stu1124. 1406.1209.
- McCray R (2017), The Physics of Supernova 1987A, Alsabti AW and Murdin P, (Eds.), Handbook of Supernovae, pp. 2181.
- Menzies JW, Catchpole RM, van Vuuren G, Winkler H, Laney CD, Whitelock PA, Cousins AWJ, Carter BS, Marang F, Lloyd Evans THH, Roberts G, Kilkenny D, Spencer Jones J, Sekiguchi K, Fairall AP and Wolstencroft RD (1987), Aug. Spectroscopic and photometric observations of SN 1987A : the first 50days. *MNRAS* 227: 39P–49. doi:10.1093/mnras/227.1.39P.
- Metzger BD, Margalit B, Kasen D and Quataert E (2015), Dec. The diversity of transients from magnetar birth in core collapse supernovae. *MNRAS* 454: 3311–3316. doi:10.1093/mnras/stv2224. 1508.02712.
- Mezzacappa A, Endeve E, Messer OEB and Bruenn SW (2020), Dec. Physical, numerical, and computational challenges of modeling neutrino transport in core-collapse supernovae. *Living Reviews in Computational Astrophysics* 6 (1), 4. doi:10.1007/s41115-020-00010-8. 2010.09013.
- Milisavljevic D and Fesen RA (2008), Apr. The Nature of the Ultraluminous Oxygen-Rich Supernova Remnant in NGC 4449. *ApJ* 677 (1): 306–316. doi:10.1086/528929. 0709.0181.
- Milisavljevic D and Fesen RA (2013), Aug. A Detailed Kinematic Map of Cassiopeia A's Optical Main Shell and Outer High-velocity Ejecta. *ApJ* 772 (2), 134. doi:10.1088/0004-637X/772/2/134. 1306.2310.
- Milisavljevic D and Fesen RA (2015), Jan. The bubble-like interior of the core-collapse supernova remnant Cassiopeia A. *Science* 347 (6221): 526–530. doi:10.1126/science.1261949. 1501.07283.
- Milisavljevic D and Fesen RA (2017), The Supernova - Supernova Remnant Connection, Alsabti AW and Murdin P, (Eds.), Handbook of Supernovae, pp. 2211.
- Milisavljevic D, Fesen RA, Gerardy CL, Kirshner RP and Challis P (2010), Feb. Doublets and Double Peaks: Late-Time [O I] λ 16300, 6364 Line Profiles of Stripped-Envelope, Core-Collapse Supernovae. *ApJ* 709 (2): 1343–1355. doi:10.1088/0004-637X/709/2/1343. 0904.4256.
- Milisavljevic D, Fesen RA, Chevalier RA, Kirshner RP, Challis P and Turatto M (2012), May. Late-time Optical Emission from Core-collapse Supernovae. *ApJ* 751, 25. doi:10.1088/0004-637X/751/1/25. 1203.0006.

- Milisavljevic D, Soderberg AM, Margutti R, Drout MR, Howie Marion G, Sanders NE, Hsiao EY, Lunnan R, Chornock R, Fesen RA, Parrent JT, Levesque EM, Berger E, Foley RJ, Challis P, Kirshner RP, Dittmann J, Bieryla A, Kamble A, Chakraborti S, De Rosa G, Fausnaugh M, Hainline KN, Chen CT, Hickox RC, Morrell N, Phillips MM and Stritzinger M (2013), Jun. SN 2012au: A Golden Link between Superluminous Supernovae and Their Lower-luminosity Counterparts. *ApJ* 770 (2), L38. doi:10.1088/2041-8205/770/2/L38. 1304.0095.
- Milisavljevic D, Patnaude DJ, Chevalier RA, Raymond JC, Fesen RA, Margutti R, Conner B and Banovetz J (2018), Sep. Evidence for a Pulsar Wind Nebula in the Type Ib Peculiar Supernova SN 2012au. *ApJ* 864 (2), L36. doi:10.3847/2041-8213/aadd4e. 1809.01141.
- Milisavljevic D, Temim T, De Looze I, Dickinson D, Laming JM, Fesen R, Raymond JC, Arendt RG, Vink J, Posselt B, Pavlov GG, Fox OD, Pinarski E, Subrayan B, Schmidt J, Blair WP, Rest A, Patnaude D, Koo BC, Rho J, Orlando S, Janka HT, Andrews M, Barlow MJ, Burrows A, Chevalier R, Clayton G, Fransson C, Fryer C, Gomez HL, Kirchschrager F, Lee JJ, Matsuura M, Niculescu-Duvaz M, Pierel JDR, Plucinsky PP, Priestley FD, Ravi AP, Sartorio NS, Schmidt F, Shahbandeh M, Slane P, Smith N, Sravan N, Weil K, Wesson R and Wheeler JC (2024), Apr. A JWST Survey of the Supernova Remnant Cassiopeia A. *ApJ* 965 (2), L27. doi:10.3847/2041-8213/ad324b. 2401.02477.
- Minkowski R (1941), Aug. Spectra of Supernovae. *PASP* 53 (314): 224. doi:10.1086/125315.
- Modjaz M, Kirshner RP, Blondin S, Challis P and Matheson T (2008), Nov. Double-Peaked Oxygen Lines Are Not Rare in Nebular Spectra of Core-Collapse Supernovae. *ApJ* 687 (1): L9. doi:10.1086/593135. 0801.0221.
- Modjaz M, Li W, Butler N, Chornock R, Perley D, Blondin S, Bloom JS, Filippenko AV, Kirshner RP, Kocovski D, Poznanski D, Hicken M, Foley RJ, Stringfellow GS, Berlind P, Barrado y Navascues D, Blake CH, Bouy H, Brown WR, Challis P, Chen H, de Vries WH, Dufour P, Falco E, Friedmann A, Ganeshalingam M, Garnavich P, Holden B, Illingworth G, Lee N, Liebert J, Marion GH, Olivier SS, Prochaska JX, Silverman JM, Smith N, Starr D, Steele TN, Stockton A, Williams GG and Wood-Vasey WM (2009), Sep. From Shock Breakout to Peak and Beyond: Extensive Panchromatic Observations of the Type Ib Supernova 2008D Associated with Swift X-ray Transient 080109. *ApJ* 702 (1): 226–248. doi:10.1088/0004-637X/702/1/226. 0805.2201.
- Modjaz M, Gutiérrez CP and Arcavi I (2019), Aug. New regimes in the observation of core-collapse supernovae. *Nature Astronomy* 3: 717–724. doi:10.1038/s41550-019-0856-2. 1908.02476.
- Moriya TJ, Sorokina EI and Chevalier RA (2018), Mar. Superluminous Supernovae. *Space Sci. Rev.* 214 (2), 59. doi:10.1007/s11214-018-0493-6. 1803.01875.
- Morozova V, Piro AL and Valenti S (2018), May. Measuring the Progenitor Masses and Dense Circumstellar Material of Type II Supernovae. *ApJ* 858 (1), 15. doi:10.3847/1538-4357/aab9a6. 1709.04928.
- Mösta P, Ott CD, Radice D, Roberts LF, Schnetter E and Haas R (2015), Dec. A large-scale dynamo and magnetoturbulence in rapidly rotating core-collapse supernovae. *Nature* 528 (7582): 376–379. doi:10.1038/nature15755. 1512.00838.
- Müller B (2019), Oct. Neutrino Emission as Diagnostics of Core-Collapse Supernovae. *Annual Review of Nuclear and Particle Science* 69: 253–278. doi:10.1146/annurev-nucl-101918-023434. 1904.11067.
- Müller B (2020), Jun. Hydrodynamics of core-collapse supernovae and their progenitors. *Living Reviews in Computational Astrophysics* 6 (1), 3. doi:10.1007/s41115-020-0008-5. 2006.05083.
- Müller B (2024), Mar. Supernova Simulations. *arXiv e-prints*, arXiv:2403.18952doi:10.48550/arXiv.2403.18952. 2403.18952.
- Müller E, Fryxell B and Arnett D (1991), Nov. Instability and clumping in SN 1987A. *A&A* 251: 505–514.
- Müller B, Heger A, Liptai D and Cameron JB (2016a), Jul. A simple approach to the supernova progenitor-explosion connection. *MNRAS* 460 (1): 742–764. doi:10.1093/mnras/stw1083. 1602.05956.
- Müller B, Heger A, Liptai D and Cameron JB (2016b), Jul. A simple approach to the supernova progenitor-explosion connection. *MNRAS* 460 (1): 742–764. doi:10.1093/mnras/stw1083. 1602.05956.
- Müller B, Melson T, Heger A and Janka HT (2017a), Nov. Supernova simulations from a 3D progenitor model - Impact of perturbations and evolution of explosion properties. *MNRAS* 472: 491–513. doi:10.1093/mnras/stx1962.
- Müller B, Melson T, Heger A and Janka HT (2017b), Nov. Supernova simulations from a 3D progenitor model - Impact of perturbations and evolution of explosion properties. *MNRAS* 472 (1): 491–513. doi:10.1093/mnras/stx1962. 1705.00620.
- Müller T, Prieto JL, Pejcha O and Clocchiatti A (2017c), Jun. The Nickel Mass Distribution of Normal Type II Supernovae. *ApJ* 841 (2), 127. doi:10.3847/1538-4357/aa72f1. 1702.00416.
- Müller B, Tauris TM, Heger A, Banerjee P, Qian YZ, Powell J, Chan C, Gay DW and Langer N (2019), Apr. Three-dimensional simulations of neutrino-driven core-collapse supernovae from low-mass single and binary star progenitors. *MNRAS* 484 (3): 3307–3324. doi:10.1093/mnras/stz216. 1811.05483.
- Nagao T, Patat F, Cikota A, Baade D, Mattila S, Kotak R, Kuncarayakti H, Bulla M and Ayala B (2024), Jan. Spectropolarimetry of Type II supernovae. II. Intrinsic supernova polarization and its relation to photometric and spectroscopic properties. *A&A* 681, A11. doi:10.1051/0004-6361/202346715. 2308.00996.
- Ng CY and Romani RW (2004), Jan. Fitting Pulsar Wind Tori. *ApJ* 601 (1): 479–484. doi:10.1086/380486. astro-ph/0310155.
- Ng CY, Romani RW, Brisken WF, Chatterjee S and Kramer M (2007), Jan. The Origin and Motion of PSR J0538+2817 in S147. *ApJ* 654 (1): 487–493. doi:10.1086/510576. astro-ph/0611068.
- Nicholl M, Smartt SJ, Jerkstrand A, Inserra C, McCrum M, Kotak R, Fraser M, Wright D, Chen TW, Smith K, Young DR, Sim SA, Valenti S, Howell DA, Bresolin F, Kudritzki RP, Tonry JL, Huber ME, Rest A, Pastorello A, Tomasella L, Cappellaro E, Benetti S, Mattila S, Kankare E, Kangas T, Leloudas G, Sollerman J, Taddia F, Berger E, Chornock R, Narayan G, Stubbs CW, Foley RJ, Lunnan R, Soderberg A, Sanders N, Milisavljevic D, Margutti R, Kirshner RP, Elias-Rosa N, Morales-Garoffolo A, Taubenberger S, Botticella MT, Gezari S, Urata Y, Rodney S, Riess AG, Scolnic D, Wood-Vasey WM, Burgett WS, Chambers K, Flewelling HA, Magnier EA, Kaiser N, Metcalfe N, Morgan J, Price PA, Sweeney W and Waters C (2013), Oct. Slowly fading super-luminous supernovae that are not pair-instability explosions. *Nature* 502 (7471): 346–349. doi:10.1038/nature12569. 1310.4446.
- Nomoto K (1987), Nov. Evolution of 8–10 M_{sun} Stars toward Electron Capture Supernovae. II. Collapse of an O + NE + MG Core. *ApJ* 322: 206. doi:10.1086/165716.
- Nomoto K, Sparks WM, Fesen RA, Gull TR, Miyaji S and Sugimoto D (1982), Oct. The Crab Nebula's progenitor. *Nature* 299 (5886): 803–805. doi:10.1038/299803a0.
- Nomoto K, Hashimoto M, Tsujimoto T, Thielemann FK, Kishimoto N, Kubo Y and Nakasato N (1997), Feb. Nucleosynthesis in type II supernovae. *Nucl. Phys. A* 616: 79–90. doi:10.1016/S0375-9474(97)00076-6. astro-ph/9706024.
- Nomoto K, Tominaga N, Umeda H, Kobayashi C and Maeda K (2006), Oct. Nucleosynthesis yields of core-collapse supernovae and hypernovae, and galactic chemical evolution. *Nucl. Phys. A* 777: 424–458. doi:10.1016/j.nuclphysa.2006.05.008. astro-ph/0605725.
- Obergaulinger M and Reichert M (2020), Nucleosynthesis in jet-driven and jet-associated supernovae, *Handbook of Nuclear Physics*. ISBN: 978-981-15-8818-1. Springer, pp. 90.
- O'Connor EP and Couch SM (2018), Oct. Exploring Fundamentally Three-dimensional Phenomena in High-fidelity Simulations of Core-collapse Supernovae. *ApJ* 865 (2), 81. doi:10.3847/1538-4357/aadcf7. 1807.07579.
- Ofek EO, Sullivan M, Cenko SB, Kasliwal MM, Gal-Yam A, Kulkarni SR, Arcavi I, Bildsten L, Bloom JS, Horesh A, Howell DA, Filippenko AV,

- Laher R, Murray D, Nakar E, Nugent PE, Silverman JM, Shaviv NJ, Surace J and Yaron O (2013), Feb. An outburst from a massive star 40 days before a supernova explosion. *Nature* 494 (7435): 65–67. doi:10.1038/nature11877. 1302.2633.
- Orlando S, Miceli M, Pumo ML and Bocchino F (2016), May. Modeling SNR Cassiopeia A from the Supernova Explosion to its Current Age: The Role of Post-explosion Anisotropies of Ejecta. *ApJ* 822, 22. doi:10.3847/0004-637X/822/1/22. 1603.03690.
- Orlando S, Ono M, Nagataki S, Miceli M, Umeda H, Ferrand G, Bocchino F, Petruk O, Peres G, Takahashi K and Yoshida T (2020), Apr. Hydrodynamic simulations unravel the progenitor-supernova-remnant connection in SN 1987A. *A&A* 636, A22. doi:10.1051/0004-6361/201936718. 1912.03070.
- Orlando S, Wongwathanarat A, Janka HT, Miceli M, Ono M, Nagataki S, Bocchino F and Peres G (2021), Jan. The fully developed remnant of a neutrino-driven supernova. Evolution of ejecta structure and asymmetries in SNR Cassiopeia A. *A&A* 645, A66. doi:10.1051/0004-6361/202039335. 2009.01789.
- Owen PJ and Barlow MJ (2015), Mar. The Dust and Gas Content of the Crab Nebula. *ApJ* 801 (2), 141. doi:10.1088/0004-637X/801/2/141. 1501.01510.
- Özel F and Freire P (2016), Sep. Masses, Radii, and the Equation of State of Neutron Stars. *ARA&A* 54: 401–440. doi:10.1146/annurev-astro-081915-023322. 1603.02698.
- Pannuti TG, Rho J, Borkowski KJ and Cameron PB (2010), Dec. Mixed-morphology Supernova Remnants in X-rays: Isothermal Plasma in HB21 and Probable Oxygen-rich Ejecta in CTB 1. *AJ* 140 (6): 1787–1805. doi:10.1088/0004-6256/140/6/1787. 1009.3987.
- Pannuti TG, Rho J, Kargaltsev O, Rangelov B, Kosakowski AR, Winkler PF, Keohane JW, Hare J and Ernst S (2017), Apr. CTIO, ROSAT HRI, and Chandra ACIS Observations of the Archetypical Mixed-morphology Supernova Remnant W28 (G6.4-0.1). *ApJ* 839 (1), 59. doi:10.3847/1538-4357/aa615c. 1703.08141.
- Park S, Hughes JP, Burrows DN, Slane PO, Nousek JA and Garmire GP (2003), Dec. 0103-72.6: A New Oxygen-rich Supernova Remnant in the Small Magellanic Cloud. *ApJ* 598 (2): L95–L98. doi:10.1086/380599. astro-ph/0309271.
- Pastorello A, Mattila S, Zampieri L, Della Valle M, Smartt SJ, Valentini S, Agnoletto I, Benetti S, Benn CR, Branch D, Cappellaro E, Dennefeld M, Eldridge JJ, Gal-Yam A, Harutyunyan A, Hunter I, Kjeldsen H, Lipkin Y, Mazzali PA, Milne P, Navasardyan H, Ofek EO, Pian E, Shemmer O, Spiro S, Stathakis RA, Taubenberger S, Turatto M and Yamaoka H (2008), Sep. Massive stars exploding in a He-rich circumstellar medium - I. Type Ibn (SN 2006jc-like) events. *MNRAS* 389 (1): 113–130. doi:10.1111/j.1365-2966.2008.13602.x. 0801.2277.
- Patat F, Cappellaro E, Danziger J, Mazzali PA, Sollerman J, Augusteyn T, Brewer J, Doublier V, Gonzalez JF, Hainaut O, Lidman C, Leibundgut B, Nomoto K, Nakamura T, Spyromilio J, Rizzi L, Turatto M, Walsh J, Galama TJ, van Paradijs J, Kouveliotou C, Vreeswijk PM, Frontera F, Masetti N, Palazzi E and Pian E (2001), Jul. The Metamorphosis of SN 1998bw. *ApJ* 555 (2): 900–917. doi:10.1086/321526. astro-ph/0103111.
- Patnaude DJ, Lee SH, Slane PO, Badenes C, Heger A, Ellison DC and Nagataki S (2015), Apr. Are Models for Core-collapse Supernova Progenitors Consistent with the Properties of Supernova Remnants? *ApJ* 803 (2), 101. doi:10.1088/0004-637X/803/2/101. 1502.04374.
- Pavlov GG, Zavlin VE, Aschenbach B, Trümper J and Sanwal D (2000), Mar. The Compact Central Object in Cassiopeia A: A Neutron Star with Hot Polar Caps or a Black Hole? *ApJ* 531 (1): L53–L56. doi:10.1086/312521. astro-ph/9912024.
- Pavlov GG, Sanwal D and Teter MA (2004), Jan., Central Compact Objects in Supernova Remnants, Camilo F and Gaensler BM, (Eds.), *Young Neutron Stars and Their Environments*, IAU Symposium, 218, pp. 239, astro-ph/0311526.
- Pejcha O and Prieto JL (2015), Jun. On the Intrinsic Diversity of Type II-Plateau Supernovae. *ApJ* 806 (2), 225. doi:10.1088/0004-637X/806/2/225. 1501.06573.
- Perley DA, Sollerman J, Schulze S, Yao Y, Fremling C, Gal-Yam A, Ho AYQ, Yang Y, Kool EC, Irani I, Yan L, Andreoni I, Baade D, Bellm EC, Brink TG, Chen TW, Cikota A, Coughlin MW, Dahiwal A, Dekany R, Duev DA, Filippenko AV, Hoefflich P, Kasliwal MM, Kulkarni SR, Lunnan R, Masci FJ, Maund JR, Medford MS, Riddle R, Rosnet P, Shupe DL, Strotjohann NL, Tzanidakis A and Zheng W (2022), Mar. The Type Icn SN 2021csp: Implications for the Origins of the Fastest Supernovae and the Fates of Wolf-Rayet Stars. *ApJ* 927 (2), 180. doi:10.3847/1538-4357/ac478e. 2111.12110.
- Popov DV (1993), Sep. An Analytical Model for the Plateau Stage of Type II Supernovae. *ApJ* 414: 712. doi:10.1086/173117.
- Prentice SJ, Mazzali PA, Pian E, Gal-Yam A, Kulkarni SR, Rubin A, Corsi A, Fremling C, Sollerman J, Yaron O, Arcavi I, Zheng W, Kasliwal MM, Filippenko AV, Cenko SB, Cao Y and Nugent PE (2016), May. The bolometric light curves and physical parameters of stripped-envelope supernovae. *MNRAS* 458 (3): 2973–3002. doi:10.1093/mnras/stw299. 1602.01736.
- Quimby RM, Wheeler JC, Höflich P, Akerlof CW, Brown PJ and Rykoff ES (2007), Sep. SN 2006bp: Probing the Shock Breakout of a Type II-P Supernova. *ApJ* 666 (2): 1093–1107. doi:10.1086/520532. 0705.3478.
- Raymond JC (2018), Feb. Shock Waves in Supernova Ejecta. *Space Sci. Rev.* 214 (1), 28. doi:10.1007/s11214-017-0453-6.
- Raynaud R, Guilet J, Janka HT and Gastine T (2020), Mar. Magnetar formation through a convective dynamo in protoneutron stars. *Science Advances* 6 (11): eaay2732. doi:10.1126/sciadv.aay2732. 2003.06662.
- Reed JE, Hester JJ, Fabian AC and Winkler PF (1995), Feb. The Three-dimensional Structure of the Cassiopeia A Supernova Remnant. I. The Spherical Shell. *ApJ* 440: 706. doi:10.1086/175308.
- Renaud M, Vink J, Decourchelle A, Lebrun F, den Hartog PR, Terrier R, Couvreur C, Knödseder J, Martin P, Prantzos N, Bykov AM and Bloemen H (2006), Aug. The Signature of ^{44}Ti in Cassiopeia A Revealed by IBIS/ISGRI on INTEGRAL. *ApJ* 647 (1): L41–L44. doi:10.1086/507300. astro-ph/0606736.
- Rest A, Welch DL, Suntzeff NB, Ooster L, Lanning H, Olsen K, Smith RC, Becker AC, Bergmann M, Challis P, Clocchiatti A, Cook KH, Damke G, Garg A, Huber ME, Matheson T, Minniti D, Prieto JL and Wood-Vasey WM (2008), Jul. Scattered-Light Echoes from the Historical Galactic Supernovae Cassiopeia A and Tycho (SN 1572). *ApJ* 681 (2): L81. doi:10.1086/590427. 0805.4607.
- Rest A, Foley RJ, Sinnott B, Welch DL, Badenes C, Filippenko AV, Bergmann M, Bhatti WA, Blondin S, Challis P, Damke G, Finley H, Huber ME, Kasen D, Kirshner RP, Matheson T, Mazzali P, Minniti D, Nakajima R, Narayan G, Olsen K, Sauer D, Smith RC and Suntzeff NB (2011), May. Direct Confirmation of the Asymmetry of the Cas A Supernova with Light Echoes. *ApJ* 732, 3. doi:10.1088/0004-637X/732/1/3. 1003.5660.
- Reynolds SP, Borkowski KJ, Hwang U, Hughes JP, Badenes C, Laming JM and Blondin JM (2007), Oct. A Deep Chandra Observation of Kepler's Supernova Remnant: A Type Ia Event with Circumstellar Interaction. *ApJ* 668 (2): L135–L138. doi:10.1086/522830. 0708.3858.
- Rho J and Petre R (1998), Aug. Mixed-Morphology Supernova Remnants. *ApJ* 503 (2): L167–L170. doi:10.1086/311538.
- Rho J, Kozasa T, Reach WT, Smith JD, Rudnick L, DeLaney T, Ennis JA, Gomez H and Tappe A (2008a), Jan. Freshly Formed Dust in the Cassiopeia A Supernova Remnant as Revealed by the Spitzer Space Telescope. *ApJ* 673 (1): 271–282. doi:10.1086/523835. 0709.2880.
- Rho J, Kozasa T, Reach WT, Smith JD, Rudnick L, DeLaney T, Ennis JA, Gomez H and Tappe A (2008b), Jan. Freshly Formed Dust in the Cassiopeia A Supernova Remnant as Revealed by the Spitzer Space Telescope. *ApJ* 673 (1): 271–282. doi:10.1086/523835. 0709.2880.
- Richmond MW, Treffers RR, Filippenko AV and Paik Y (1996), Aug. UVRI Photometry of SN 1993J in M81: Days 3 to 365. *AJ* 112: 732. doi:10.1086/118048.
- Rodríguez Ó, Meza N, Pineda-García J and Ramirez M (2021), Aug. The iron yield of normal Type II supernovae. *MNRAS* 505 (2): 1742–1774. doi:10.1093/mnras/stab1335. 2105.03268.
- Ryder SD, Van Dyk SD, Fox OD, Zapartas E, de Mink SE, Smith N, Brunsden E, Azalee Bostroem K, Filippenko AV, Shivvers I and Zheng

- W (2018), Mar. Ultraviolet Detection of the Binary Companion to the Type IIb SN 2001ig. *ApJ* 856 (1), 83. doi:10.3847/1538-4357/aaaf1e. 1801.05125.
- Sarangi A, Matsuura M and Micelotta ER (2018), Apr. Dust in Supernovae and Supernova Remnants I: Formation Scenarios. *Space Sci. Rev.* 214 (3), 63. doi:10.1007/s11214-018-0492-7.
- Sato T, Yoshida T, Umeda H, Nagataki S, Ono M, Maeda K, Hirai R, Hughes JP, Williams BJ and Maeda Y (2020), Apr. A Subsolar Metallicity Progenitor for Cassiopeia A, the Remnant of a Type IIb Supernova. *ApJ* 893 (1), 49. doi:10.3847/1538-4357/ab822a. 2003.08922.
- Scheck L, Kifonidis K, Janka HT and Müller E (2006), Oct. Multidimensional supernova simulations with approximative neutrino transport. I. Neutron star kicks and the anisotropy of neutrino-driven explosions in two spatial dimensions. *A&A* 457: 963–986. doi:10.1051/0004-6361:20064855.
- Schlegel EM (1990), May. A new subclass of type II supernovae? *MNRAS* 244: 269–271.
- Schneider FRN, Podsiadlowski P and Müller B (2021), Jan. Pre-supernova evolution, compact-object masses, and explosion properties of stripped binary stars. *A&A* 645, A5. doi:10.1051/0004-6361/202039219. 2008.08599.
- Schulze S, Yaron O, Sollerman J, Leloudas G, Gal A, Wright AH, Lunnan R, Gal-Yam A, Ofek EO, Perley DA, Filippenko AV, Kasliwal MM, Kulkarni SR, Neill JD, Nugent PE, Quimby RM, Sullivan M, Strotjohann NL, Arcavi I, Ben-Ami S, Bianco F, Bloom JS, De K, Fraser M, Fremling CU, Horesh A, Johansson J, Kelly PL, Knežević N, Knežević S, Maguire K, Nyholm A, Papadogiannakis S, Petrushevska T, Rubin A, Yan L, Yang Y, Adams SM, Bufano F, Clubb KI, Foley RJ, Green Y, Harmanen J, Ho AYQ, Hook IM, Hosseinzadeh G, Howell DA, Kong AKH, Kotak R, Matheson T, McCully C, Milisavljevic D, Pan YC, Poznanski D, Shivvers I, van Velzen S and Verbeek KK (2021), Aug. The Palomar Transient Factory Core-collapse Supernova Host-galaxy Sample. I. Host-galaxy Distribution Functions and Environment Dependence of Core-collapse Supernovae. *ApJS* 255 (2), 29. doi:10.3847/1538-4365/abff5e. 2008.05988.
- Shahbandeh M, Hsiao EY, Ashall C, Teffs J, Hoefflich P, Morrell N, Phillips MM, Anderson JP, Baron E, Burns CR, Contreras C, Davis S, Diamond TR, Folatelli G, Galbany L, Gall C, Hachinger S, Holmbo S, Karamahmetoglu E, Kasliwal MM, Kirshner RP, Krisciunas K, Kumar S, Lu J, Marion GH, Mazzali PA, Piro AL, Sand DJ, Stritzinger MD, Suntzeff NB, Taddia F and Uddin SA (2022), Feb. Carnegie Supernova Project-II: Near-infrared Spectroscopy of Stripped-envelope Core-collapse Supernovae. *ApJ* 925 (2), 175. doi:10.3847/1538-4357/ac4030. 2110.12083.
- Shigeyama T, Nomoto K, Tsujimoto T and Hashimoto MA (1990), Sep. Low-Mass Helium Star Models for Type Ib Supernovae: Light Curves, Mixing, and Nucleosynthesis. *ApJ* 361: L23. doi:10.1086/185818.
- Shivvers I, Modjaz M, Zheng W, Liu Y, Filippenko AV, Silverman JM, Matheson T, Pastorello A, Graur O, Foley RJ, Chornock R, Smith N, Leaman J and Benetti S (2017), May. Revisiting the Lick Observatory Supernova Search Volume-limited Sample: Updated Classifications and Revised Stripped-envelope Supernova Fractions. *PASP* 129 (975): 054201. doi:10.1088/1538-3873/aa54a6. 1609.02922.
- Silverman JM, Pickett S, Wheeler JC, Filippenko AV, Vinkó J, Marion GH, Cenko SB, Chornock R, Clubb KI, Foley RJ, Graham ML, Kelly PL, Matheson T and Shields JC (2017), May. After the Fall: Late-Time Spectroscopy of Type IIP Supernovae. *MNRAS* 467 (1): 369–411. doi:10.1093/mnras/stx058. 1610.07654.
- Smartt SJ (2015), Apr. Observational Constraints on the Progenitors of Core-Collapse Supernovae: The Case for Missing High-Mass Stars. *Publ. Astron. Soc. Aust.* 32, e016. doi:10.1017/pasa.2015.17. 1504.02635.
- Smith N (2013), Sep. The Crab nebula and the class of Type II-n-P supernovae caused by sub-energetic electron-capture explosions. *MNRAS* 434 (1): 102–113. doi:10.1093/mnras/stt1004. 1304.0689.
- Soderberg AM, Berger E, Page KL, Schady P, Parrent J, Pooley D, Wang XY, Ofek EO, Cucchiara A, Rau A, Waxman E, Simon JD, Bock DCJ, Milne PA, Page MJ, Barentine JC, Barthelmy SD, Beardmore AP, Bietenholz MF, Brown P, Burrows A, Burrows DN, Byrnes G, Cenko SB, Chandra P, Cummings JR, Fox DB, Gal-Yam A, Gehrels N, Immler S, Kasliwal M, Kong AKH, Krimm HA, Kulkarni SR, Maccarone TJ, Mészáros P, Nakar E, O'Brien PT, Overzier RA, de Pasquale M, Racusin J, Rea N and York DG (2008), May. An extremely luminous X-ray outburst at the birth of a supernova. *Nature* 453 (7194): 469–474. doi:10.1038/nature06997. 0802.1712.
- Soderberg AM, Chakraborti S, Pignata G, Chevalier RA, Chandra P, Ray A, Wieringa M, Copete A, Chaplin V, Connaughton V, Barthelmy SD, Bietenholz MF, Chugai N, Stritzinger MD, Hamuy M, Fransson C, Fox O, Levesque EM, Grindlay JE, Challis P, Foley RJ, Kirshner RP, Milne PA and Torres MAP (2010), Jan. A relativistic type Ibc supernova without a detected γ -ray burst. *Nature* 463 (7280): 513–515. doi:10.1038/nature08714. 0908.2817.
- Sollerman J, Kozma C, Fransson C, Leibundgut B, Lundqvist P, Ryde F and Woudt P (2000), Jul. SN 1998bw at Late Phases. *ApJ* 537 (2): L127–L130. doi:10.1086/312763. astro-ph/0006406.
- Sollerman J, Holland ST, Challis P, Fransson C, Garnavich P, Kirshner RP, Kozma C, Leibundgut B, Lundqvist P, Patat F, Filippenko AV, Panagia N and Wheeler JC (2002), May. Supernova 1998bw - the final phases. *A&A* 386: 944–956. doi:10.1051/0004-6361:20020326. astro-ph/0204498.
- Spyromilio J, Stathakis RA and Meurer GR (1993), Jul. Clumping and small-scale mixing in supernova 1987A. *MNRAS* 263: 530–534. doi:10.1093/mnras/263.2.530.
- Stockinger G, Janka HT, Kresse D, Melson T, Ertl T, Gabler M, Gessner A, Wongwathanarat A, Tolstov A, Leung SC, Nomoto K and Heger A (2020), Aug. Three-dimensional models of core-collapse supernovae from low-mass progenitors with implications for Crab. *MNRAS* 496 (2): 2039–2084. doi:10.1093/mnras/staa1691. 2005.02420.
- Stritzinger M, Taddia F, Fransson C, Fox OD, Morrell N, Phillips MM, Sollerman J, Anderson JP, Boldt L, Brown PJ, Campillay A, Castellon S, Contreras C, Folatelli G, Habergham SM, Hamuy M, Hjorth J, James PA, Krzeminski W, Mattila S, Persson SE and Roth M (2012), Sep. Multi-wavelength Observations of the Enduring Type II-n Supernovae 2005ip and 2006jd. *ApJ* 756 (2), 173. doi:10.1088/0004-637X/756/2/173. 1206.5575.
- Sukhbold T, Ertl T, Woosley SE, Brown JM and Janka HT (2016), Apr. Core-collapse Supernovae from 9 to 120 Solar Masses Based on Neutrino-powered Explosions. *ApJ* 821 (1), 38. doi:10.3847/0004-637X/821/1/38. 1510.04643.
- Tanaka M, Maeda K, Mazzali PA, Kawabata KS and Nomoto K (2017), Mar. Three-dimensional Explosion Geometry of Stripped-envelope Core-collapse Supernovae. II. Modeling of Polarization. *ApJ* 837 (2), 105. doi:10.3847/1538-4357/aa6035. 1702.03127.
- Tananbaum H (1999), Sep. Cassiopeia A. *IAU Circ.* 7246: 1.
- Tartaglia L, Sand DJ, Groh JH, Valenti S, Wyatt SD, Bostroem KA, Brown PJ, Yang S, Burke J, Chen TW, Davis S, Förster F, Galbany L, Haislip J, Hiramatsu D, Hosseinzadeh G, Howell DA, Hsiao EY, Jha SW, Koupryanov V, Kuncarayakti H, Lyman JD, McCully C, Phillips MM, Rau A, Reichart DE, Shahbandeh M and Strader J (2021), Jan. The Early Discovery of SN 2017ahn: Signatures of Persistent Interaction in a Fast-declining Type II Supernova. *ApJ* 907 (1), 52. doi:10.3847/1538-4357/abca8a. 2008.06515.
- Taubenberger S, Valenti S, Benetti S, Cappellaro E, Della Valle M, Elias-Rosa N, Hachinger S, Hillebrandt W, Maeda K, Mazzali PA, Pastorello A, Patat F, Sim SA and Turatto M (2009), Aug. Nebular emission-line profiles of Type Ib/c supernovae - probing the ejecta asphericity. *MNRAS* 397 (2): 677–694. doi:10.1111/j.1365-2966.2009.15003.x. 0904.4632.
- Temim T, Slane P, Raymond JC, Patnaude D, Murray E, Ghavamian P, Renzo M and Jacovich T (2022), Jun. SNR G292.0+1.8: A Remnant of a Low-mass Progenitor Stripped-envelope Supernova. *ApJ* 932 (1), 26. doi:10.3847/1538-4357/ac6bf4. 2205.01798.
- Temim T, Laming JM, Kavanagh PJ, Smith N, Slane P, Blair WP, De Looze I, Bucciantini N, Jerkstrand A, Gountanis NM, Sankrit R, Milisavljevic D, Rest A, Lyutikov M, DePasquale J, Martin T, Drissen L, Raymond J, Fox OD, Modjaz M, Spitkovsky A and Strolger LG (2024), Jun. Dissecting

- the Crab Nebula with JWST: Pulsar Wind, Dusty Filaments, and Ni/Fe Abundance Constraints on the Explosion Mechanism. *ApJ* 968 (2), L18. doi:10.3847/2041-8213/ad50d1. 2406. 00172.
- Thielemann FK, Nomoto K and Hashimoto MA (1996), Mar. Core-Collapse Supernovae and Their Ejecta. *ApJ* 460: 408. doi:10.1086/176980.
- Timmes FX, Woosley SE and Weaver TA (1995), Jun. Galactic Chemical Evolution: Hydrogen through Zinc. *ApJS* 98: 617. doi:10.1086/192172. astro-ph/9411003.
- Tominaga N, Blinnikov SI and Nomoto K (2013), Jul. Supernova Explosions of Super-asymptotic Giant Branch Stars: Multicolor Light Curves of Electron-capture Supernovae. *ApJ* 771 (1), L12. doi:10.1088/2041-8205/771/1/L12. 1305. 6813.
- Valenti S, Elias-Rosa N, Taubenberger S, Stanishev V, Agnoletto I, Sauer D, Cappellaro E, Pastorello A, Benetti S, Riffeser A, Hopp U, Navasardyan H, Tsvetkov D, Lorenzi V, Patat F, Turatto M, Barbon R, Cirotti S, Di Mille F, Frandsen S, Fynbo JPU, Laursen P and Mazzali PA (2008), Feb. The Carbon-rich Type Ic SN 2007gr: The Photospheric Phase. *ApJ* 673 (2): L155. doi:10.1086/527672. 0712. 1899.
- Valenti S, Taubenberger S, Pastorello A, Aramyan L, Botticella MT, Fraser M, Benetti S, Smartt SJ, Cappellaro E, Elias-Rosa N, Ergon M, Magill L, Magnier E, Kotak R, Price PA, Sollerman J, Tomasella L, Turatto M and Wright DE (2012), Apr. A Spectroscopically Normal Type Ic Supernova from a Very Massive Progenitor. *ApJ* 749 (2), L28. doi:10.1088/2041-8205/749/2/L28. 1203. 1933.
- van Baal BFA, Jerkstrand A, Wongwathanarat A and Janka HT (2023), Jul. Modelling supernova nebular lines in 3D with EXTRASS. *MNRAS* 523 (1): 954–973. doi:10.1093/mnras/stad1488. 2305. 08933.
- van Baal BFA, Jerkstrand A, Wongwathanarat A and Janka HT (2024), Aug. Diagnostics of 3D explosion asymmetries of stripped-envelope supernovae by nebular line profiles. *MNRAS* 532 (4): 4106–4131. doi:10.1093/mnras/stae1603. 2404. 01763.
- Vartanyan D, Burrows A, Wang T, Coleman MSB and White CJ (2023), May. Gravitational-wave signature of core-collapse supernovae. *Phys. Rev. D* 107 (10), 103015. doi:10.1103/PhysRevD.107.103015. 2302. 07092.
- Vink J (2004), Feb. X- and γ -ray studies of Cas A: exposing core collapse to the core. *New Astronomy Reviews* 48 (1-4): 61–67. doi:10.1016/j.newar.2003.11.008. astro-ph/0310518.
- Vink J (2020). Physics and Evolution of Supernova Remnants. doi:10.1007/978-3-030-55231-2.
- Vogt FPA, Bartlett ES, Seitzzahl IR, Dopita MA, Ghavamian P, Ruiter AJ and Terry JP (2018), Apr. Identification of the central compact object in the young supernova remnant 1E 0102.2-7219. *Nature Astronomy* 2: 465–471. doi:10.1038/s41550-018-0433-0. 1803. 01006.
- Wanajo S (2023), Mar. Nucleosynthesis in neutrino-heated ejecta and neutrino-driven winds of core-collapse supernovae; neutrino-induced nucleosynthesis. *arXiv e-prints*, arXiv:2303.09442doi:10.48550/arXiv.2303.09442. 2303. 09442.
- Wanajo S, Janka HT and Müller B (2011), Jan. Electron-capture Supernovae as The Origin of Elements Beyond Iron. *ApJ* 726 (2), L15. doi:10.1088/2041-8205/726/2/L15. 1009. 1000.
- Wang L and Wheeler JC (2008), Sep. Spectropolarimetry of supernovae. *ARA&A* 46: 433–474. doi:10.1146/annurev.astro.46.060407.145139. 0811. 1054.
- Waxman E and Katz B (2017), Shock Breakout Theory, Alsabti AW and Murdin P, (Eds.), Handbook of Supernovae, pp. 967.
- West JL, Safi-Harb S, Jaffe T, Kothes R, Landecker TL and Foster T (2016), Mar. The connection between supernova remnants and the Galactic magnetic field: A global radio study of the axisymmetric sample. *A&A* 587, A148. doi:10.1051/0004-6361/201527001. 1510. 08536.
- Wheeler JC and LeVreault R (1985), Jul. The peculiar type I supernova in NGC 991. *ApJ* 294: L17–L20. doi:10.1086/184500.
- Winkler PF and Kirshner RP (1985), Dec. Discovery of fast-moving oxygen filaments in Puppis A. *ApJ* 299: 981–986. doi:10.1086/163764.
- Winteler C, Käppeli R, Perego A, Arcones A, Vassetz N, Nishimura N, Liebendörfer M and Thielemann FK (2012), May. Magnetorotationally Driven Supernovae as the Origin of Early Galaxy r-process Elements? *ApJ* 750 (1), L22. doi:10.1088/2041-8205/750/1/L22. 1203. 0616.
- Wongwathanarat A, Janka HT and Müller E (2013), Apr. Three-dimensional neutrino-driven supernovae: Neutron star kicks, spins, and asymmetric ejection of nucleosynthesis products. *A&A* 552: A126. doi:10.1051/0004-6361/201220636.
- Wongwathanarat A, Janka HT, Müller E, Pllumbi E and Wanajo S (2017), Jun. Production and Distribution of ^{44}Ti and ^{56}Ni in a Three-dimensional Supernova Model Resembling Cassiopeia A. *ApJ* 842 (1), 13. doi:10.3847/1538-4357/aa72de. 1610. 05643.
- Woosley SE (2010), Aug. Bright Supernovae from Magnetar Birth. *ApJ* 719 (2): L204–L207. doi:10.1088/2041-8205/719/2/L204. 0911. 0698.
- Woosley SE and Bloom JS (2006), Sep. The Supernova Gamma-Ray Burst Connection. *ARA&A* 44 (1): 507–556. doi:10.1146/annurev.astro.43.072103.150558. astro-ph/0609142.
- Woosley S and Janka T (2005), Dec. The physics of core-collapse supernovae. *Nature Physics* 1 (3): 147–154. doi:10.1038/nphys172. astro-ph/0601261.
- Woosley SE and Weaver TA (1995), Nov. The Evolution and Explosion of Massive Stars. II. Explosive Hydrodynamics and Nucleosynthesis. *ApJS* 101: 181. doi:10.1086/192237.
- Woosley SE, Heger A and Weaver TA (2002), Nov. The evolution and explosion of massive stars. *Reviews of Modern Physics* 74 (4): 1015–1071. doi:10.1103/RevModPhys.74.1015.
- Yang H and Chevalier RA (2015), Jun. Evolution of the Crab Nebula in a Low Energy Supernova. *ApJ* 806 (2), 153. doi:10.1088/0004-637X/806/2/153. 1505. 03211.
- Young PA, Fryer CL, Hungerford A, Arnett D, Rockefeller G, Timmes FX, Voit B, Meakin C and Eriksen KA (2006), Apr. Constraints on the Progenitor of Cassiopeia A. *ApJ* 640 (2): 891–900. doi:10.1086/500108. astro-ph/0511806.
- Zapartas E, de Mink SE, Justham S, Smith N, de Koter A, Renzo M, Arcavi I, Farmer R, Götzberg Y and Toonen S (2019), Nov. The diverse lives of progenitors of hydrogen-rich core-collapse supernovae: the role of binary interaction. *A&A* 631, A5. doi:10.1051/0004-6361/201935854. 1907. 06687.
- Zha S, O'Connor EP and da Silva Schneider A (2021), Apr. Progenitor Dependence of Hadron-quark Phase Transition in Failing Core-collapse Supernovae. *ApJ* 911 (2), 74. doi:10.3847/1538-4357/abc4c. 2103. 02268.
- Zhou Y (2017), Dec. Rayleigh-Taylor and Richtmyer-Meshkov instability induced flow, turbulence, and mixing. I. *Phys. Rep.* 720: 1–136. doi:10.1016/j.physrep.2017.07.005.